Kinetic Energy Flux Associated with Natural and Simulated Rainfall Events and Instrumentation Used in the Evaluation

---

A Thesis presented to the Faculty of the Graduate School

University of Missouri-Columbia

In Partial Fulfillment

of the Requirements for the Degree

Master of Science

---

by

KEITH COOLEY

Dr. Neil Fox and Dr. Allen Thompson

Thesis Supervisors

August 2011

The undersigned, appointed by the Dean of the Graduate School,
have examined the thesis entitled

Kinetic Energy Flux Associated with Natural and Simulated Rainfall Events and Instrumentation Used in the Evaluation

Presented by Keith Cooley

A candidate for the degree of Master of Science

And hereby certify that in their opinion it is worthy of acceptance.

Dr. Neil I. Fox

Dr. Allen L. Thompson

Dr. Patrick S. Market

Acknowledgements

When I first began my undergraduate studies at the University of Missouri-Columbia, I would have never believed that I had the potential to complete the requirements for a Master's degree; however, after a lot of hard work I finally made it. To begin with, I would like to thank God for allowing me to meet all of the wonderful folks at exactly the right time and place to allow all of this to happen. Keeping God very near to my family has made it possible for my family and me to achieve many things. Next, I would like to give special thanks to my lovely wife Christie for supporting me throughout all the hours of studying and all of the trips to South Farm to collect rainfall data. She has sacrificed many things including placing her education on hold so that I would be able to complete mine. She is an exceptional wife and I have been very blessed over the past 8 years of our marriage and look forward to many more years with her.

I would also like to give thanks to the rest of my family members including my parents, Brenda and Chester; sister, Pamela; brother-in-law, Josh; niece and nephew, Abby and Alex as well as my father-in-law and mother-in-law, Rodger and Mary Ann McCoy. I know it has been rough on all of you as much as it has been on Christie and me being at such great distances away from each other. One major sacrifice that you guys gave is the amount of time that we are able to spend with each other. I want to thank each of you for supporting and encouraging me as I've made this journey.

Another area of support was provided by my co-advisers and also committee members, Dr. Neil Fox and Dr. Allen Thompson. I would like to thank both of you for providing this opportunity to continue my education and for providing me with

guidance while conducting the research and writing my thesis. I want to thank you both for believing in me and encouraging me to continue my education. I would also like to thank another committee member, Dr. Patrick Market, for providing additional support and guidance in completing my thesis.

I would like to thank Gordon Ellison and Cliff Mongler for providing their support by helping to raise the gravity-fed simulator and by providing assistance in assembling and altering the equipment as needed. I would also like to thank Larry Bliven for providing the Rain Imaging System (RIS) and technical support for the instrument setup. There are several undergraduate students that also deserve thanks as they've provided support in many areas such as equipment setup, data compilation and organization, radar support as well as many other areas. Specifically, the undergraduate students are Josh Kastman, Quinn Pallardy, Briona Chester, Elizabeth McGiffin, Traci Fehnel as well as many others that provided support. I would like to thank Katie Crandall, a graduate student, for setting up the equipment, providing radar support and for providing support while writing this thesis.

Last, but most certainly not least, I would like to thank the MU Research Board for providing the support and funding necessary to complete this research. Through this funding it was possible for me to maintain my focus on the research as well as obtain new equipment to further collect and analyze rainfall events.

Table of Contents

List of Figures

List of Tables

Abstract

There have been many studies that focus on the evaluation of the raindrop-size distribution and the parameters that are based upon this distribution, ranging from radar reflectivity to kinetic energy flux at the surface. The main focus of this study was to analyze several naturally occurring and simulated rainfall events using rainfall detection equipment such as a Rain Imaging System and a Parsivel Disdrometer to determine how critical accurate observation of the drop-size distribution is in the assessment of the kinetic energy. Some of the objectives were to evaluate the accuracy of each instrument and, for each event, to determine the total kinetic energy flux at the surface as well as some of the attributes that affect it.

It was found that the moderate to heavy rainfall events maintain a higher kinetic energy flux, while the lighter events tend to maintain much lower fluxes. It was shown that the kinetic energy flux is not solely a function of rainfall rate; rather, it is also largely a function of the drop-size distribution. While analyzing the distributions, it was noticed that events with similar storm structures tended to have very similar drop-size distributions as well as maximum drop sizes. Also discovered in this analysis was that the kinetic energy flux calculated using the rainfall rate, as is used for the RUSLE equation, is a reasonable estimate when compared with the summed kinetic energy flux.

Another finding was that using the Gunn and Kinzer (1949) equation for determining drop-terminal velocity provided an accurate parameterization. This was completed by comparing kinetic energy flux using theoretical-terminal velocity and actual velocity, as measured by the disdrometer. Using rainfall simulators it was possible to compare the simulated distribution to that of the naturally occurring distribution and to calibrate the instrumentation to ensure that accuracy was being

achieved; however, it was found that the Rain Imaging System did not perform with satisfactory results. It did appear, however, that the gravity-fed rainfall simulator produced a drop-size distribution that was very similar to the distribution in naturally occurring rainfall events. When using a drop-redistribution screen to obtain the distribution, it was discovered that the screen height above the ground may reduce the drops potential to reach terminal velocity as the drops adhere and then drip from the screen at lower heights causing the kinetic energy flux to be underestimated.

Chapter 1
Introduction

Kinetic energy flux due to heavy rainfall events is currently a topic of interest and has been over the past several years as it is likely that soil erosion increases with the kinetic energy flux; however, determining the best way to quantify this value has been somewhat difficult. Some suggest that determining kinetic energy flux is best quantified by making it a function of rainfall rate (Schwab et. al 1993), while others suggest that kinetic energy flux might be best determined by analyzing the drop-size distribution (DSD) (Sempere-Torres et. al 1992). There is great interest in being able to parameterize the kinetic energy flux as it might be possible that the data could then be placed into soil erosion models to determine areas at greatest risk of soil erosion. Many different types of simulators have been developed in order to simulate the naturally occurring DSD; however, this has proved to be a very difficult task.

Simulators are not the only issues that come with evaluating the DSD data. It is also necessary to maintain the proper equipment to sense the drops. Over the past several years many methods have been developed to analyze the DSD. One of the more basic methods, yet very laborious, is the flour-pellet method, which is where raindrops are allowed to fall into flour and then they are sifted out and binned (Kincaid et al. 1996). More recently other devices have been developed to analyze the DSDs which make use of greater technologies such as the laser disdrometers as well as high-speed video cameras. Each of these methods has limitations and needs to be evaluated further for validation. Another important aspect about the DSD is that this information might be used in classifying specific types of rainfall events. If it is found that specific storm classifications maintain a similar DSD then it is possible that kinetic energy flux and rainfall rated could be determined on a broader scale.

This type of information would be of particular use with radar as it would be possible to determine areas at greater risk of soil loss as well as flash flooding due to very intense rainfall rates based on the regular occurrence of the specified storm classification.

1.1 Statement of Thesis

The focus of this study is on the kinetic energy flux associated with rainfall events as well as the instrumentation used in the evaluation.

Kinetic energy flux plays a large role in dislodging soil from the surface. In many cases this is due to the very large raindrops that form in some of the more intense convection. These intense storms are of greatest interest as the raindrops tend to dislodge the soil and then the runoff will begin to wash the soil away causing a greater amount of soil loss. In this study, the focus will be placed on the kinetic energy as this is the basis for modeling soil loss. It is necessary to be able calculate the kinetic energy flux accurately before the information can be applied to further studies. This study will yield kinetic energy results based on the DSDs detected from simulated data as well as the DSDs from natural events. A detailed evaluation of each of the instruments used in this study will also be completed to determine if the instruments are detecting drop sizes accurately. The specific objectives of this study are to:

- Validate the Rain Imaging System and the OTT disdrometer
- Determine if the terminal velocity equation proposed by Gunn and Kinzer (1949) accurately represents actual terminal velocity
- Determine if kinetic energy flux increases with rainfall rate or if it is more of a function of the DSD

- Evaluate simulated and natural rainfall data to determine if the simulated data accurately represents natural data
- Analyze the variations in DSD and KE with natural storms of different types

The specific hypotheses to be tested in this experiment are as follows:

- The rainfall simulator represents natural rainfall data
- Changes in the DSD are due to different types of storms, most notably, pulse thunderstorms which likely maintain larger raindrops

Chapter 2
Literature Review

Soil erosion is a very large problem and will very likely continue to be for the foreseeable future. This phenomenon is defined by Fornis et al. (2005) as a process consisting of detachment of individual particles from the soil mass and their transport by erosive agents. Raindrop erosion is a very significant part of this process as the raindrops impacting a bare surface will cause erosion due to detachment as well as splash. As the larger raindrops detach the soil, excessive rainfall can then cause the water to begin running off, transporting those particles broken free through interrill and rill erosion. Interrill erosion is defined as soil movement by splash and the transport by very shallow overland flow, while rill erosion is defined as erosion by concentrated flow within small rivulets.

Fornis et al. (2005) suggest that the two parameters most widely used in determining rainfall detachment are raindrop momentum and kinetic energy (KE). Two methods are used in this thesis to determine the kinetic energy associated with rainfall events. The first method is the method used in determining soil loss in the RUSLE equation. Using this method, a relationship is made between the rainfall intensity and the total kinetic energy regardless of the drop-size distribution (Schwab et al., 1993). The relationship is as follows:

$$E = 0.119 + 0.0873 \log_{10} i \tag{2.1}$$

where,

E = kinetic energy (MJ $ha^{-1}mm^{-1}$)

i = rainfall intensity (mm hr^{-1})

The second method is the determination of kinetic energy based on the drop-size distribution; where, the kinetic energy is summed up across the entire drop size spectrum. The main focus of this thesis will be on the kinetic energy associated with select rain events and the drop-size distribution; however, the method used for the RUSLE will be used for comparison. The equation for kinetic energy, determined by using the drop-size distribution, can be defined mathematically as:

$$KE = \frac{1}{2} m {v_T}^2 \tag{2.2}$$

where,

m = droplet mass (kg)

v_T = terminal velocity (m s^{-1})

By analyzing this equation it is possible to see that larger raindrops will tend to add a significant amount of kinetic energy to any given storm as they contain a much greater mass. The velocity will tend to have a much larger impact on the kinetic energy of an individual drop as this value is squared.

As the equation is analyzed further it becomes necessary to understand the ways that the mass and velocity are derived. One must understand that it is very difficult, if not impossible, to measure the mass of each individual raindrop, so it is necessary to use another equation which is as follows:

$$m = \rho \times V \tag{2.3}$$

where,

ρ =water density (kg m^{-3})

V = volume of spherical drop (m^3)

The equivalent volume is determined by assuming that the raindrops each fall as a sphere and by using the equivalent diameter, D_e (mm), (van Djik et al., 2002) in the following equation:

$$V = \frac{1}{6}\pi {D_e}^3 \tag{2.4}$$

It is known that raindrops are not spherical as the effects of surface tension and aerodynamic pressure distort the raindrop into more of an ovular shape (McDonald, 1954). Many studies suggest that the larger raindrops fall with a flat bottom surface and a round top surface. It is worth noting that it is very difficult, at this point, to measure both the horizontal axis and vertical axis in order to derive a more exact diameter of the raindrops; instead, many researchers use the equivalent diameter which is based upon other variables such as the area or the volume of the raindrop. Using these parameters, it is possible to determine the equivalent diameter of the raindrop by setting the volume (area) of the raindrop equal to the volume (area) of a sphere (circle). The method used for determining the equivalent diameter is dependent upon whether the instrument measures the volume or the area.

2.1 Terminal Velocity

After evaluating mass in Equation 2.2, it then becomes necessary to evaluate the velocity or terminal velocity variable in the equation, which is defined by Salmi and Ikonen (2005) as the point at which gravity, drag and buoyancy forces acting upon the raindrop are in equilibrium. The variable v represents measured terminal velocity when it is possible to use instrumentation to derive the actual raindrop velocity; otherwise, v_T will generally represent the theoretical terminal velocity as this tends to be more applicable due to cost and logistics. Due to the fact that this term is squared in order to determine the amount of kinetic energy associated with

the raindrops, it is imperative that an appropriate equation is used to determine theoretical- terminal velocity.

Over the past several years there have been many studies that relate the terminal velocity to the diameter of the raindrop. One such study uses data from experimentation by Gunn and Kinzer (1949) to develop a theoretical terminal velocity equation and is as follows:

$$v_T(D) = 9.4\left[1 - e^{-1.57 \times D^{1.15}}\right] \tag{2.5}$$

Two inducing rings, mounted one above the other and separated by a distance of approximately 1 meter, were used by Gunn and Kinzer (1949) to obtain the experimental terminal velocity data. As the drops were formed a charge was placed on them. As they fell through the inducing rings a potential pulse was placed on the grid of a vacuum tube. The time at which the charged droplet passed the first and second ring was measured with the difference indicating the elapsed time for the drop to travel 1 m (Gunn and Kinzer, 1949).

Another study by Atlas and Ulbrich (1977) determined that the terminal fall velocity of a raindrop can be based on the following equation:

$$v_T(D) = 1767D^{0.067} \tag{2.6}$$

where,

$v_T(D)$ = velocity of the raindrop (cm s^{-1})

D = diameter of the raindrop (cm)

It is required that the values for D must be within the range of 0.05 cm and 0.50 cm (Atlas and Ulbrich, 1977). This is largely due to the underestimation of terminal velocity below the lower boundary and the overestimation of terminal velocity above the upper boundary, as will be shown in greater detail in later sections.

Salmi and Ikonen (2005) proposed another equation, which was compared with Gunn and Kinzer's (1949) work, to represent the terminal velocity of raindrops as:

$$v(D) = 9.4\left[1 - e^{-0.556D^{1.13}}\right] \tag{2.7}$$

where,

v(D) = terminal velocity (m s^{-1})

D = drop diameter (mm)

In developing this equation, the use of a rainfall simulator along with a parallel-beam linear sensor was used. This equipment made it possible to measure the velocity of the raindrop as the upper beam was blocked and then a second beam was blocked at time Δt. As these beams are at a set distance apart with very little, if any, accelerations to the raindrop, it is then possible to determine the distance the drop traveled over a certain length of time, which provides terminal velocity. There are no formulae that represent the entire spectrum of raindrop velocities, but it assumed that the Gunn and Kinzer (1949) equation would be a better fit than most as it begins to slow the increase in velocities as the raindrops begin to increase in size above approximately 4 mm as shown in Figure 2.1:

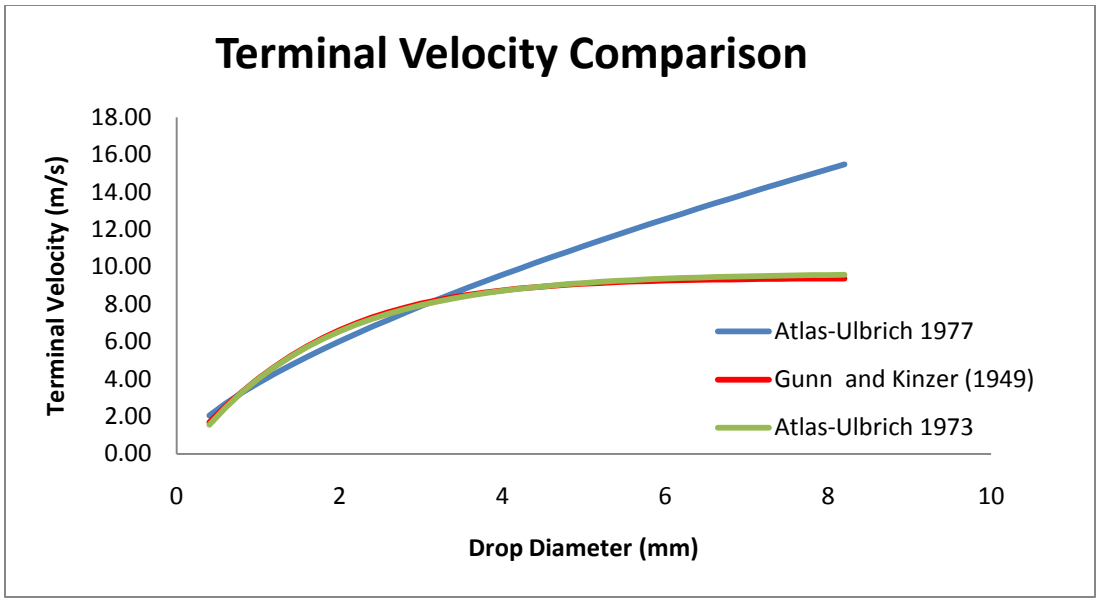

Figure 2.1: Comparison of drop diameter-terminal velocity relationships using the equations proposed by Gunn and Kinzer (1949) and Atlas and Ulbrich (1977).

2.2 Rain Rate Representation

Rain rate is the only parameter that can be used to validate the measurements taken by the instrumentation. This is important as it is one of the variables that can be evaluated and compared with actual rain gauge data. If the rain rate from the rain gauge is aligned closely with the rain rate found from the instrumentation, then it is likely that the instrument is detecting the drop sizes accurately. In order to use the drop-size data from the instrumentation, it is necessary to examine the following rain rate equation:

$$R = \frac{\pi}{6}\int_0^{D_{max}} N(D)D^3 v(D)dD \qquad (2.8)$$

where,

R = rain rate (mm s^{-1})

$N(D)$ = concentration of drops per unit volume (mm^{-3})

By analyzing the equation, one can visualize that the total volume for each rain drop is summed up across the spectrum and then allowed to spread out over the sample area which then gives a depth (mm). The results can be gathered from the rain gauge for the same time period and a comparison made to test for instrument accuracy. While Equation 2.8 shows the actual rain rate, it would be even more useful to substitute the values for the drop-size distribution as well as terminal velocity, which is fairly straight-forward; however, the equations used are based on the methods an individual decides to use such as the differing equations for terminal velocity $v_T(D)$, and the differing forms of the drop-size distribution $N(D)$.

2.3 Drop-Size Distribution

Raindrop-size distribution is very important in determining several different parameters as is evident by realizing that nearly all of the aforementioned equations are based upon the raindrop size. In an attempt to estimate the raindrop-size distribution as accurately as possible it is necessary to explore different expressions for the distribution. One representation of the drop-size distribution was proposed by Marshall and Palmer (1948), which is related solely to the lower rainfall rates associated with stratiform rain. This is due largely to the fact that a majority of their studies were conducted in southeastern Canada, where convective-type precipitation is limited at best. Through their studies, using records of raindrops on dyed filter papers, Marshall and Palmer (1948) were able to develop the following exponential equation:

$$N(D) = N_0 e^{-\Lambda D} \tag{2.9}$$

where N(D) is the concentration of drops $(mm^{-3}\, mm^{-1})$, N_0 is a parameter related to the intercept of the equation and it is estimated, by Marshall and Palmer (1948), to be approximately $(8.0 \times 10^6 m^{-4})$ for lighter rainfall rates (Testud et al., 2000).

The last variable in the equation, Λ, is represented by the following equation:

$$\Lambda = \frac{3.67}{D_0} \tag{2.10}$$

where,

Λ (mm^{-1}) = parameter related to the median drop size

D_0 = the median drop size (mm)

The drop size in which half of the volume is contained in raindrops larger and half of the volume is contained in raindrops smaller than D_0 is known as the median drop size (Testud et al. 2000). This tends to work best for stratiform events, but if it becomes necessary to evaluate heavier convective events then the intercept term, N_0, should be made variable (Testud et al. 2000).

In order to vary this term, it is necessary to revise the DSD, which assumes that the DSD maintains a gamma fit. Ulbrich (1983) showed that heavier and varying rainfall intensity events are much better represented by the gamma distribution and the equation is as follows:

$$N(D) = N_0 D^{\mu} e^{-\Lambda D} \tag{2.11}$$

where,

$N(D)$ is the concentration of drops $(mm^{-3}mm^{-1})$, Λ is determined as a function of μ, which is represented using the following equation:

$$\Lambda = \frac{3.67+\mu}{D_0} \tag{2.12}$$

where D_0 is the value in which half of the volume lies above and half of the volume lies below this diameter and μ generally ranges from -2 to approximately +6 (Ulbrich 1983). The variable N_0 in Equation 2.11 is again the parameter related to the intercept of the equation, which in this case varies with μ as suggested by Ulbrich (1983).

It was suggested by Ulbrich (1983) that N_0 should be parameterized by one of the following equations:

$$N_0 = 6 \times 10^4 e^{(3.2\mu)} \tag{2.13}$$

$$N_0 = 1.5 \times 10^4 e^{(3.14\mu)} \tag{2.14}$$

Equation 2.13 is described by Ulbrich (1983) as being representative of the DSD from empirical analysis of integral parameters of different rainfall event types. The specified equation generally overestimates the values for the μ to N_0 relationship, which is the concentration of drops compared to the μ values. The relationship compared to that of the experimental results shows that the correlation coefficient (R^2) is on the order of roughly 0.98 (Ulbrich 1983). Ulbrich (1983) described Equation 2.14 as being a good fit when analyzing raindrop data from moment to moment, where the correlation coefficient is greater than 0.95.

To aid in the understanding of the equations, it is worth discussing how the μ-values influence the overall shape of the DSD. Using the gamma distribution, with

the μ-value, Gilmore (2007) showed that the overall distribution of raindrops is graphically narrower, which would tend to represent the larger raindrops more accurately. Since the larger raindrops will contribute the largest amount to the overall kinetic energy, then it is necessary to use the gamma distribution equation with variable μ-values.

It is also evident by the differing values for N_0 that the drop-size distributions change when looking at different types of storms and storm structures. In general it would seem more intuitive that larger drops would form in convective events; however, some research would suggest that this is not the case. Tokay and Short (1996) determined, when comparing stratiform and convective precipitation at the same rainfall rates, that the larger drops tended to occur in the stratiform events. A comparison will be made in this thesis to determine if specific storm types or structures have any sort of impact on the drop-size distribution.

2.4 Rainfall Simulators

There are two main types of rainfall simulators as described by Renard (1975). The first type is the nozzle simulator, in which drops are produced through a pressurized fitting that can simulate abnormally long-duration and high-intensity storms (Blanquies et al. 2003). They all operate in generally the same fashion but the size and pressure application vary. One advantage of these simulators is that it is not necessary to elevate the nozzle to extreme heights as the drops generally reach terminal velocity much quicker due to the pressurized water. This is largely due to the jet spraying downward toward the surface, which means that the drops already maintain a significant velocity from the simulator. An example of a nozzle simulator can be seen in Figure 2.2.

Figure 2.2: An example of a square nozzle-type rainfall simulator of the Agricultural Engineering Building of the University of Missouri-Columbia.

The second type of rainfall simulator is the drop former. This type of simulator does not rely on pressure from a pump; rather, it is relies solely upon gravity to form the drops. Initially researchers used yarn or fine chicken wire to develop smaller drops; however, the issue with this type of setup was the inability to control the rainfall rate. The researchers were only able to sample one rainfall rate based upon the drip rate of the yarn or chicken wire. This problem was reduced as researchers began to use other types of drop formation.

As time progressed, new designs were developed using stainless steel or polyethylene tubing (Renard, 1975). Using these simulators it is possible to control rain rate by adjusting the length and the diameter of the tubes. If the length is increased, then there tends to be more friction within the tube allowing for a decreased rain rate; whereas the shorter tube will reduce friction allowing for an

increased rain rate. Larger and smaller raindrops are allowed to form depending upon the direction in which the diameter is shifted.

It is very difficult to simulate naturally occurring rainfall as the spatial distribution of the drops is largely based on the spacing of the drippers along with the dripper diameter and the size distribution. Some of the advantages are that the simulators are generally cost efficient to operate and it is possible to control when and where data collection occurs. The simulator can also be valuable for instrument calibration as it is possible to maintain a controlled drop size by using similar size tubing. One disadvantage of using the simulators is that the initial cost is fairly expensive (Renard, 1975); however, this cost can be recovered by having the ability to sample events at more convenient times. In most cases the test area is very small, meaning that the data has to be extrapolated over a much larger area which can lead to larger errors and, as previously mentioned, the DSD may not match that of natural rainfall events. There are also issues of temporal variations in natural rainfall compared to the steady tendencies of a rainfall simulator as it is difficult to simulate natural wind. It is also possible that the simulated drops will not reach terminal velocity if the simulator is not positioned at a height which allows for this to occur. With the large number of disadvantages to advantages, rainfall simulators still provide valuable information about terminal velocity even if there are issues with the DSD, provided that the height of the simulator is adequate.

2.5 Instruments for Sensing the DSD

One of the first methods for determining the DSD is known as the flour-pellet method, where rain drops would fall into a pan of sifted wheat flour and then the pan was removed after sampling. The drops were then sifted to determine the total number of each drop size. This tends to be reasonably accurate and some of the newer instruments, such as the laser disdrometers, have been validated using this method (Kincaid et al. 1996). There are several disadvantages to using this method, one of which is that it is not possible to determine the raindrop velocity as it falls into the pan, while another disadvantage is that it is very laborious due to the sifting, sorting and counting of the flour pellets, which limits the sample to very short time intervals.

As technology has advanced the instrumentation has become more high-tech. Kincaid et al. (1996) show a couple of examples of these newer technologies which include laser and photographic data collection. It is suggested that the laser method is able to measure the diameter of the raindrop by blocking some portion of a detector array. It is also explained by Kincaid et al. (1996) that the laser systems are able to determine the velocity by measuring the beam blockage as well as the time that it was blocked. Some of the largest errors that were found when using the laser system were due to overlapping images which produce larger raindrops, with smaller errors being due to small drops near the edge of the beam.

Kincaid et al. (1996) also used a photographic method in which raindrops fell into oil which kept the drop from breaking up and dispersing into the fluid, while a camera rapidly captured the images for later analysis. The main advantage of using this system is due to the lack of calibration measures needed and that the only errors come from magnification and the resolution of the camera. Comparisons have

been made with other instruments and methods in order to validate the photographic method (Kincaid et al. 1996). There are other photographic methods that have been used more recently as well; for example, Gilmore (2007) used the Rain Imaging System (RIS) to analyze raindrops using high-speed photography. Using this method it is possible to determine the drop-size distribution by using pattern recognition software, which analyzes each raindrop and places it into a bin; however, there are questions as to how in-focus and out-of-focus raindrops are analyzed. One disadvantage noted for these photographic methods is that it is not possible to analyze drop velocity; therefore, it is necessary to use theoretical terminal velocity to calculate parameters such as kinetic energy without comparing with actual velocity. This also places limitations on precipitation discrimination as liquid and ice structures will fall with different rates of speed (Yuter et al. 2006).

Chapter 3
Equipment and Instrumentation

In this study it was necessary to utilize several meteorological instruments to acquire natural rainfall data and simulated rainfall data. A majority of the natural rainfall data was collected at the Atmospheric and Climatic Experiment Station at the South Farm of the University of Missouri-Columbia, where much of the instrumentation was located. It was necessary to relocate during some rainfall events to collect the higher intensity rainfall which occurred north of the station. When relocation was required, rain gauge data was acquired from locations closest to the data collection point. Simulated rainfall data were collected from two rainfall simulators located in the Hydrology Lab within the Agricultural Engineering Building on the University of Missouri campus.

3.1 Atmospheric and Climatic Experiment Station

The Atmospheric and Climatic Experiment Station proved to be very useful in the data collection process. This station, located at South Farm Field Research Center southeast of Columbia, MO, is home to several different meteorological devices and is shown in Figure 3.1. One setup maintained at the station is a Campbell Scientific weather station, which encompasses several different devices to measure the following:

- 2-meter temperature
- 2-meter humidity
- Barometric pressure
- 3-meter wind speed
- Max wind speed
- 3-meter wind direction

The Campbell Scientific weather station also maintains a tipping-bucket rain gauge, which records data in 2-minute intervals and then archives them every 10 minutes. Each tip of the bucket is counted as 0.254 mm (0.01 inch) and is archived as such. The most useful information provided by the weather station was the 3-meter wind speed, max wind speed and rainfall data from the tipping-bucket rain gauge.

Figure 3.1: The ACES at Columbia, MO, the location where a majority of the data collection occurred.

The rain gauge data provided by the Campbell Scientific weather station was used for comparison with two other rain gauges located much closer to the Rain Imaging System (RIS) as well as the OTT Parsivel Disdrometer. One of the rain gauges was positioned on top of the Atmospheric and Climatic Experiment Station at approximately 4 meters above ground level (AGL), while the other was positioned much closer to the rain imaging equipment at approximately 1 meter (AGL). Data collection and archiving was similar with each rain gauge as each was designed by Campbell Scientific.

3.2 Rainfall Simulators Used in This Study

The gravity-fed rainfall simulators used in this research were located in the Hydrology Lab within the Agricultural Engineering Building. One of the simulators was a smaller version of the larger rainfall simulator located in the rain tower, which is shown in Figure 3.2. The small simulator would not permit terminal velocity to be

tested, but it did permit testing of the imager sensitivity to raindrop focus. Both rainfall simulators operate by using an air-inlet tube to maintain a constant pressure above the tubing-tips. As the air-inlet tube is adjusted higher inside the vacuum tank, the pressure increases above the tubing tip causing the rainfall rate to increase. Both simulators used tubes having a 0.76 mm inside diameter; however, they differ in the fact that the tubes in the large simulator are 457.2 mm (18 in) long while the tubes in the small simulator are 304.8 mm (12 in). The longer tubes were added to the large simulator to decrease the overall rain rate as the greater length increases the friction applied to the fluid flow. This should not vary the raindrop size that is released from the tubing tips as this is largely a function of the tube diameter and surface tension.

The large gravity rainfall simulator, shown in Figure 3.3, is positioned in the rain tower so that the tubing tips are located approximately 14 m above ground level, which allows the drops to obtain a velocity that is shown to be approximately 95% of their terminal velocity (Regmi and Thompson, 2000). This information, along with drop-size data collected without the drop redistribution screen, can be used to calibrate the drop detecting instruments. If the simulators are utilized with the drop-redistribution screen, the DSD produced can be compared with that of natural rainfall events; however, if the drop-redistribution screen is not utilized, then the drops should be fairly uniform since each drop originates from drippers of uniform diameter. The drop-redistribution screen tends to cause the drops to break-up and fall as smaller drops as they impact the screen; however, some of the drops actually adhere to the screen allowing larger drops to form which provides a larger maximum drop size in the distribution. The manner in which the distribution is impacted is largely a function of the screen distance away from the drippers. For example, the closer the screen is to the drippers the larger the drops tend to be as the drop

velocity is not great enough to splash through without adhering to the screen. The greater distances will allow for the drops to readily break-up providing smaller drops in the distribution (Regmi and Thompson, 2000).

Figure 3.2: The smaller gravity-fed rainfall simulator with the single dripper circled near the center of the simulator

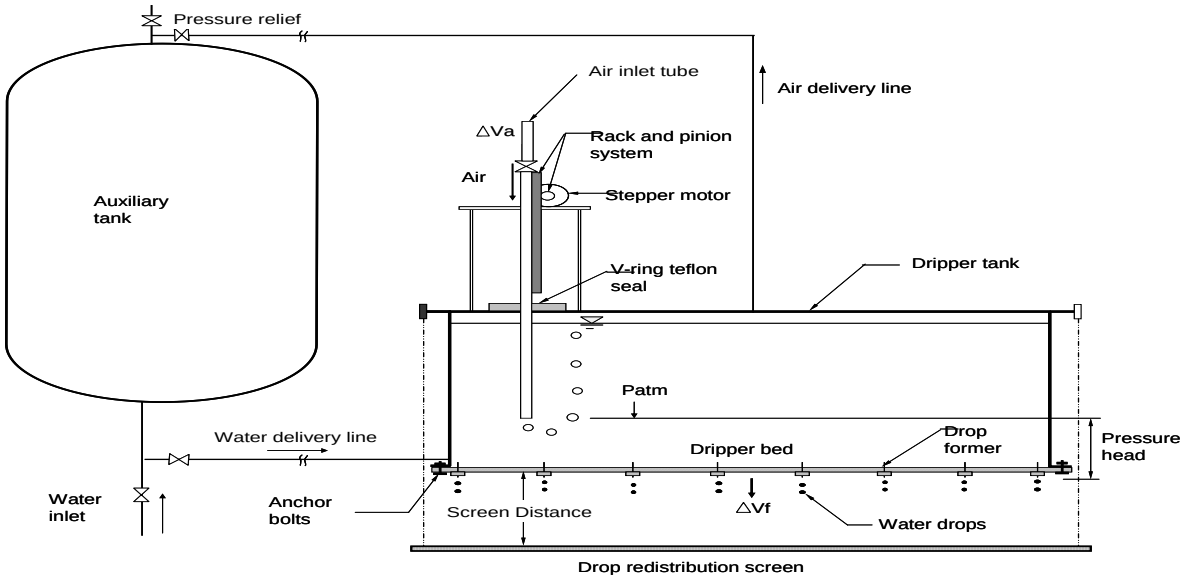

Figure 3.3: Design schematic of the large rainfall simulator located in the Hydrology Lab. (From Regmi and Thompson, 2000)

3.3 Rain Imaging System (RIS)

In order to collect the DSD data it was necessary to acquire the appropriate instrumentation. One device used was the Rain Imaging System (RIS), which was on loan from National Aeronautics and Space Administration (NASA) and was constructed to collect data from both rainfall and snowfall events. The RIS consists of three main hardware components: the flood lamp, camera and personal computer. The flood lamp consists of a 110 V, 300 W bulb with a sand blasted glass cover, which reduces the amount of glare. The light is used to create a shadow of the raindrop and produce a bright spot in the center of the droplet. The camera, shown in Figure 3.4, is placed approximately 3 m (≈10ft) in front of the flood lamp, while the center of the focal volume is located at approximately 2 m (≈6.5 ft) in front of the camera. The camera maintains the following attributes:

- 32 x 24 mm^2 focal plane
- 60 frames per second image capture rate
- High speed image compression for long-term deployment

The software used with the RIS was developed by NASA using pattern recognition software. The software is meant to determine the total area that is shadowed by the raindrop from which the equivalent diameter is derived. While determining the total area, it is necessary to determine if the raindrop is in-focus or out-of-focus as the out-of-focus raindrops will appear as larger drops due to larger shadow areas. The software was designed to analyze "bright spots" near the center of the raindrop, in order to ensure that the raindrops were within the focal volume, as shown in Figure 3.5. If the raindrop maintained a bright spot then the drop was accepted, and if not the drop was eliminated from the analysis (Jones et al. 2003). The software also

maintained the capability of rejecting raindrops that fell along the edges of the focal plane, which aides in error reduction in the small-diameter portion of the DSD.

Figure 3.4: Setup for data collection at South Farm including the Campbell Scientific rain gauge, OTT Parsivel Disdrometer and the Rain Imaging System.

3.4 Rain Imaging System (RIS) Calibration

As with any instrument it is necessary to evaluate the errors that are likely to occur during data collection; therefore, the RIS was tested using both the small rainfall simulator and the large rainfall simulator. Using the small rainfall simulator it was possible to test the RIS to determine if the software was correctly detecting particle size. In order to test the system it was necessary to perform three 5-minute tests which required the removal of all the drippers, except for a single dripper, from the small rainfall simulator. Once this was completed, the RIS was set up with the focal volume centered below the single dripper, following the aforementioned setup guidelines, which allowed for the single drop to fall into that volume. Theoretically the drop formed from the single dripper should be fairly uniform with only slight variations in the drop diameters.

To verify the drop diameters, it was necessary to place a beaker below the sample volume so that each drop was collected while being counted manually. The volume of water was weighed which revealed the total mass (kg) and by using a value of 1000 kg m^{-3} for the density of water, it was possible to derive the volume of water that remained in the beaker. After the volume within the beaker was determined, it was possible to determine the average drop diameter by assuming that the volume was evenly distributed among the drop population; rephrased, the total volume was divided by the total drops. By setting the average drop volume equal to the volume of a sphere, as in Equation 2.3, it was possible to determine the average drop diameter. A comparison was made between the average volume diameter calculation and the average drop diameter detected by the RIS. The results for the tests are as follows:

No. of Drops Counted Manually	No. of Drops Detected (RIS)	Mean Drop Diameter Mass Calculation (mm)	Mean Drop Diameter RIS (mm)	Standard Deviation RIS (+/-)
326	136	4.21	4.21	.074
345	154	4.19	4.29	.098
274	132	4.18	4.19	.140

Table 3.1: Comparison of values between the RIS and mass calculation of the average drop diameter all tested at 20 cm head.

Using Table 3.1, it is possible to see that the RIS maintains a very good estimate of drop diameter at the predefined setup distance, with only slight variations from that of the manual calculations. It is noticeable that the drop counts detected by the RIS are significantly lower than the manual count. This is likely a result of top-edge and bottom-edge touches as these drops are rejected from the analysis via the RIS software. It then became necessary to test the imager to ensure that the drop size does not increase due to the out-of-focus image also known as the "circle of confusion". In other words the data were further evaluated to determine if the less-focused drops would increase or decrease the average diameter due to droplets closer to or farther from the pre-set focal plane. To conduct this test, it was necessary to move the dripper at set increments toward and away from the suggested focal point. Data were collected from the following positions:

- 13.34 cm (5.25 in) Closer to the Camera (CTC)
- 26.67 cm (10.5 in) Closer to the Light (CTL)
- 26.67 cm (10.5 in) CTC
- 40.01 cm (15.75 in) CTL
- 40.01 cm (15.75 in) CTC

The 13.34 cm CTL was not shown in the list as the file was corrupt and time did not permit another sample to be taken; however, it is likely that this distance would have had little effect based on the other tests CTL, shown in Table 3.2. This setup allowed for the evaluation of the drop diameter as the drop was moved both closer and farther away from the in-focus focal volume. The following data were collected from the aforementioned setup:

	13.34 cm CTC	26.67 cm CTC	26.67 cm CTL	40.01 cm CTC	40.01 cm CTL
No. of Drops	59	23	93	22	23
Mean Drop Size (mm)	5.04	5.86	4.34	6.44	4.52
Bias (mm)	0.85	1.68	0.20	2.27	0.40

Table 3.2: Measurement recorded by the RIS at set distances closer to the camera (CTC) and closer to the light (CTL). The biasing is based on the average drop-size diameter (4.2 mm) as calculated manually.

The data in Table 3.2 indicates that the drops that are supposed to be rejected are actually being accepted by the software, which causes a rather large overestimation of drop size when compared to the manually calculated average diameter of 4.2 mm, especially when the drops fall between the in-focus distance and the camera. It is also notable that the drops are overestimated, but to a lesser extent, as the drops fall between the in-focus distance and the light. Some errors are greater than 2 mm larger than the drop should be, and this will have a large effect since the velocity, mass, kinetic energy, rainfall rate and all other parameters will be overestimated.

During this testing it was possible to test the RIS by using the large rainfall simulator which did not require the drop samples to be shifted toward and away from the camera as the simulator was large enough to cover the entire focal volume. The drop-redistribution screens were not in place during testing to maintain uniform drop size across the focal volume, which should prove to be true as the drops were formed from uniform tubing size. It can be seen in Figure 3.6 that most of the drops are located around the 4 to 5 mm range, but there are also a number of larger drops that are detected as well.

It is likely that the error is being introduced by drops that are out-of-focus. This can be seen in greater detail by analyzing the images of the raindrops in Figure 3.4, where it is possible to see that drops that are outside of the focal volume are not rejected. This is notable as the larger drops do not have the bright spot in the center of the image and tend to have rough edges, which is largely the result of the analysis software that is being used to evaluate and bin the data. The software could be altered in the future to accept fewer out-of-focus drops, which would then aid in the reduction of the oversized drops. Once this correction is made it is possible that the instrument could provide valuable data as there would be only minor issues with splash; however, more testing would be needed to determine the sample volume as the focal depth would need to be determined to find the accurate drop concentration.

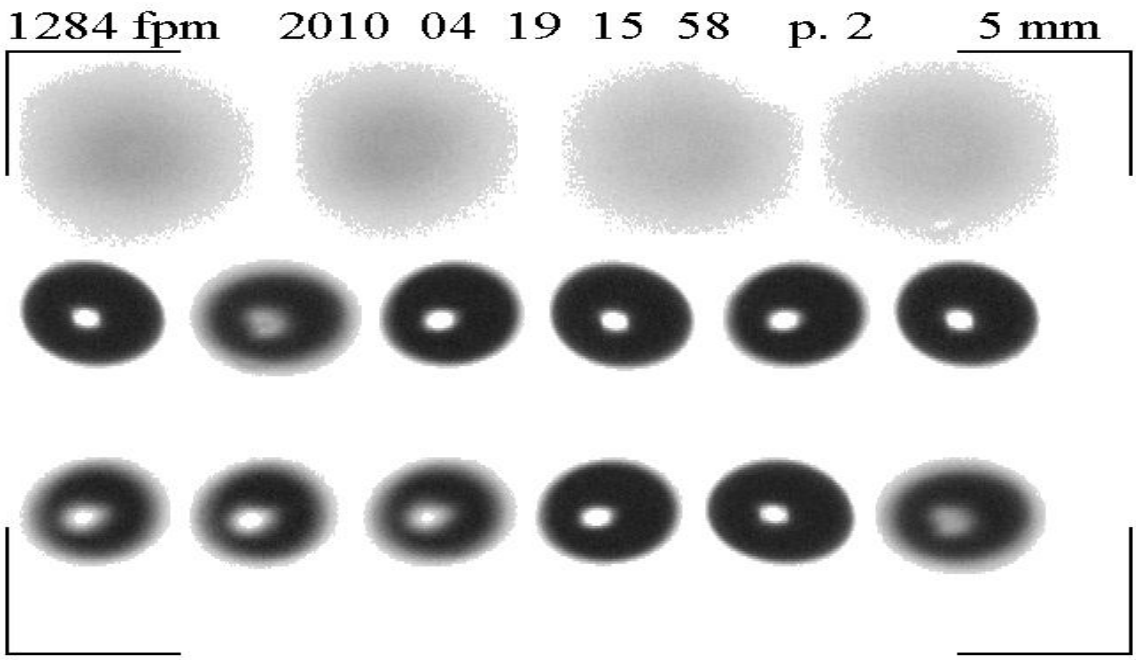

Figure 3.5: Droplet images sampled from in-focus and out-of-focus positions to evaluate RIS software for properly detecting actual droplet dimensions. The top row is out-of-focus while the middle and bottom rows are mostly in-focus.

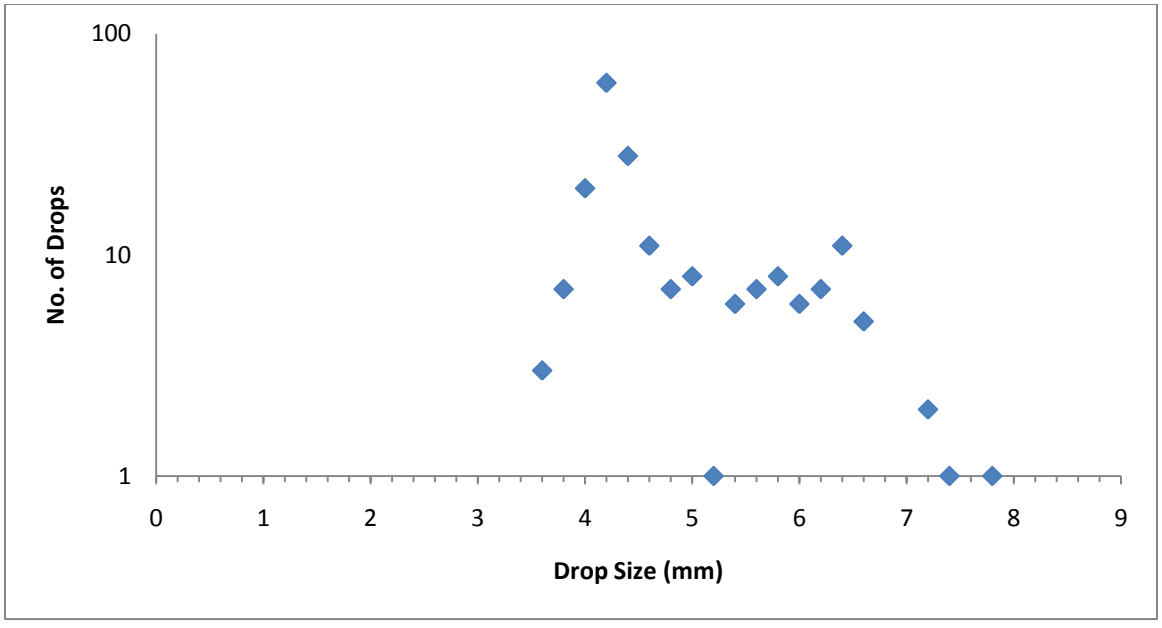

Figure 3.6: Drop size distribution produced by the RIS, where the drops were formed by drippers of uniform diameter. The larger drops, greater than 5 mm, indicate out-of-focus drops.

3.5 OTT Parsivel Disdrometer

The Parsivel disdrometer was used to collect data useful for comparison with data from the RIS. The disdrometer is a very convenient piece of equipment as it consists of an emitter and receiver in a single protective housing that is mounted upon a tripod. The disdrometer functions as an optical sensor where a laser diode with dimensions of 30 X 180 mm^2 runs between the protective housings as shown in Figure 3.7. The laser detects particles by analyzing the voltage output at the receiver. If the receiver maintains the maximum voltage output it is understood that there are no particles being detected within the beam; however, if the voltage output is reduced then the diameter is derived from the reduction and the maximum diameter is output into an excel file. The disdrometer is also capable of determining the drop velocity since it is able to calculate the amount of time it takes for a drop of a specific diameter to pass through the beam. The velocity data also serves as a quality control tool since some of the particles can fall at the edge of the sample area giving them an apparent smaller size. When this happens the raindrop will have an apparent higher velocity than drops in the specified class. When these drops are detected, the software will reject the raindrop as erroneous data. The velocity data is also used to discriminate precipitation as previously mentioned since hail, rain and snow flakes will tend to have differing velocities. In this study the velocity data will also be used to determine areas where splash occurred as the drops will tend to move at greatly reduced velocities.

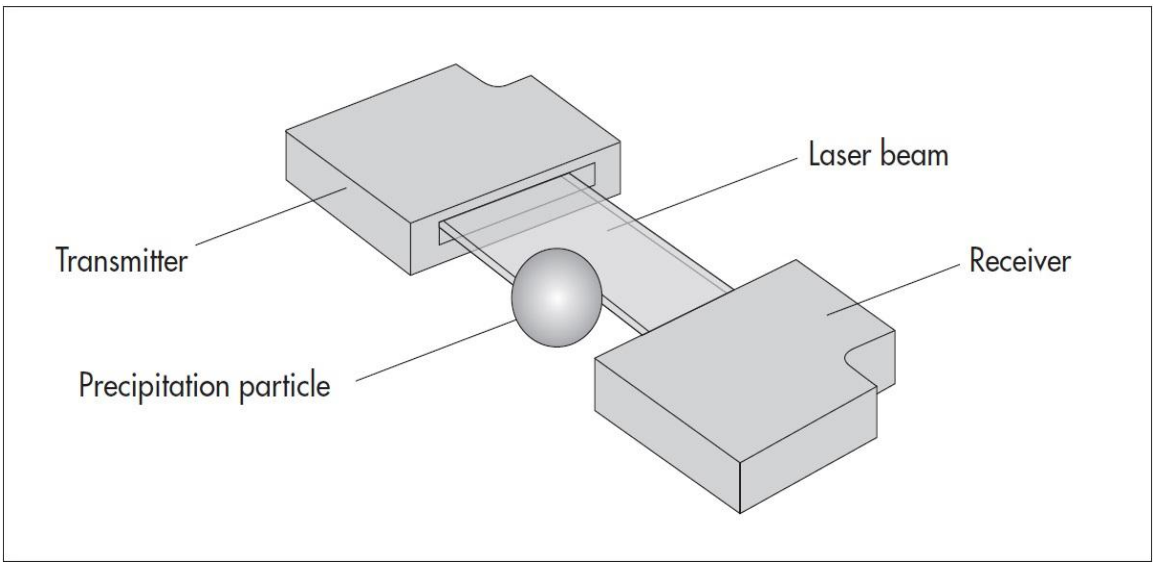

Figure 3.7: Schematic of a precipitation particle as it blocks a portion of the laser beam running between the protective housings. (From OTT, 2006)

During the precipitation detection process, the raindrop data are placed into a two-dimensional matrix where the drops are binned based upon the drop terminal velocity as well as the drop size within the bin. The instrument does not output the individual raindrop sizes; rather, it bins them and uses the drop size of the center of the bin in order to classify the sizes. This can be a rather large source of error especially when determining rainfall properties, since the bin width ranges from 0.125 mm in the lower bins to 1 mm in the upper bins. The width of the upper bins will generally affect accuracy by a greater amount as the drops in those bins can either fall at the upper or lower end of the bin, which changes the terminal velocity as well as the raindrop mass. The software provided by the manufacturer allows for a graphical depiction of the rainfall velocities as well as the drop-size distribution; however, more detail was required to determine the values for kinetic energy. In order to analyze this parameter it was necessary to write a software program to analyze raw data to produce the total number of drops for each class size. It should also be noted that the drops 7 mm and larger were excluded from the dataset as is

common practice since drops of that magnitude are not likely to exist naturally or they are rare at best (van Dijk et al. 2002). Once this program was written it was then possible to do both a graphical analysis as well as a numerical analysis on the data.

3.6 OTT Parsivel Disdrometer Calibration

As previously mentioned, it was necessary to calibrate the disdrometer in order to determine the types of errors that can occur during data collection. This permits correction of some data problems as well as providing a better understanding of the instrument. During this process it was necessary to utilize the large rainfall simulator without the drop-redistribution screen in place, which would again allow for a uniform DSD. The drippers that were installed in the large simulator were of the same diameter as the single dripper of the small rainfall simulator; therefore, a majority of the drops produced in the large simulator should be approximately 4.2 mm in diameter based on the mass-drop size calculation. The initial test was performed without any modification to the instrument other than the attached power supply box and tripod. This permitted identification of a rather large error which was due to splash. The splash accounted for a large increase in drops that maintained both a slower velocity as well a small diameter; however, small drops were not the only issue as some of the drops splashed on the lens which resulted in an increase in the measured diameter. The DSD from the initial test can be seen below in Figure 3.8.

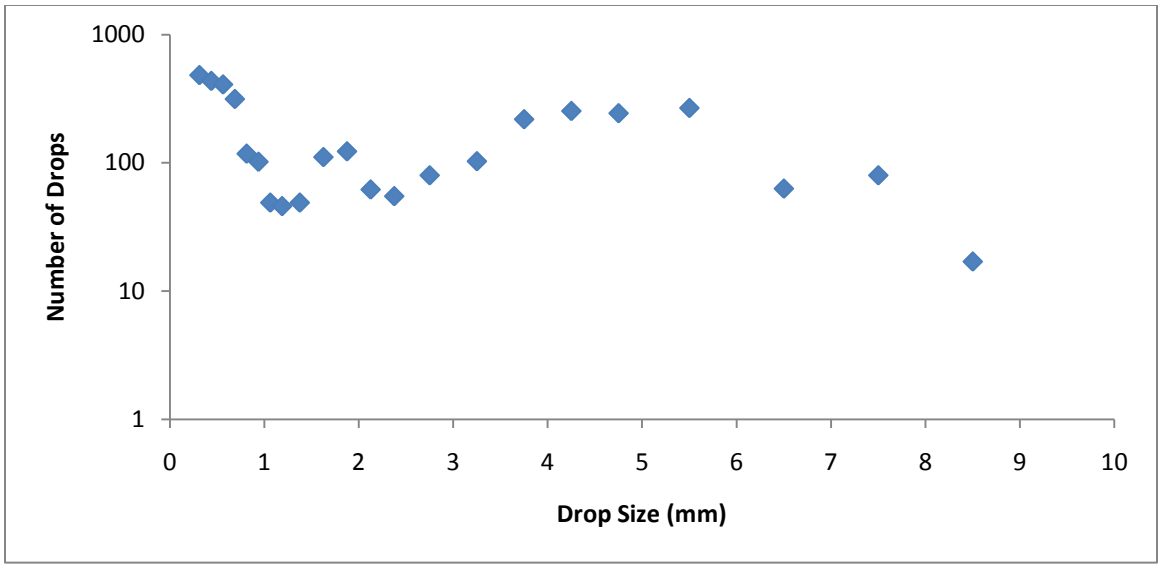

Figure 3.8: DSD produced by the simulator with no drop-redistribution screen or alterations to the disdrometer over a 10-minute interval.

Figure 3.8 shows that most of the drops were centered within the 4 to 6 mm range; however, there were several drops detected outside of this range which was unexpected. One item to note about the distribution is that there were a large number of drops detected below 1mm. This indicates that there is a large amount of splash that is occurring from the instrument. By observing the instrument at a very close distance it was possible to see that some of the small drops were being created as the drops were impacting the disdrometer housing. The disdrometer was designed, by the manufacturer, with spray protection on the disdrometer housing which consists of a stainless steel mesh, which appeared to work very well, although some drops were splashing back into the beam which overestimated the amount of smaller raindrops. To correct for this it was necessary to place a 12.7 mm (0.50 in) flange on each side of the housing closest to the beam. The flange location on the instrument can be seen in Figure 3.10. The idea is that if the drops land on the housing near the beam, the flange would deflect the small particles away.

After the flange was installed a second set of testing was performed to determine if the flanges reduced the splashing issue. The results are shown in Figure 3.9. One aspect about this distribution is that there appeared to be less of a problem with splash on the lens as there were fewer of the large drops greater than 6 mm; however, it doesn't appear as if the flange reduced the amount of small particles below 1 mm. It should also be noted that special care was taken in each test to ensure that splash from the floor was not able to impact the distribution. Loose plastic film and wire mesh were distributed around the disdrometer to dampen the impact of the drops on the concrete floor. When examining the instrumentation at a close distance it appeared as if this method eliminated or drastically reduced splash from the floor. Without the dampening effects of the aforementioned material the larger drops tended to have an impact normal to the concrete surface causing the splash to reach heights high enough to impact the sample area.

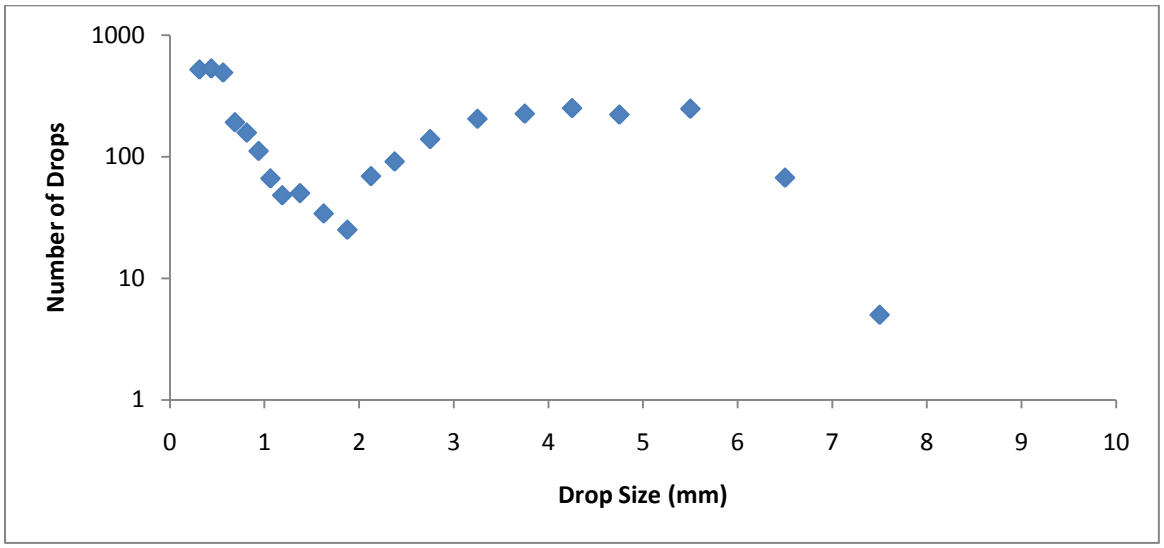

Figure 3.9: Depicts the drops size distribution with the added flange on the disdrometer.

After determining the flange reduced splash on the lens, alternate ways to reduce particles that were being detected erroneously were investigated. To do this, the instrument was observed from a close distance to determine where the splash originated. It was determined that the splash was originating from the power supply box placed below the disdrometer. This explained why the raindrops maintained a slower velocity since they were actually splashing upward into the laser beam and slowed by gravity. An attempt was made to correct this by placing a small piece of wire mesh on the upward-facing portion of the power supply box. A picture of the wire mesh can be seen below in Figure 3.10. A third test was then completed to determine if this screen reduced the overall error due to splash in both the lower and upper end of the spectrum and the result of this can be seen below in Figure 3.11.

Figure 3.10: Wire mesh placed on the upward-facing portion of the power supply box, indicated by the right-pointing arrow. The flange was located at the end of the left-pointing arrow.

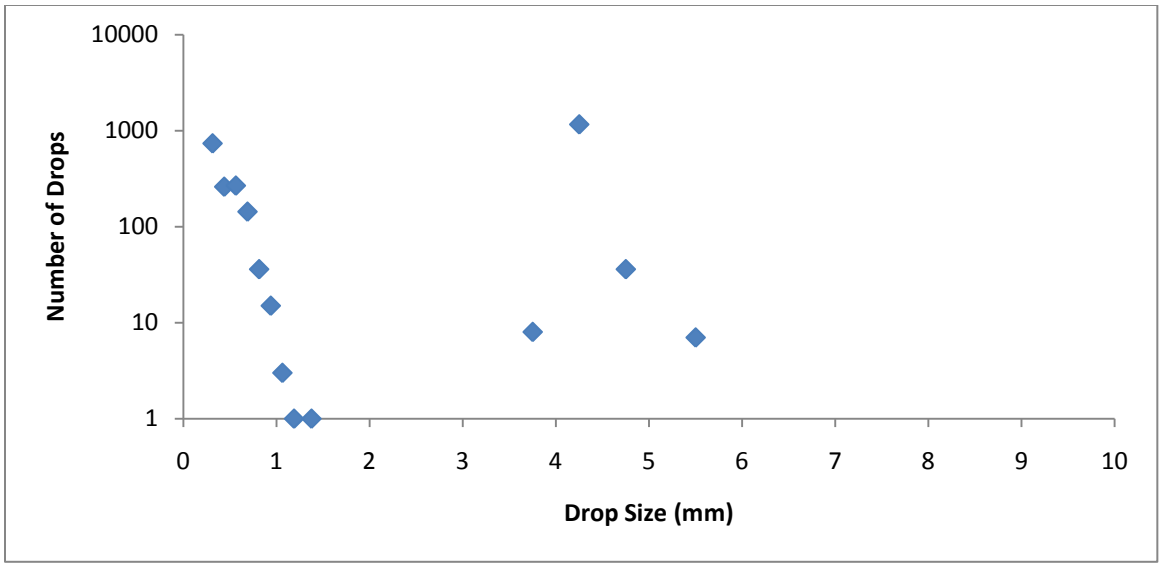

Figure 3.2: The drop-size distribution with both the flange and the wire mesh installed.

The distribution in Figure 3.11 indicates that there is a drastic reduction in splash with both alterations, but it appears as if the wire mesh placed on the power supply box has the largest impact. Another very important thing to note in Figure 3.11 is the fact that a majority of the drops are located in the 4 to 4.5 mm bins which is where it was expected that the largest drop concentration should occur as determined by the mass-drop diameter calculation. This is a result of reducing the amount of splash from the power-supply box, eliminating the splash on the lens. It is noticeable that the smaller drops are not reduced, but it would be impossible to reduce the entire splash as the sample area is collocated with the instrument. It must be noted that the results of the last test will not necessarily represent the results of natural events, which will be shown in later sections, as there is no wind simulation in the rain tower. The last comparison made was among the three tests that were completed using the factory instrument with no alterations, with the flange added and the wire mesh on the power box. Figure 3.12 shows a comparison between the DSDs observed using the three arrangements. It is possible to see that

with both the flange and wire mesh in place the drop concentration is reduced in all columns, except the lowest column, and increased near the 4.0 to 4.5 mm bins. Therefore, it appears the issues, caused by the splash, are significantly reduced in the simulated environment, so data collection from natural rainfall events and the rainfall simulator was then begun.

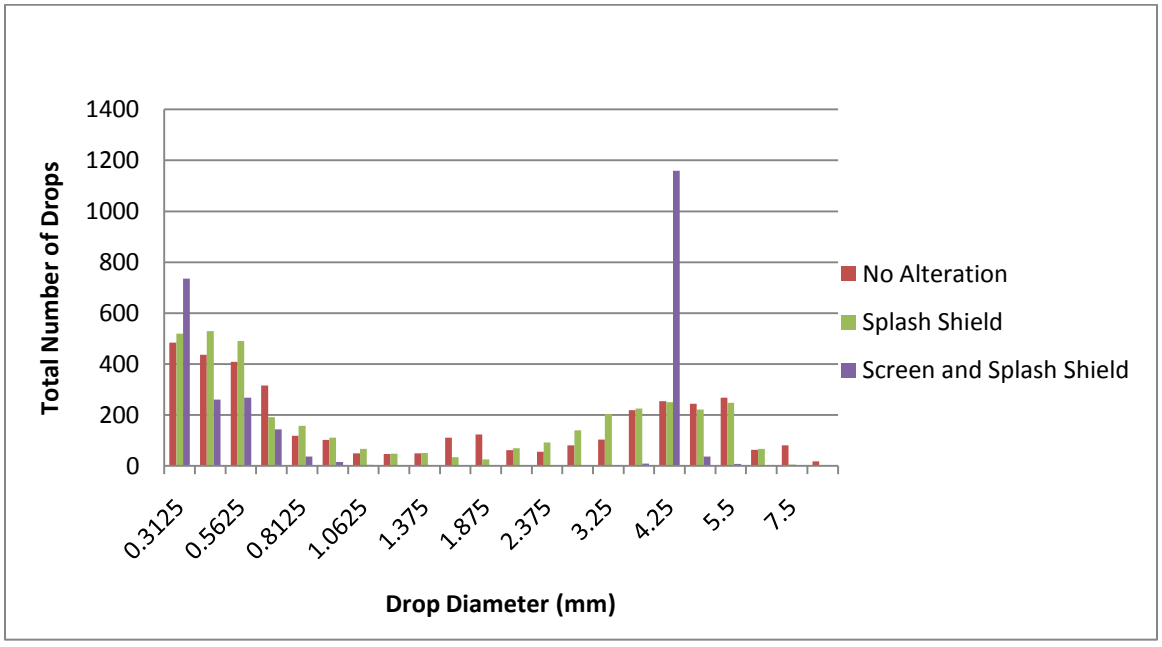

Figure 3.3: Comparison of each of the calibration tests completed.

3.6.1 Disdrometer Splash Correction

During data collection it was noticed that some of the data had a larger amount of drops that were generally small in diameter and had greatly reduced velocities. Much of this was due to splash originating from the instrument, but some of it was a result of strong wind splashing the drops onto the lens. Splash on the lens was observed in the rainfall tower before the wire mesh was placed on the power supply box and it was noticed that the water on the lens added to the overall drop sizes. In some case this error was very large. The drops formed were expected to be 4.2 mm, but with the splash on the lens some of the drops reached 11 mm. There is no way to correct this form of error as the water on the lens tends to increase the drop diameters across the spectrum; however, if the splash is due to drop contact with the instrument, but does not impact the lens, then it is possible to eliminate these slower-moving drops based on the Gunn and Kinzer (1949) equation. For example, if a drop is moving at a greatly reduced velocity compared to that which is parameterized by the Gunn and Kinzer (1949) equation, then the drop was determined to be splash and was removed. A graphical example can be seen below in Figures 3.13 and 3.14. The correction was applied across the entire spectrum, where drops that had velocities that were 25 percent or more lower than that of the Gunn and Kinzer (1949) values were counted as splash. This resulted in few drops being counted as splash in bins larger than the 1.875 mm diameter bin as many of the splashed drops tended to be very small, which can be seen by comparing Figure 3.13 and 3.14. Results of this correction can be seen quantitatively in the results section for each event.

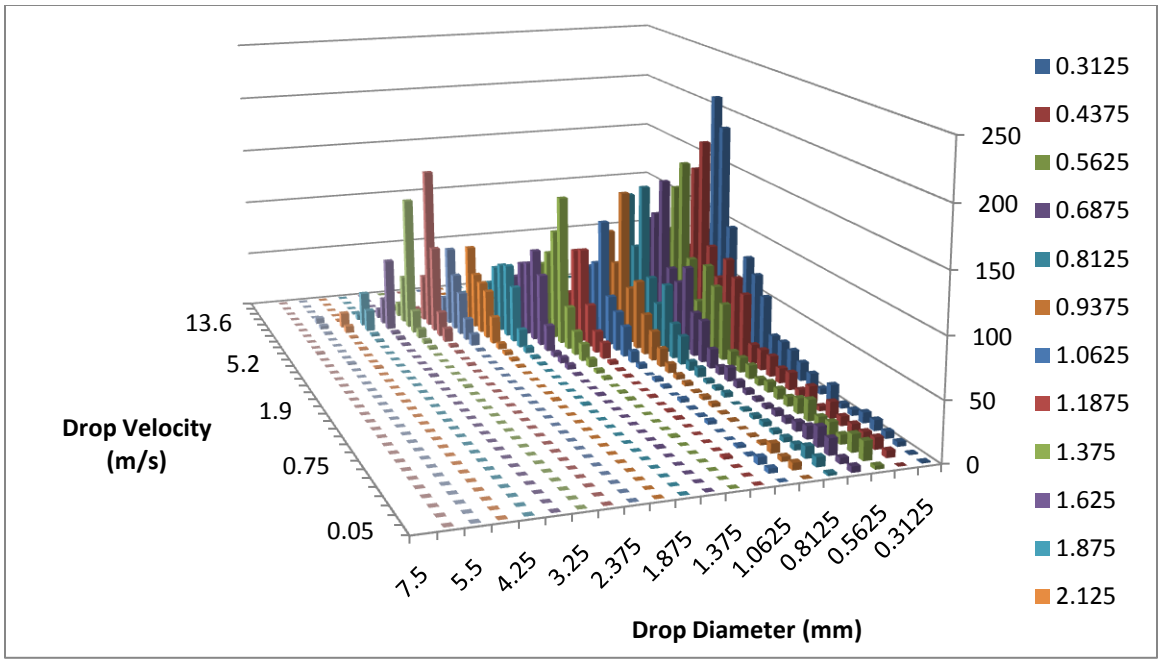

Figure 3.4: The distribution of drops in each size and velocity bin without splash correction.

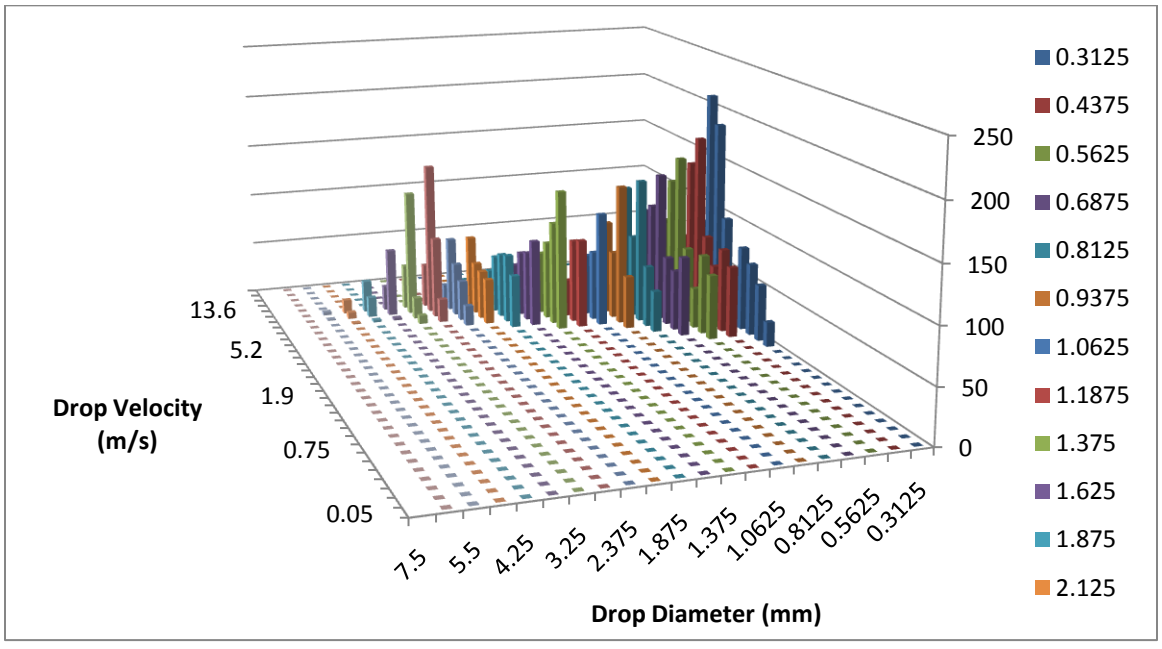

Figure 3.5: The distribution of drops in each size and velocity bin without splash correction.

3.7 RIS and OTT Disdrometer Comparison

After evaluating each instrument it was then necessary to collect data with both instruments sampling a similar area. To do this, the OTT Parsivel disdrometer was lowered to where the housing and laser were at a height of approximately 0.6 m (2 ft), and then the RIS sample volume was placed about 0.3 m (1 ft) directly above. The tests were then conducted at 10-minute intervals at eight different screen positions, which were at 26, 51, 80, 104, 126, 152, 178 and 206 cm which can be seen in Table 3.3. A comparison was then made to determine if the rainfall rates were being accurately detected by each instrument. Initially the RIS was underestimating the rainfall rate, but after some minor adjustments to the depth-of-focus the rainfall rates were much closer to that of the disdrometer and mass calculation. The depth-of-focus is very difficult to determine and the apparent depth-of-focus tends to vary with drop size; however, if a relation was made to the individual drop sizes then the equation could be placed in the algorithm to determine the apparent sample volume. As it is very difficult to determine the distances in which a drop is in-focus or out-of-focus, it was necessary to adjust the focal depth to match the rainfall rate. This is the only portion of the focal volume that may vary as the width and length remain at the previously mentioned dimensions of 32 x 24. To see how the distribution changed from larger drops to smaller drops see Figure 3.15 below.

Table 3.3: Comparison of rainfall rate determined by the mass measurement (RR_M), disdrometer (RR_D) and RIS (RR_{RIS}) along with RIS depth of focus.

Time (UTC)	Screen Height (cm)	RR_M (mm hr^{-1})	RR_D (mm hr^{-1})	RR_{RIS} (mm hr^{-1})	Depth of Focus (mm)
1518-1528	26	36.44	33.97	35.97	4.5
1538-1548	51	35.62	33.01	33.32	4.5
1602-1612	80	37.39	36.55	31.18	3.2
1618-1628	104	32.62	33.93	30.38	2
1636-1646	126	32.84	31.87	34.28	1.5
1702-1712	152	30.83	31.32	32.53	1.1
1720-1730	178	29.91	31.09	29.96	1
1736-1746	206	22.09	30.83	22.17	1

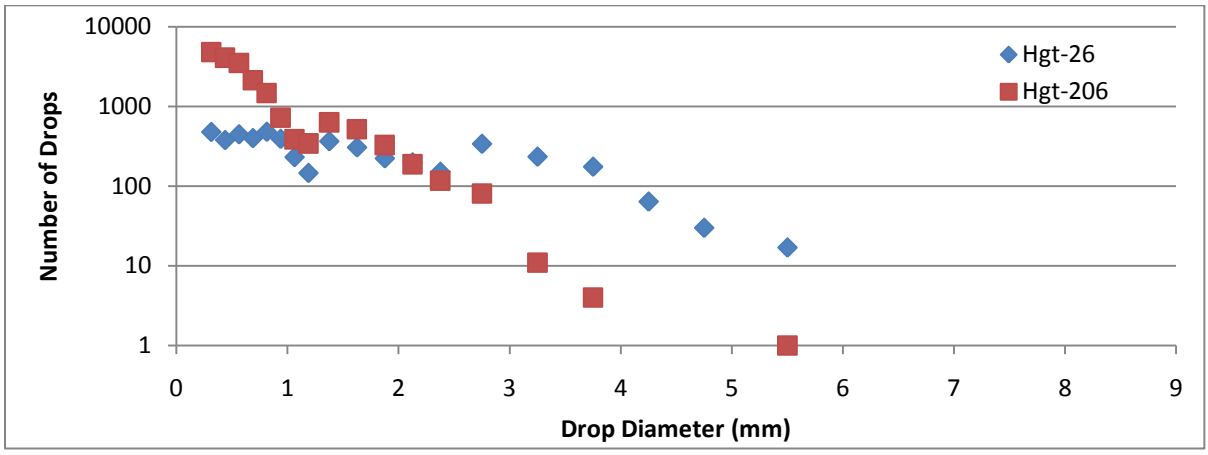

Figure 3.6: Comparison of DSD data collected using the RIS. The diamond shapes represent the distribution with the screen at 26 cm from the drippers and the square shapes represent the distribution with the screen at 206 cm from the drippers.

Chapter 4
Methodology

In order to collect data the previously mentioned instrumentation was deployed at South Farm in Columbia, MO as well as in the rain tower. Initially, data collection occurred with an observer in the climate center, but some of the events occurred at very late hours, so it was necessary to position the instrumentation so that data collection could occur without an observer present. It was still necessary to maintain the equipment directly before each event since the instrumentation needed to be cleaned due to spider webs as well as other types of debris that could be a source of error. The data collected were the DSD from each instrument, total rainfall and wind data.

4.1 Natural Rainfall Events

For each event it was necessary to deploy and maintain the equipment to ensure that errors were minimized and to ensure that the entire event was captured. The data were divided into 10-minute intervals for comparison with data collected in the rainfall simulator, where each event was classified as being a peak in rainfall intensity. Some of the events maintained more than one peak allowing for more than one event to be classified on the same day. The natural rainfall data were collected from May 10, 2010 to August 14, 2010 at the ACES South Farm location; however, it was also necessary to collect some data by deploying the equipment at other locations as not all desired storms occurred over the ACES location. During this time period it was possible to capture a total of 48 rainfall events ranging from very light stratiform rainfall events to very heavy convective rainfall events. A majority of the convective rainfall events captured were due to linear development

as opposed to supercell or pulse thunderstorm development. This was very helpful in reducing error due to the presence of hail, since hail is generally limited in linear storm structures; however, linear storm structures tend to maintain higher wind gusts which can cause error due to splash as well as error due to a change in the sample volumes. In order to verify that hail was not present it was also necessary to evaluate storm reports in which only one event maintained a hail report; however, these data were not included as the data were unfortunately lost due to a power outage.

In order to evaluate these events in a structured manner, it was necessary to divide the events into three separate classes. The first class was defined to be rainfall events with total precipitation less than 2.54 mm (0.10 inches) over a 10-minute interval. The second class was defined as rainfall events with total precipitation greater than or equal to 2.54 mm (0.10 inches) and less than 7.62 mm (0.30 inches) over a 10-minute interval. The third and final class was defined as rainfall events with total precipitation greater than or equal to 5.08 mm (0.20 inches) over a 10-minute interval. The main focus of this study will remain on the second and third classes as it is expected that more kinetic energy is maintained in the heavier events resulting in more erosion.

4.2 Simulated Rainfall Events

It was necessary to evaluate the DSD beneath the rain fall simulator as it is much easier to analyze the impact of drop size on soil erosion in a controlled environment. Before the simulated data can be used to represent natural rainfall events, a comparison must be made to ensure that the simulated data closely resembles the distribution from that of natural events. As previously mentioned, it was necessary to utilize a drop-redistribution screen in order to maintain drops sizes ranging from

very small diameters to large diameters dependent upon the height of the screen from the base of the drippers.

The rainfall simulator was adjusted to maintain a steady rainfall rate at a head of approximately 10 cm by adjusting the air-inlet tube, which allowed for a rainfall rate similar to the second class rainfall events. This also allowed the rainfall rate to remain low enough that several 10-minute tests could be performed without refilling the tank. According to Regmi and Thompson (2000), the rainfall rate did not change based upon the height of the drop-redistribution screen; rather, the DSD was the only notable change. With those results in mind it was necessary to examine the drop-size distribution at several screen heights, which were tested and evaluated at the following heights: 26.7, 51.7, 80.0, 104.1, 126.4, 151.8, 177.8 and 205.7 cm below the base of the drippers. A larger distance between the drop-redistribution screen and the drippers results in smaller droplets, while a smaller distance will likely allow for larger drops to form.

The imaging equipment was set up with the disdrometer sample volume directly below the RIS sample volume near the center of the rainfall simulator. There were no rain gauges deployed inside the rain tower so it was necessary to evaluate the rainfall rate by placing buckets around the equipment to capture the volume of water that fell within a 10-minute interval. The volume was then determined by using the mass measurement procedures as mentioned in the instrument section. The rainfall rates measured with the buckets were compared with the rainfall rates of both the disdrometer and the RIS to determine the accuracy of each instrument. The disdrometer and RIS were both compared against each other to determine if one performed better than the other.

4.3 Data Analysis

It was necessary to complete a quantitative analysis for each event to ensure that each instrument was measuring rainfall rates that were similar to that of the rain gauges. After instrument accuracy was verified it was necessary to analyze the amount of kinetic energy calculated for each instrument by summing the drop kinetic energy across the DSD. This evaluation was completed by using the measured velocity data from the disdrometer as well as by using the theoretical terminal velocity data from Gunn and Kinzer (1949). A comparison was then made to determine if the theoretical velocity resulted in an over or underestimation of kinetic energy flux. These values were also compared with kinetic energy flux determined by using the rainfall rate which is the method used in the RUSLE equation. Wind also contributes a significant amount to the total kinetic energy; however, this study will remain focused on the vertical aspect. It is worth noting that it is very difficult, if not impossible, to determine the exact impact of the horizontal and vertical components of kinetic energy upon soil as there are many variations in slope as well as vegetative covering that must be dealt with. This study will deal solely with the impact of the drop on a bare and flat surface where the impact is normal to the surface.

While it is informative to collect data using the aforementioned instrumentation, it is not feasible to deploy multiple instruments in order to quantify the kinetic energy with each storm. Instead, the DSD can be parameterized using the methods shown by Testud et al. (2001). In this study, however, the focus will be on the types of distributions associated with convective events and kinetic energy flux associated with the different events as opposed to the parameterization of the events. If the

storms are found to have differing DSDs then it could be possible to estimate kinetic energy flux via radar and the parameterization of the DSD as previously mentioned.

Chapter 5
5.1 Natural Events

Data were collected during the warm season across central Missouri ranging from May 2010 to August 2010. A total of 48 events were analyzed ranging from light to very heavy precipitation events. In order to maintain a more structured analysis the events were broken into three categories with Category I containing very light rainfall and Category III containing the very heavy rainfall events. As previously mentioned, most of the rainfall data collection was taken at the ACES South Farm location in Columbia, MO; however, mobile data collection occurred once during this period. This rainfall event occurred north of Interstate 70 in the north-central part of the city of Columbia. The rainfall that occurred in the mobile event was significant enough to be placed in the Category III rainfall classification. Each event was classified by analyzing a 10-minute interval encompassing the most intense portion of the event. If an event had more than one peak rainfall intensity, the event was broken into more than one event. In many cases, peak intensities occurred at the leading edge of the event as well as directly behind the event allowing for the examination of different areas of the storms.

5.2 Category I Rainfall Events

The events included in the Category I rainfall classification maintained similar rainfall characteristics with the main criteria being a lower rainfall rate. Any event that produced less than 2.54 mm (0.10 in) during a 10-minute interval was included in this classification and is shown in Table 5.1. It is expected that these rainfall events have a minimal impact upon the surface as the events in this category have the lowest amount of total kinetic energy flux due to a reduced number of raindrops overall and a reduced proportion of larger raindrops which will be shown in later

sections. This is not meant to suggest that these events have no impact upon the surface, as the events aide in increasing the amount of soil moisture, which tends to allow the soil to detach more readily. This category, which represents just under half of the total events, maintains 20 events that are listed in Table 5.1.

Table 5.1: Dates and times of each of the Category I rainfall events as well as rainfall rate and total rainfall.

Date	Time (UTC)	Rainfall Total (mm)	Rain Rate (mm/hr)
12-May	0746-0756	0.76	4.57
20-May	0812-0822	0.76	4.57
21-May	0244-0254	0.76	4.57
11-Jul	1948-1958	0.76	4.57
10-May	1948-1958	1.02	6.10
25-Jul	0040-0050	1.02	6.10
2-Jun	0830-0840	1.27	7.62
12-May	0644-0654	1.52	9.14
16-May	1830-1840	1.52	9.14
2-Jun	0716-0726	1.52	9.14
11-Jun	1724-1734	1.52	9.14
8-Jun	1624-1634	1.78	10.67
13-Jun	2144-2154	1.78	10.67
21-Jul	0132-0142	1.78	10.67
26-Jul	2038-2048	2.03	12.19
2-Jun	0644-0654	2.29	13.72
2-Jun	0736-0746	2.29	13.72
12-Jun	1948-1958	2.29	13.72
15-Jun	1750-1800	2.29	13.72
14-Aug	0310-0320	2.29	13.72

5.3 Category II Rainfall Events

The events included in the Category II classification maintained very similar properties and rainfall rates ranging from moderate to heavy. To be classified as Category II it was necessary for the event to maintain attributes that included rainfall totals greater than or equal to 2.54 mm (0.10 in) and also less than 7.62 mm (0.30 in) within a 10-minute interval. These events tend to be much heavier than the previous categorized events with rainfall rates exceeding 25.4 mm hr $^{-1}$ (1.00 in

hr $^{-1}$) and approaching 50.8 mm hr^{-1} (2.00 in hr^{-1}). Rain falling at those rates will tend to readily run off, which aids in the loss of soil that has been detached by raindrop impacts. While soil erosion is not the main focus of this study it is necessary to realize that it is with these types of events that issues with soil erosion begins to occur. A majority of the Category II events were produced from linear-convective systems as opposed to pulse or supercell thunderstorms. Each of the 21 Category II events can be seen below in Table 5.2.

Table 4.2: Dates and times of each of the Category II rainfall events as well as rainfall rate and total rainfall.

Date	Time (UTC)	Rainfall Total (mm)	Rain Rate (mm/hr)
27-Jun	2234-2244	2.54	15.24
26-Jul	2023-2032	2.79	16.76
20-Aug	1730-1740	2.79	16.76
14-Aug	0424-0434	2.79	16.76
2-Jun	0700-0710	3.05	18.29
12-Jun	2008-2018	3.05	18.29
30-Jul	2220-2230	3.05	18.29
11-May	0330-0340	3.30	19.81
20-Jul	1226-1236	3.30	19.81
26-Jul	2012-2022	3.30	19.81
8-Jun	1540-1550	3.56	21.34
30-Jul	1714-1724	3.56	21.34
12-Aug	0406-0416	3.56	21.34
12-May	0632-0642	3.81	22.86
30-Jul	2210-2220	3.81	22.86
13-May	0934-0944	4.06	24.38
8-Jun	1634-1644	4.83	28.96
30-Jul	2200-2210	5.33	32.00
27-Jun	2224-2234	5.59	33.53
21-Jul	0152-0202	6.60	39.62
24-Jun	0112-0122	6.86	41.15

5.4 Category III Rainfall Events

The events classified as Category III maintained very similar attributes with rainfall rates shown to be very heavy. In order to be placed in this category it was necessary for the events to maintain attributes that included rainfall totals greater than or equal to 7.62 mm (0.30 in) within a 10-minute interval. This category maintains only the heaviest rainfall events where rainfall rates approached and exceeded 50.8 mm hr^{-1} (2.00 in hr^{-1}). These rainfall events were of particular interest as a larger amount of kinetic energy is produced with more mass impacting the soil surface. Not only are the rainfall rates heavy enough that runoff will be significant, but also the DSD suggests that greater numbers of larger drops also impact the soil allowing for more detachment. A majority of the Category III events are due to linear-convective systems as well and are shown in Table 5.3.

Table 5.3: Dates and times of each of the Category III rainfall events as well as rainfall rate and total rainfall.

Date	Time (UTC)	Rainfall Total (mm)	Rain Rate (mm/hr)
12-Jun	1932-1942	7.62	45.72
13-Jul	0320-0330	7.62	45.72
12-Aug	0356-0406	7.62	45.72
18-Jul	1258-1308	7.87	47.24
20-Jul	1214-1224	9.40	56.39
20-Aug	1750-1800	10.92	65.53
18-Jul	1220-1230	11.18	67.06
25-Jul	0010-0020	12.19	73.15

5.5 Mobile Data

As previously mentioned at certain points during data collection it was necessary to relocate in order to sample the most intense portion of the storm. Specifically, the event that was sampled by redeploying the instrumentation immediately north of Interstate 70 in the northern portion of Columbia, MO occurred on August 20, 2010 from 2220 UTC to 2344 UTC. During this linear event the heaviest portion of the storm was expected to remain to the north of Interstate 70, but an outflow boundary allowed for development in areas farther south as shown in Figure 5.1. In this figure, the location of the deployed instrumentation is shown by the point below the blue arrow, while the rain gauge location is shown by the point at the end of the yellow arrow.

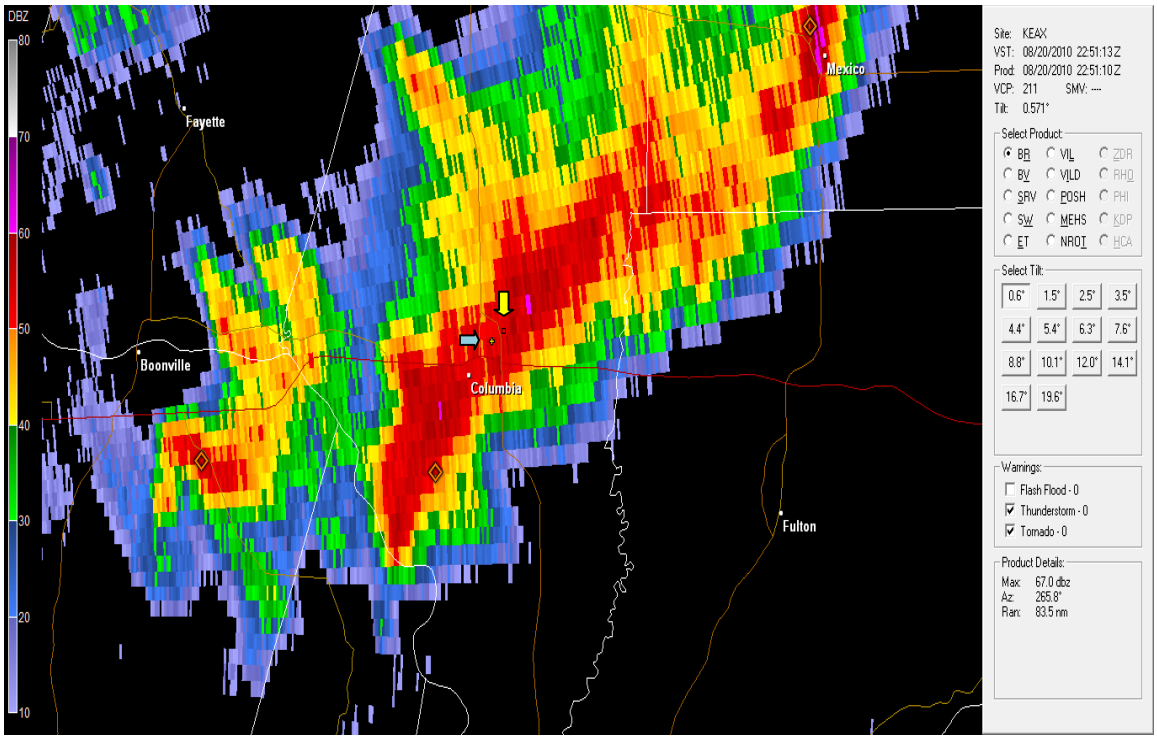

Figure 5.1: Radar base reflectivity from the National Weather Service in Pleasant Hill, MO shown at 2251 Z. The upper arrow represents the location of the disdrometer deployment and the lower arrow indicates the location of the rain gauge.

In this location up to 10.92 mm (0.43 in) of rain fell within a 10-minute time period, which places this event in the Category III classification. Even though the precipitation developed farther to the south of Interstate 70, it is worth noting that the mobile location chosen actually received more precipitation for a longer duration as another storm developed directly behind the first line as shown in Figure 5.2, which was a Category II event. This allowed for a more robust dataset than would have occurred otherwise as the second storm missed the ACES South Farm location. As there was little time to deploy a rain gauge ahead of an event of this nature it was necessary to collect data from a stationary rain gauge that was in close proximity to the deployment location, which can be seen in Figure 5.3.

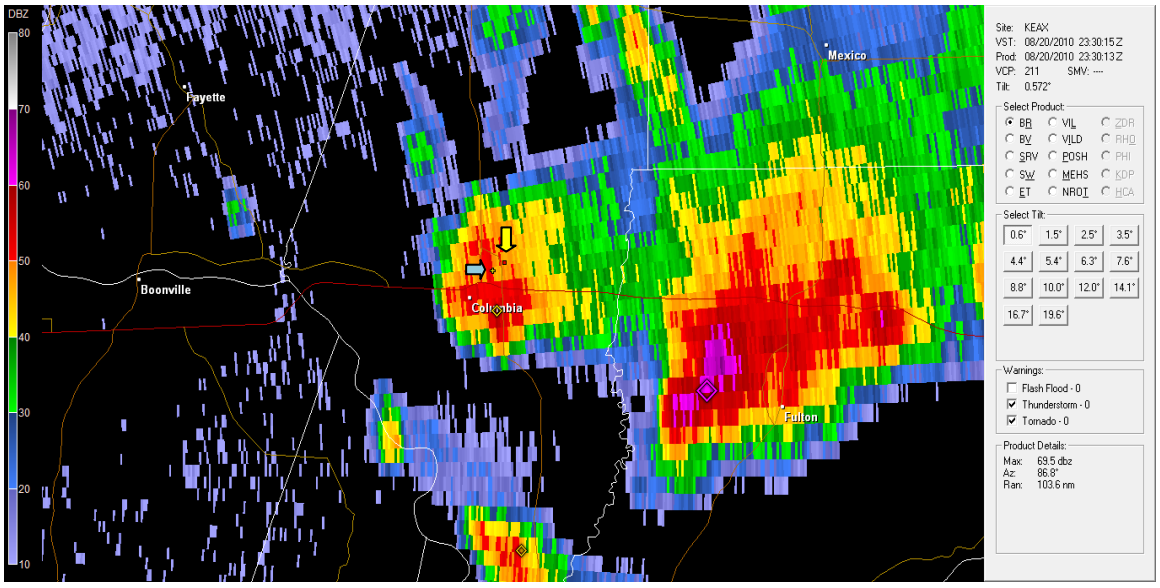

Figure 5.2: Radar base reflectivity from the National Weather Service in Pleasant Hill, MO shown at 2330 Z. The upper arrow represents the location of the disdrometer deployment and the lower arrow indicates the location of the rain gauge.

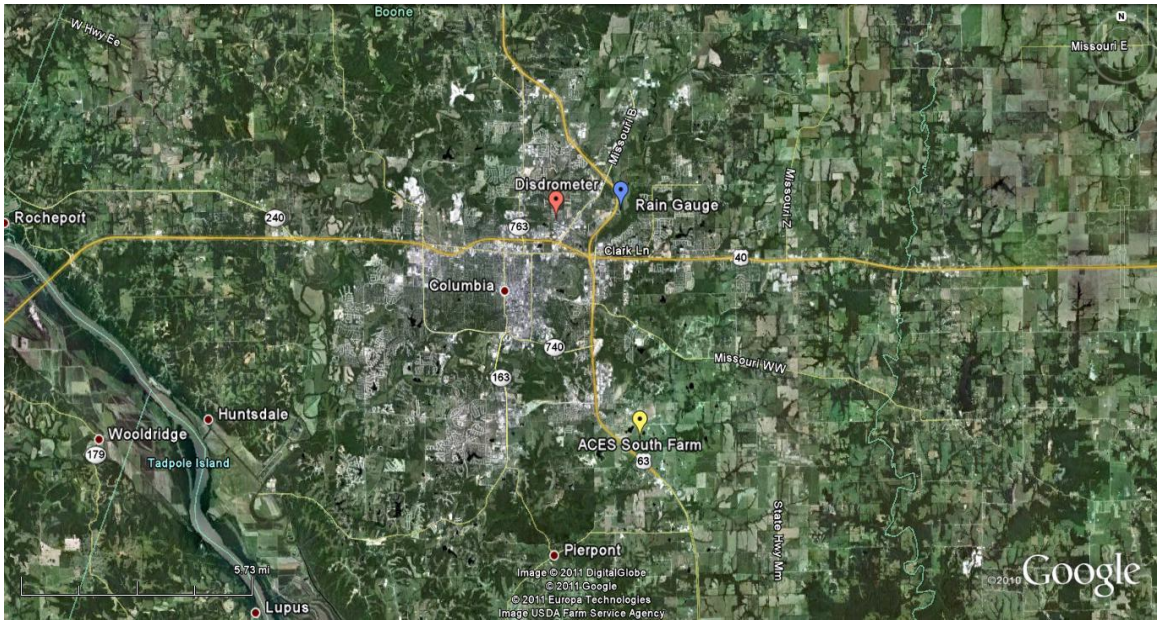

Figure 5.3: Location of the rain gauge (upper right), OTT Parsivel disdrometer (upper left) and the ACES South Farm location (lower center) relative to each other.

Chapter 6
Results and Discussion

Multiple rainfall events were evaluated to determine the DSD and the associated kinetic energy flux. It was necessary to evaluate several rainfall events ranging from light stratiform events to very heavy convective events. In section 6.1 an analysis is performed to show a comparison of the rainfall rate calculated by the OTT Parsivel disdrometer and the tipping bucket rain gauge. Also included in this evaluation is the total kinetic energy flux associated with each event using the velocity calculated by the disdrometer as well as the terminal velocity estimated using the equation proposed by Gunn and Kinzer (1949). After the initial analysis was complete it was then necessary to determine what caused any differences in kinetic energy within datasets of similar rainfall rates. Generally one would expect that if the rainfall rates are similar then certain characteristics of the rainfall must be similar such as total drop count and the DSD. To determine if that logic is correct, an evaluation of the DSD was completed, graphically, to see if one event had more large drops than the other or if the results were due solely to a greater amount of total raindrops.

Section 6.2 is focused on the DSDs produced by the rainfall simulator that were sampled by positioning the drop-redistribution screen at different heights away from the drippers. As mentioned earlier it is expected that the screen heights closer to the drippers will allow larger drops to form, while heights farther from the drippers will allow the drops to break up into smaller drops. Also, the drop velocity was tested as the drop fell from the screen at the aforementioned heights to determine if the screen had a large impact upon the velocity of the drops. Section 6.3 will focus on a comparison of both the natural and simulated DSDs to determine if the simulated data can be used to accurately represent natural rainfall events. In this

study only one range of rainfall rates were used for comparison due to time constraints, which was approximately 30-36 mm hr $^{-1}$.

6.1 Natural Event Distributions

6.1.1 Events Maintaining Large Errors

This section is focused upon the events that maintained large differences in rainfall rates calculated by the disdrometer compared to that of the rain gauge. As discussed in the instrumentation section high winds occasionally caused a problem with splash on the instrument lens which in turn caused the raindrop sizes to be overestimated in each of the bins, and in some cases raindrop sizes of 11 mm or greater were detected. Events that showed compelling evidence that splash impacted the lens, such as the unusually large raindrops, were not weighted as heavily in the overall kinetic energy flux analysis. The events shown in the previous sections did not show evidence of splash on the lens; however, they did show evidence that splash existed but it was possible to correct for this using the methods discussed in the instrument section. Many of the erroneous events maintained rainfall rates that ranged from roughly 1.3 to 1.5 times the rainfall rate of the rain gauge, which can be seen below in Table 6.1.

Table 6.1: Events that presented evidence of splash on disdrometer lens.

Date	Time (UTC)	R_T (mm)	RR_G (mm hr^{-1})	RR_{NS} (mm hr^{-1})	KE_{NS} (J m^{-2})	DC_{NS}
12-May	0746-0756	0.76	4.57	7.15	0.156	3132
12-May	0644-0654	1.52	9.14	12.12	0.231	10431
21-Jul	0132-0142	1.78	10.67	14.46	0.373	8630
27-Jun	2234-2244	2.54	15.24	22.01	0.534	5299
11-May	0330-0340	3.30	19.81	26.70	0.712	7469
20-Jul	1226-1236	3.30	19.81	29.66	0.771	14709
21-Jul	0152-0202	6.60	39.62	54.56	1.417	16725
13-Jul	0320-0330	7.62	45.72	64.46	1.720	19819
18-Jul	1220-1230	11.18	67.06	91.93	2.159	39283

6.1.2 Category I Events

There remains some question as to whether or not the increase in kinetic energy flux at the surface is due to a DSD containing a greater proportion of larger drops or a DSD that contains a greater number of total drops. To evaluate the potential causes for the increase it was necessary to create a table indicating the total amount of kinetic energy flux at the surface and the total number of drops detected. This allowed for the extraction of events that maintained similar rainfall rates with differing drop counts and kinetic energy fluxes. To keep the study complete it was necessary to evaluate one or more events from each of the categories mentioned in previous sections. Each dataset contains a column that is labeled RR_G, which is representative of a range of data rather than a single value. The rain rate values in this column can range plus or minus 1.52 mm hr^{-1}, depending on whether the tipping bucket was about to tip at the end of the sample or if it was nearly full and ready to tip at the beginning of the sample. The first dataset consists of 12 Category I rainfall events and can be seen in Table 6.2.

Table 6.2: Category I events with rainfall total (R_T), rain rate as recorded by the rain gauge (RR_G), rain rate as recorded by the disdrometer (RR_{NS}), kinetic energy flux (KE_{NS}), kinetic energy flux based on rainfall intensity (KE_R) and total drop count (DC_{NS}).

Date	Time (UTC)	R_T (mm)	RR_G (mm hr^{-1})	RR_{NS} (mm hr^{-1})	KE_{NS} (J m^{-2})	KE_R (J m^{-2})	DC_{NS}
21-May	0244-0254	0.76	4.57	3.84	0.052	0.15	3557
11-Jul	1948-1958	0.76	4.57	4.10	0.063	0.15	2232
10-May	1948-1958	1.02	6.10	7.13	0.203	0.16	4686
25-Jul	0040-0050	1.02	6.10	5.81	0.091	0.16	4578
2-Jun	0830-0840	1.27	7.62	6.05	0.106	0.18	2641
11-Jun	1724-1734	1.52	9.14	11.26	0.165	0.20	5951
16-May	1830-1840	1.52	9.14	8.44	0.120	0.20	8848
2-Jun	0716-0726	1.52	9.14	9.35	0.155	0.20	5799
26-Jul	2038-2048	2.03	12.19	15.17	0.335	0.24	4248
2-Jun	0736-0746	2.29	13.72	12.57	0.246	0.27	3823
12-Jun	1948-1958	2.29	13.72	12.89	0.180	0.27	7940
15-Jun	1750-1800	2.29	13.72	16.05	0.264	0.27	9530

Table 6.2 indicates that the kinetic energy flux generally increases as the total rainfall (R_T) and rainfall rate (RR_G) increases; however, it is not as smooth of a transition as the kinetic energy flux shown using the rainfall intensity. The difference in the two fluxes is caused by KE_R being a function of the rainfall intensity as opposed to being a function of the DSD only. There are some anomalies that occurred within the dataset, the first of which occurred on May 10, 2010 from 1948-1958 UTC. This event maintained a much greater kinetic energy flux compared to similar events around it. Most notably, the event on July 25, 2010 maintained both a similar rainfall rate and total drop count, but the kinetic energy flux was less than half of the anomaly. While the anomaly shows that the disdrometer is overestimating the rainfall rate, it is unlikely that this would cause the kinetic energy flux to double since the error equates to a rainfall rate difference of approximately 1 mm hr^{-1} which could be due to the tipping bucket being close to tipping before the event ended. It was theorized that the difference was due to larger drops in the event.

As each of these events have very similar total drop counts, the increase in kinetic energy is not due to an increase in total drops; therefore, it became necessary to analyze the DSDs of each event to determine if the increase was due to a greater amount of large drops. The comparison of both distributions can be seen below in Figure 6.1. It is evident, in this figure, that the May 10, 2010 event maintains a greater amount of large drops with a maximum drop size of 4.75 mm, while the July 25, 2010 event maintains a greater amount of smaller drops with a maximum drop size of 3.25 mm. These data suggests that the increase in kinetic energy flux is due to the larger drop sizes produced in the anomaly as these larger drops will not only have more mass but also a higher velocity. It is also worth noting that a majority of the rainfall events in the Category I section contain a similar distribution as the July 25, 2010 event, while many of the events in Category II and III are similar to the May 10, 2010 event.

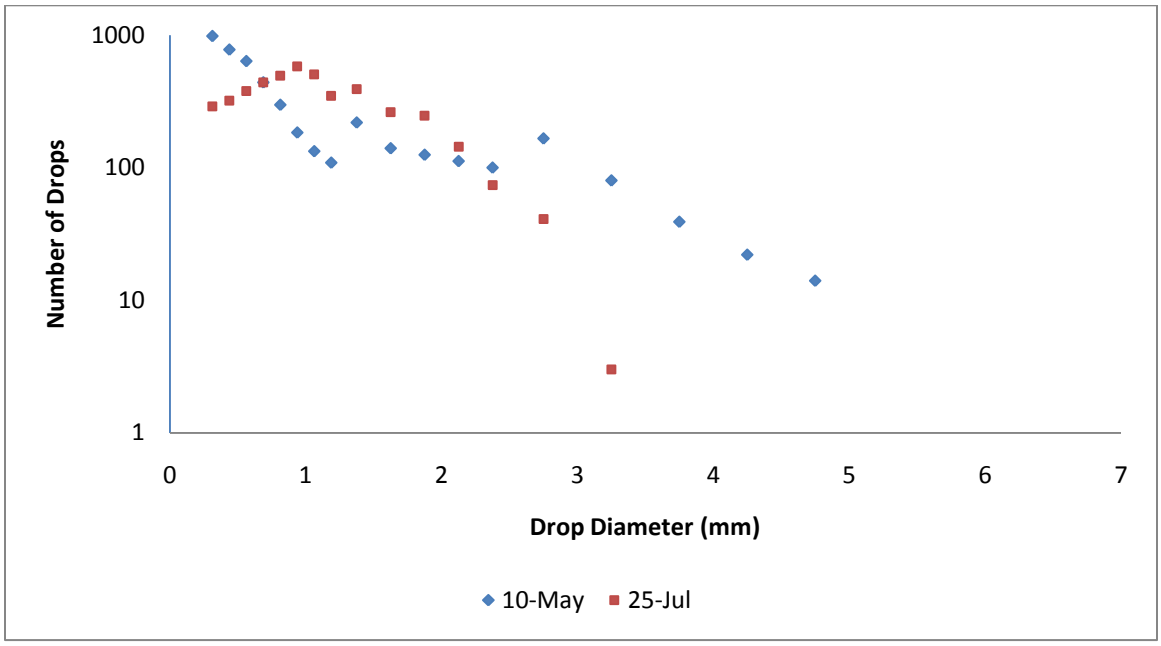

Figure 6.1: Log-scale comparison of the drop-size distributions for the May 10, 2010 and July 25, 2010 events.

After analyzing the DSD a curious difference was noticed in the two distributions, which might be explained by examining the events with radar data to determine if storm structure plays a significant role in creating such distributions. One would expect that deeper convection might aide in the production of these larger drops as collision-coalescence becomes the main process for drop growth allowing the drops to grow larger. Radar data were requested from the National Climatic Data Center (NCDC) in order to further evaluate the distributions and the images are shown below in Figures 6.2 and 6.3.

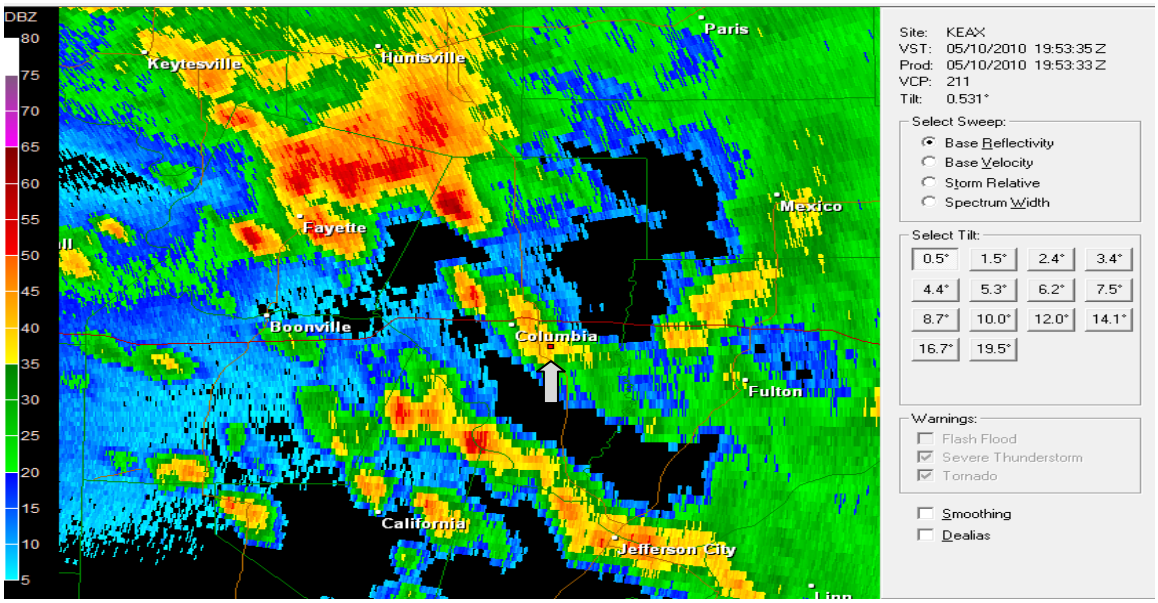

Figure 6.2: Radar reflectivity 0.5^0 tilt from the Pleasant Hill, MO Weather Forecast Office for the May 10, 2010 event. The red dot at the end of the gray arrow indicates the ACES South Farm location.

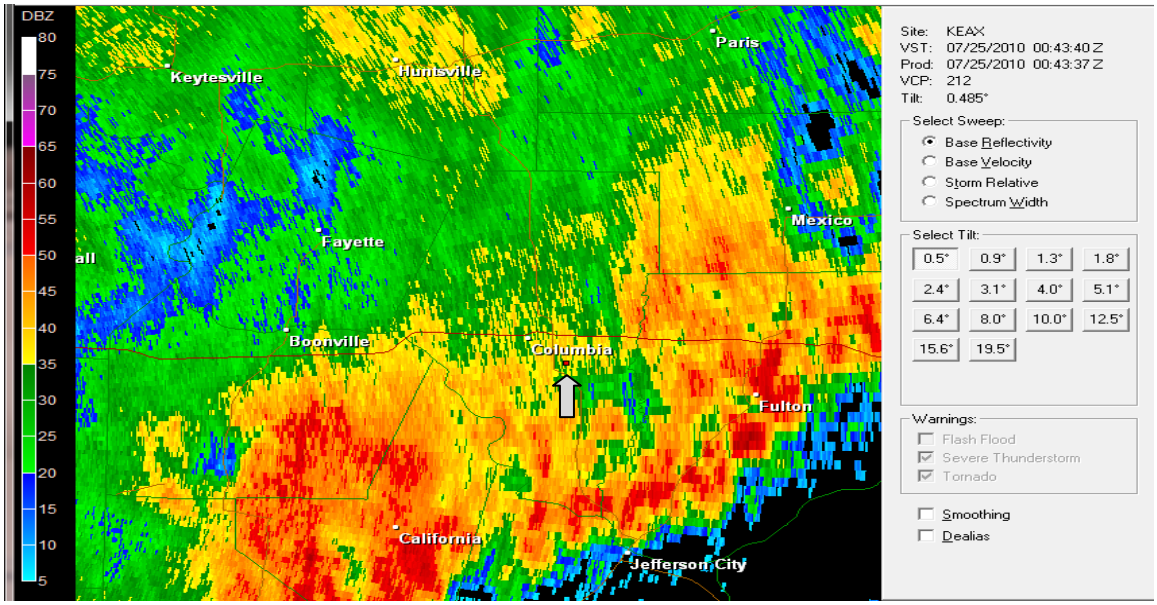

Figure 6.3: Radar reflectivity 0.5^0 tilt from the Pleasant Hill, MO Weather Forecast Office for the July 25, 2010 event. The red dot at the end of the gray arrow indicates the ACES South Farm location.

Figure 6.2 shows that the higher reflectivity remained farther to the northwest of the Columbia area while the deployment location is to the south and east of the city. The activity south of Interstate-70 tended to be fairly disorganized where the storms remained of the pulse variety. The image shows that the pulse thunderstorm moved directly over the ACES South Farm location. The next figure, Figure 6.3, shows that the area sampled was located on the back side of some very heavy convection that had moved through the area, which was also sampled and will be discussed in later sections. As is generally expected, the rainfall rates behind the initial line of convection are much lighter as this precipitation falls farther away from the greatest upward-vertical motion. Sampling near the area of greatest upward vertical motion as opposed to farther away from that area is most likely the reason for the differing drop-size distributions.

6.1.3 Category II Events

This section is focused upon the heavier rainfall events in the Category II classification. These rainfall events were generally convective in nature and maintained rainfall rates and kinetic energy fluxes that were more likely to cause issues with soil erosion due to raindrop impacts, and surface runoff dependent upon antecedent soil moisture and land practices. There were a total of 12 Category II events that can be seen below in Table 6.3.

Table 6.3: Category II events with rainfall total (R_T), rain rate as recorded by the rain gauge (RR_G), rain rate as recorded by the disdrometer (RR_{NS}), kinetic energy flux (KE_{NS}), kinetic energy flux based on rainfall intensity (KE_R) and total drop count (DC_{NS}).

Date	Time (UTC)	R_T (mm)	RR_G (mm hr^{-1})	RR_{NS} (mm hr^{-1})	KE_{NS} (J m^{-2})	KE_R (J m^{-2})	DC_{NS}
26-Jul	2022-2032	2.79	16.76	19.42	0.443	0.31	10748
14-Aug	0424-0434	2.79	16.76	14.86	0.264	0.31	8444
20-Aug	2330-2340	2.79	16.76	23.76	0.466	0.31	9156
2-Jun	0700-0710	3.05	18.29	16.02	0.320	0.34	5105
12-Jun	2008-2018	3.05	18.29	17.25	0.355	0.34	3781
30-Jul	2220-2230	3.05	18.29	20.98	0.441	0.34	9900
26-Jul	2012-2022	3.30	19.81	17.89	0.307	0.36	12099
30-Jul	1714-1724	3.56	21.34	19.06	0.275	0. 39	11393
12-May	0632-0642	3.81	22.86	20.19	0.399	0.41	11692
30-Jul	2210-2220	3.81	22.86	20.61	0.402	0.41	12624
13-May	0934-0944	4.06	24.38	22.09	0.486	0.44	9118
8-Jun	1634-1644	4.83	28.96	27.99	0.533	0.52	13227

The general trend, as shown in Table 6.3, of the Category II events follows that of the Category I events, where kinetic energy flux increases as total rainfall (R_T) and rainfall rate (R_G) each increase; however, it appears as if the KE fluxes are much closer to that of the KE_R than in the lower intensity events, which could indicate that the kinetic energy flux calculation used in the RUSLE equation is of better use in heavier rainfall events with larger drop sizes. In this classification it was discovered

again that some of the events did not follow the overall trend, so they were analyzed further to determine what caused these differences. The first anomaly occurred July 26, 2010 from 2022-2032 UTC where the kinetic energy flux was approximately double that of a very similar event which occurred on August 14, 2010. Both events had very similar rainfall rates with the August 14 event containing fewer total drops than the anomaly. To evaluate the differences it was necessary to analyze the DSD to see if the higher kinetic energy flux is due to larger drops in the dataset. This comparison can be seen in Figure 6.4.

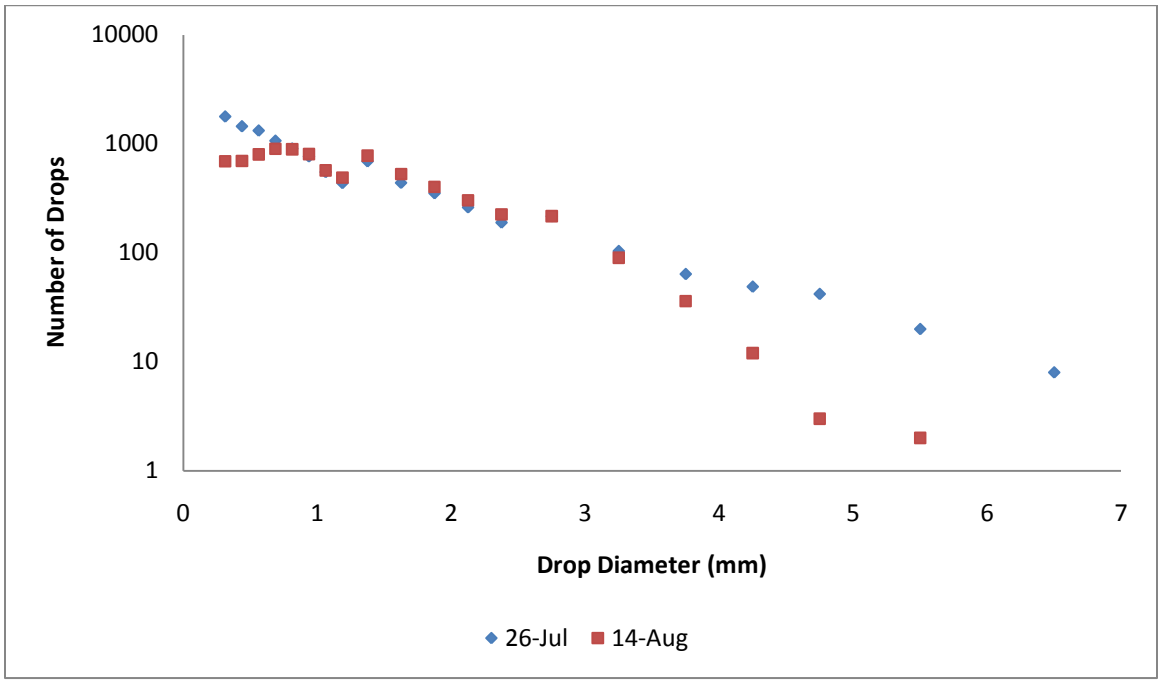

Figure 6.4: Log-scale comparison of the DSDs for the July 26, 2010 from 2022 to 2032 UTC and August 14, 2010 events.

By analyzing Figure 6.4 it is possible to see that the July 26 event contains a greater number of larger raindrops which are greater than 3 mm in diameter. Below the 3 mm diameter the distributions are very similar for both events. The July 26 event maintains a maximum drop size of 6.5 mm while the August 14 event contains a maximum drop size of 5.5 mm. Figure 6.4 shows that the maximum drop size is

fairly close to that of the anomaly; however, the number of larger drops is significantly lower in the August 14 event. The results from this graphical analysis are very similar to the results shown in the Category I analysis. As previously mentioned these curious results warranted further analysis using radar data to see if the type of storm may have had an impact on the DSD.

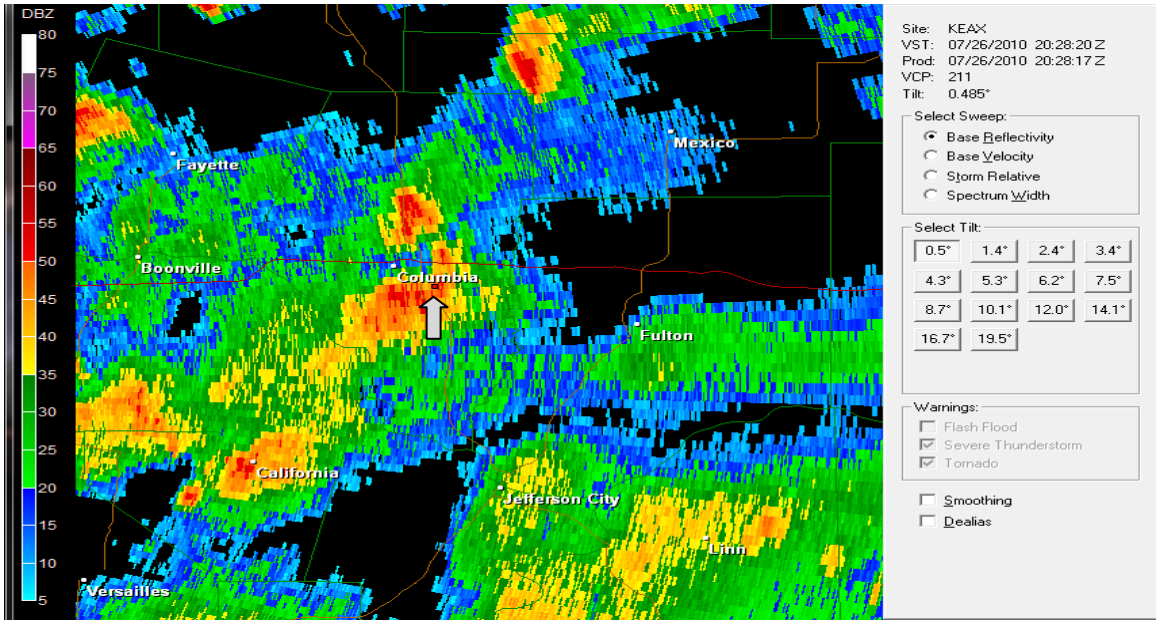

Figure 6.5: Radar reflectivity 0.5^0 tilt from the Pleasant Hill, MO Weather Forecast Office for the July 26, 2010 event. The red dot at the end of the gray arrow indicates the ACES South Farm location.

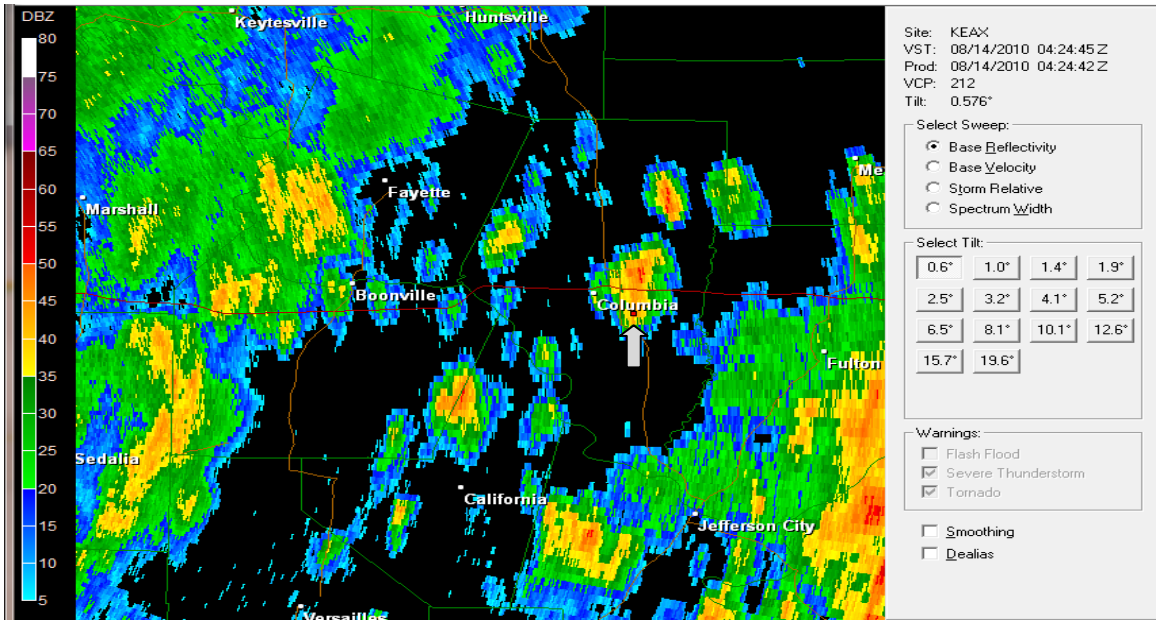

Figure 6.6: Radar reflectivity 0.5^0 tilt from the Pleasant Hill, MO Weather Forecast Office for the August 14, 2010 event. The red dot at the end of the gray arrow indicates the ACES South Farm location.

Each of the events shown in Figures 6.5 and 6.6 are indicative of a fairly disorganized air mass across the area with a majority of the heavier precipitation closer to the Columbia, MO area. The events appear as if they maintain very similar characteristics; however, the August 14 event shows lower reflectivity over the ACES location. This means that the most intense portion of the storm was not sampled on August 14, which is where the two events differ as the most intense portion was sampled over the ACES location during the July 26 event. As it is known that higher reflectivities are directly related to precipitation diameter, it is likely that the difference in the DSD is due to the area of the storm sampled.

Another anomaly occurred on July 30, 2010 from 2220 to 2230 UTC where the kinetic energy flux was much higher than the events with similar rainfall rates. To determine the cause of the kinetic energy flux it was necessary to evaluate the DSD to determine if this was due to a greater quantity of larger drops as the other event comparisons have been. A comparison was made with a similar event that occurred

June 12, 2010 as this event had a similar rainfall rate yet roughly one-third of the total number of raindrops. The comparison of the DSDs can be seen in Figure 6.7, where it is evident that the July 30 event maintains more raindrops in the smaller diameters below 3 mm. In this comparison both events maintained a maximum drop size of 6.5 mm. The events also maintained a similar number of raindrops that were larger than 3 mm; however, the July 30 event maintained an amount of smaller drops significant enough to increase the total kinetic energy. This would suggest that the increase in kinetic energy is not due solely to the larger drops in this case, but also due to the increase in overall drops as there would tend to be more mass in the event. It is again necessary to analyze the types of storms that may have produced such distributions by viewing radar imagery for each event, which can be seen in Figures 6.8 and 6.9.

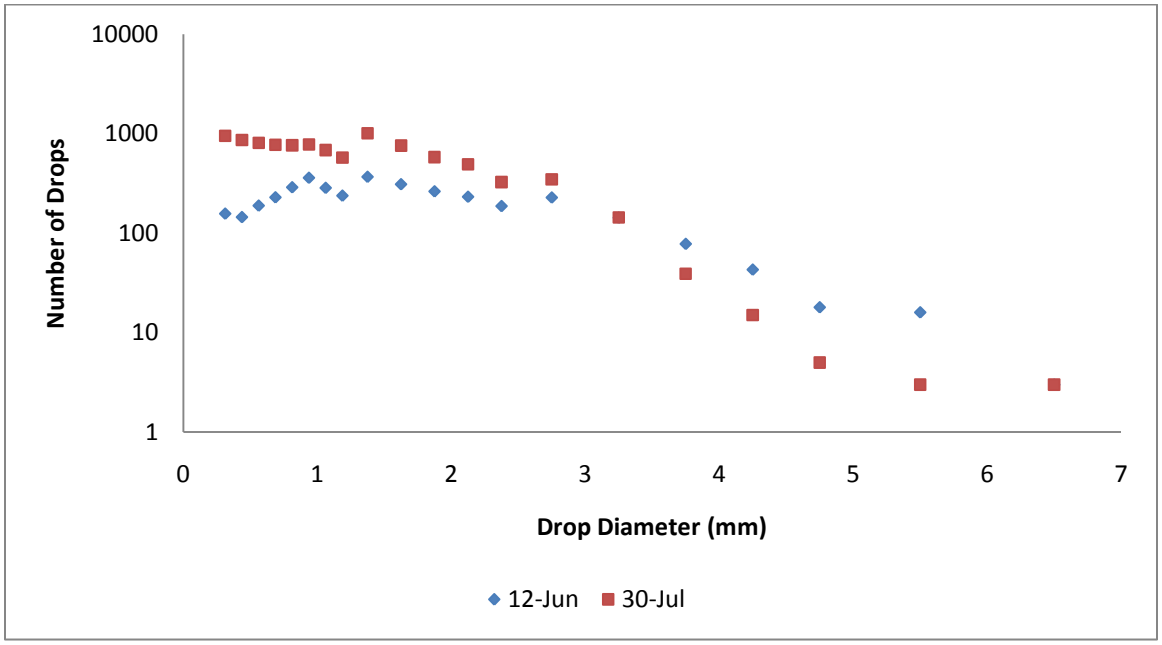

Figure 6.7: Comparison of the drop-size distributions for the July 30, 2010 from 2220 to 2230 UTC and June 12, 2010 events.

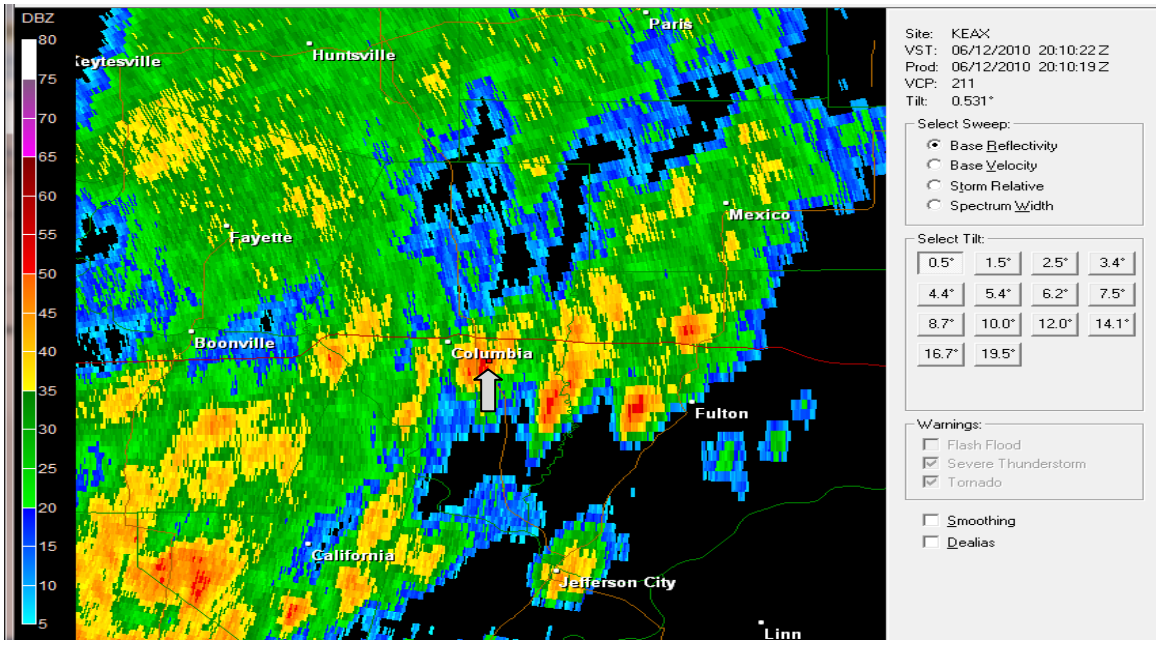

Figure 6.8: Radar reflectivity 0.5^0 tilt from the Pleasant Hill, MO Weather Forecast Office for the June 12, 2010 event. The red dot at the end of the gray arrow indicates the ACES South Farm location.

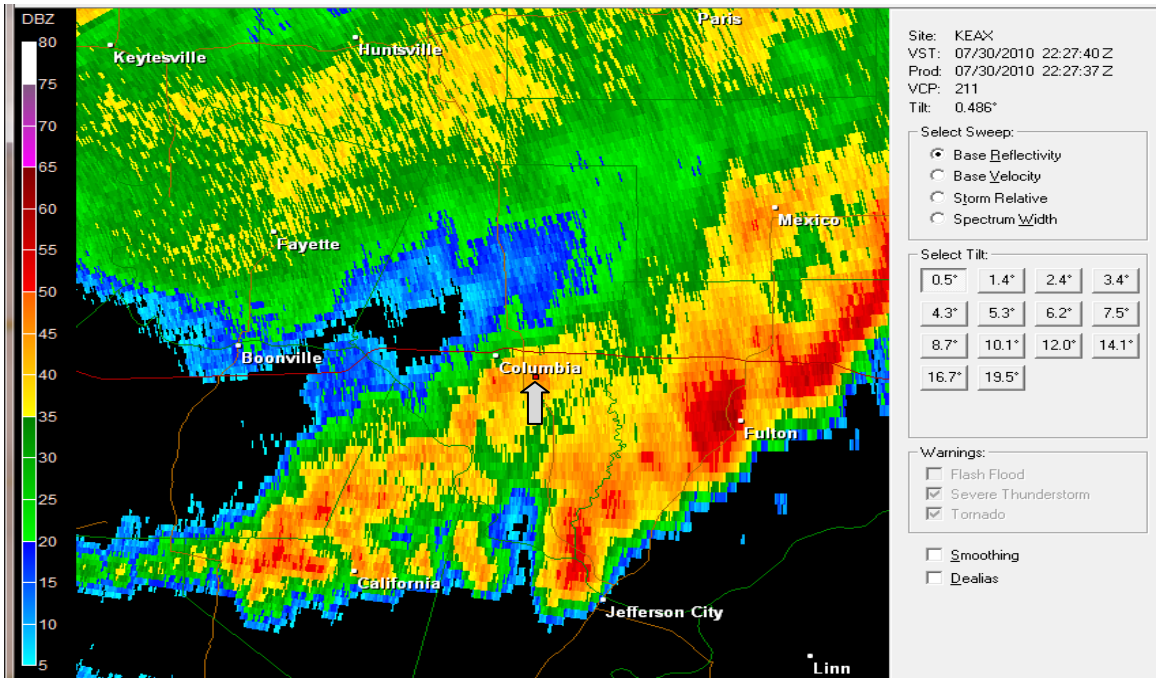

Figure 6.9: Radar reflectivity 0.5^0 tilt from the Pleasant Hill, MO Weather Forecast Office for the July 30, 2010 (2220 to 2230 UTC) event. The red dot at the end of the gray arrow indicates the ACES South Farm location.

Figure 6.8 shows that the storm sampled is part of a fairly disorganized system, where the storm that passed over the ACES location was not as broad as the event shown in Figure 6.9. The July 30 event was part of a much broader linear system; however, the part of the storm sampled is not along the leading edge where the greatest vertical motion exists. Based on previous events this allows for a reduction in the larger drops. The radar imagery in Figure 6.8 shows that the radar reflectivity is higher than the reflectivity in Figure 6.9 as a result of a greater concentration of larger drops. This is very likely the reason that the DSD shows that the June 12 event has more of these drops. The July 30 event maintained a steadier rainfall for the entire 10-minute period, whereas the June 12 event maintained a more intense rainfall for about a 5-minute period with a sharp decrease in reflectivity after the most intense part of the storm. This sharp decrease is likely due to fewer drops, overall, which effectively kept the kinetic energy flux lower than the July 30 event.

A majority of the events analyzed have been focused upon anomalies that have kinetic energy flux that is higher than events of similar rainfall rate; however, in the Category II events list there is at least one event, July 30 from 1714 to 1724 UTC, that had a high rainfall rate with kinetic energy flux that is much lower than the surrounding events. In order to keep the study complete it was necessary to analyze this event to determine what might have caused such an anomaly to occur. In order to determine this it was first necessary to analyze the DSD, which can be seen in Figure 6.10.

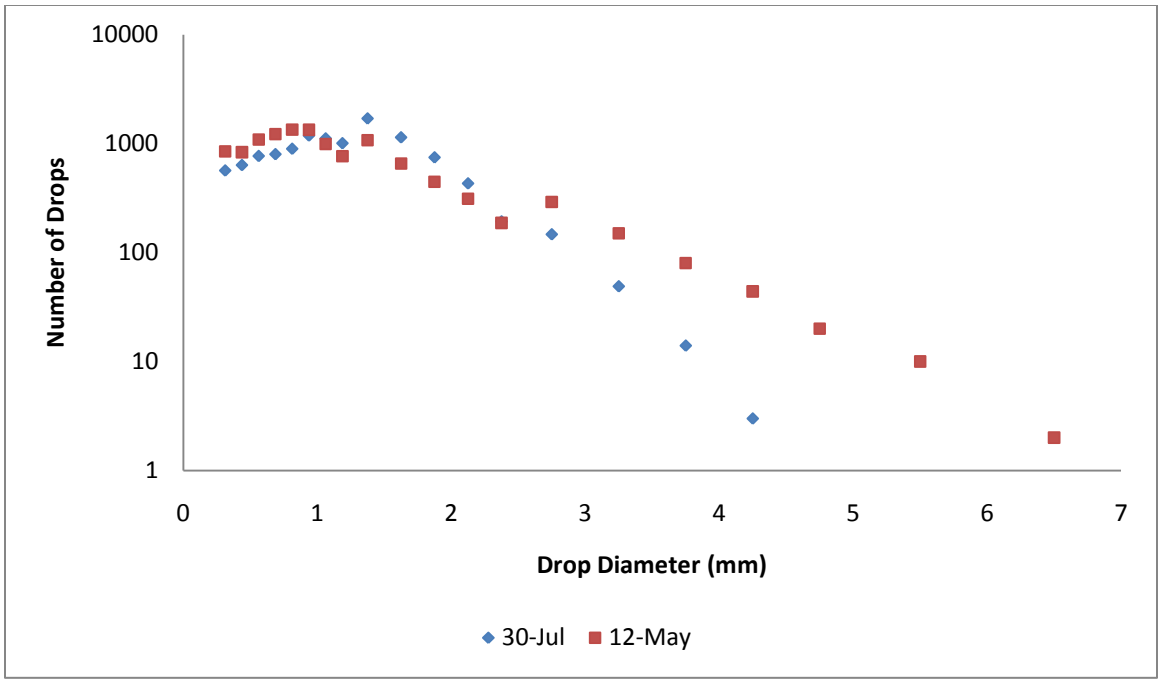

Figure 6.10: Log-scale comparison of the DSDs for the July 30, 2010 from 1714 to 1724 UTC and May 12, 2010 events.

When analyzing the DSDs in Figure 6.10 a curious difference was noticed. The DSD for the July 30 event tended to have the peak number of smaller droplets shifted higher in total drops for the peak as well as farther right. This means, for the July 30 event, that the average drop size below 3 mm is much larger than that of the May 12 event. This would effectively indicate that rainfall rate is more sensitive to an increase in smaller drops than the kinetic energy flux. The maximum drop size in the July 30 event is 4.25 mm, while the maximum drop size in the May 12 event is 6.5 mm. The greater number of large drops in the May 12 event is likely the cause of the increased amount of kinetic energy flux. After looking at the DSDs, radar imagery was then analyzed to determine if certain storm types changed the distribution, which can be seen in Figures 6.11 and 6.12.

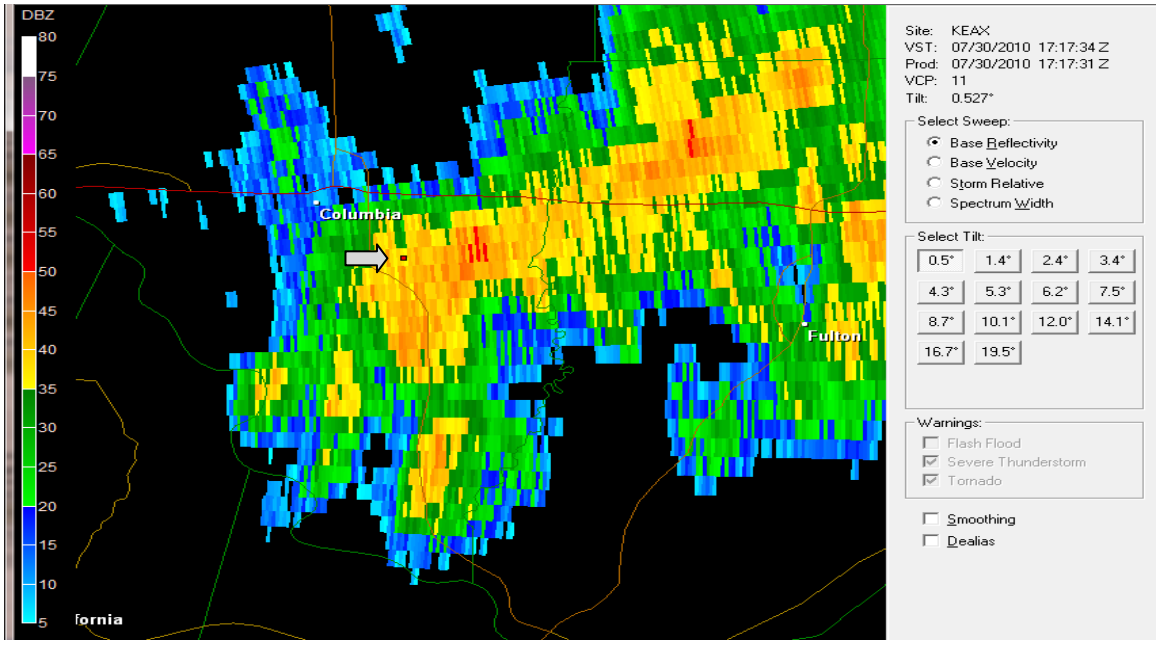

Figure 6.11: Radar reflectivity 0.5^0 tilt from the Pleasant Hill, MO Weather Forecast Office for the July 30, 2010 (1714 to 1724 UTC) event. The red dot at the end of the gray arrow indicates the ACES South Farm location.

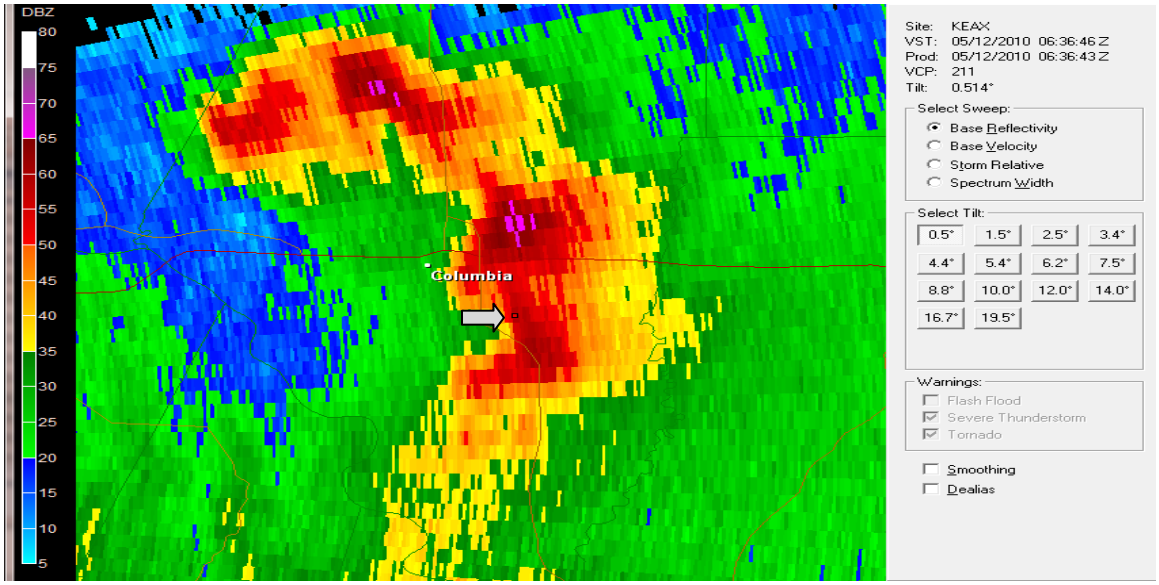

Figure 6.12: Radar reflectivity 0.5^0 tilt from the Pleasant Hill, MO Weather Forecast Office for the May 12, 2010 event. The red dot at the end of the gray arrow indicates the ACES South Farm location.

Most of the events analyzed have followed a very similar trend with the larger raindrops appearing in areas that maintain the higher reflectivity. This event appears to be no different, as the May 12 event maintains a higher reflectivity and also maintains a greater kinetic energy flux, where the July 30 event has lower reflectivity as a result of the smaller drop diameters. One would expect to see drop diameters that are somewhat higher as the reflectivity indicates that the drop diameters could be slightly larger. The highest reflectivity in the May 12 event appears to be just north of Columbia and could be an indication of the presence of hail. It must be kept in mind that the imagery is taken from the Pleasant Hill, MO NWS Radar which means the elevation of the radar beam is approximately 3200 m above the surface so the hail may melt before reaching the surface. The St. Louis, MO NWS Radar is a bit closer but much of the radar data needed for these studies was not available. This area of concern was not sampled during the event.

6.1.4 Category III Events

This section is focused on some of the most impressive events with very high rainfall rates as well as rainfall totals. Many of these events maintained rainfall rates that exceeded 25.4 mm hr^{-1} and some approaching and exceeding 50.8 mm hr^{-1}. Rainfall rates of these magnitudes can cause several problems from raindrop detachment to soil erosion from surface runoff. Not only are the rainfall rates impressive, but also the kinetic energy fluxes are triple that of some of the Category II events. Each event in the Category III classification will be analyzed as these events are likely to result in a greater amount of soil detachment and erosion. The events are listed in order from lowest rainfall rate to the highest rainfall rate and can be seen below in Table 6.4.

Table 6.4: Category III events with rainfall total (R_T), rain rate as recorded by the rain gauge (RR_G), rain rate as recorded by the disdrometer (RR_{NS}), kinetic energy flux (KE_{NS}), kinetic energy flux based on rainfall intensity (KE_R), total drop count (DC_{NS}) and maximum drop size (MDS).

Date	Time (UTC)	R_T (mm)	RR_G (mm hr^{-1})	RR_{NS} (mm hr^{-1})	KE_{NS} (J m^{-2})	KE_R (J m^{-2})	DC_{NS}	MDS (mm)
30-Jul	2200-2210	5.33	32.00	35.56	0.64	0.57	24023	4.75
24-Jun	0112-0122	6.86	41.15	33.03	0.74	0.75	14131	5.5
12-Jun	1932-1942	7.62	45.72	41.10	0.74	0.84	24666	6.5
20-Jul	1214-1224	9.40	56.39	66.98	1.54	1.05	52945	5.5
20-Aug	2246-2256	10.92	65.53	74.03	1.40	1.97	34706	6.5
25-Jul	0010-0020	12.19	73.15	77.75	1.67	1.41	36168	4.75

The events in Table 6.4 seem to follow the general trend of the tables previously shown, where there is a tendency for the kinetic energy flux to increase as the rainfall rate increases. The kinetic energy flux determined in KE_R is very representative of the data found by using the DSD, which would again suggest that the rainfall intensity is a reasonable way to analyze kinetic energy flux in heavier rainfall events. In this category there are no real anomalies except for the curious rapid increase in kinetic energy flux between the event that occurred July 20, 2010 and both events that occurred on June 24, 2010 and June 12, 2010. The rainfall rates did not double, but the kinetic energy flux did. It appears as if the total drops may have had some impact on this increase as the drop count doubled from the June 12 event and nearly tripled from the June 24 event. The distribution will be shown for each event with the majority of the analysis being focused upon this rapid increase in kinetic energy flux without a rapid increase in rainfall rates.

Most of the events shown in Figure 6.13 share very similar DSDs but with differing maximum drop sizes. This was not expected as it was initially thought that much of the kinetic energy in each event comes from the very large drops, which is valid if the kinetic energy flux were accounted for per unit raindrop. It is curious though that these events had the most kinetic energy flux yet many of the events do

not contain a drop count in the largest bin size. It does appear, however, that the increase in kinetic energy flux is due to a significant increase in the total drop count when compared to the less intense events. As expected, more mass that falls through the plain should cause an increase in kinetic energy flux.

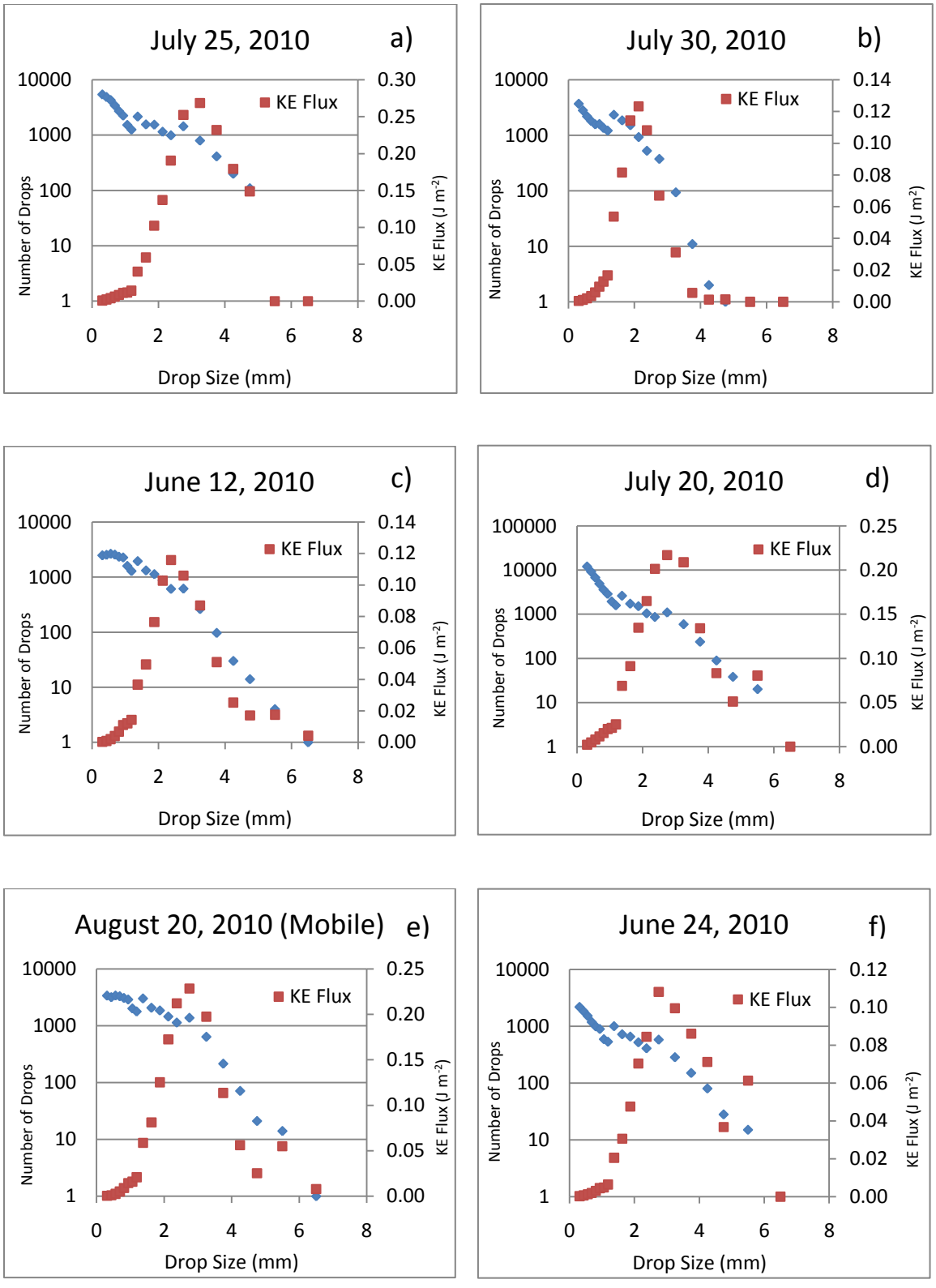

Figure 6.13: Log-scale DSD for each of the Category III events in order by least rainfall rate to greatest.

The June 12 and the August 20, 2010 events, Figures 6.13 A and B respectively, were the only events to have a drop count in this largest bin size, but it was only a single raindrop that was detected. In general, the kinetic energy flux curve maintains a distribution that has a majority of the kinetic energy flux occurring between the 2 and 4 mm drop sizes. This is the point at which the total number in the bin size coexists with the increasing kinetic energy flux. It appears as if the greatest difference in the three events is actually due to the increase in total raindrops, which would mean there are more drops in each individual bin adding to the total mass reaching the surface during the event. There is great interest in the impacts of raindrops larger than 6 mm, but these events maintained very few of these drops to analyze. It is likely that it will be very difficult to collect raindrops of that magnitude as these may occur in super cell thunderstorms, which would likely be associated with severe hail and potentially tornadoes. Each of these modes of severe weather increases the risk to the observer as well as the observation equipment.

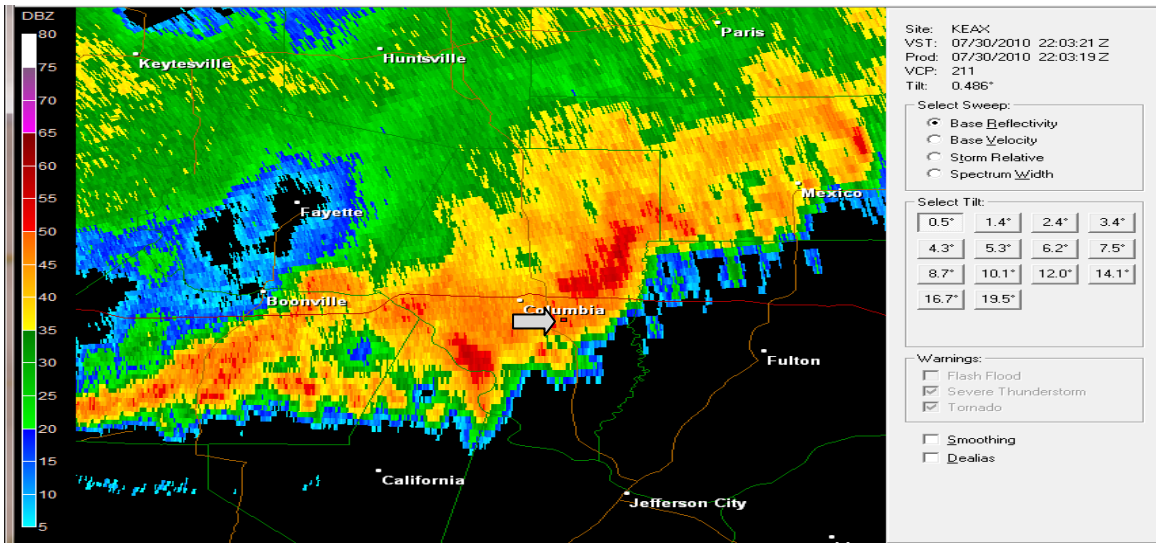

Figure 6.14: Radar reflectivity 0.5^0 tilt from the Pleasant Hill, MO Weather Forecast Office for the July 30, 2010 event. The red dot at the end of the gray arrow indicates the ACES South Farm location.

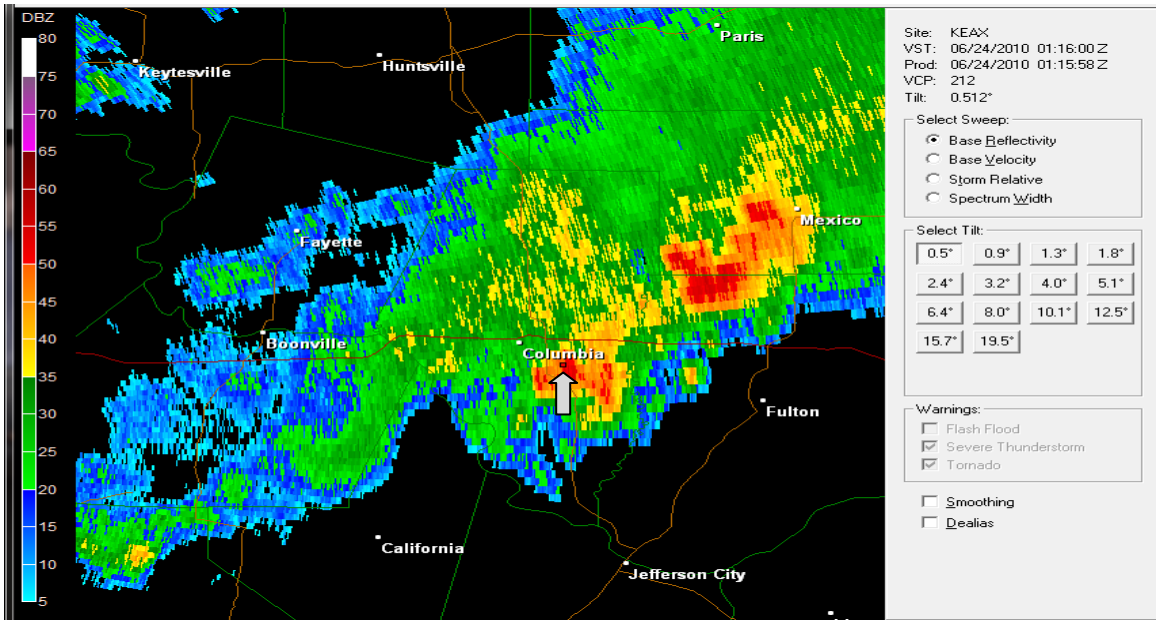

Figure 6.15: Radar reflectivity 0.5^0 tilt from the Pleasant Hill, MO Weather Forecast Office for the June 24, 2010 event. The red dot at the end of the gray arrow indicates the ACES South Farm location.

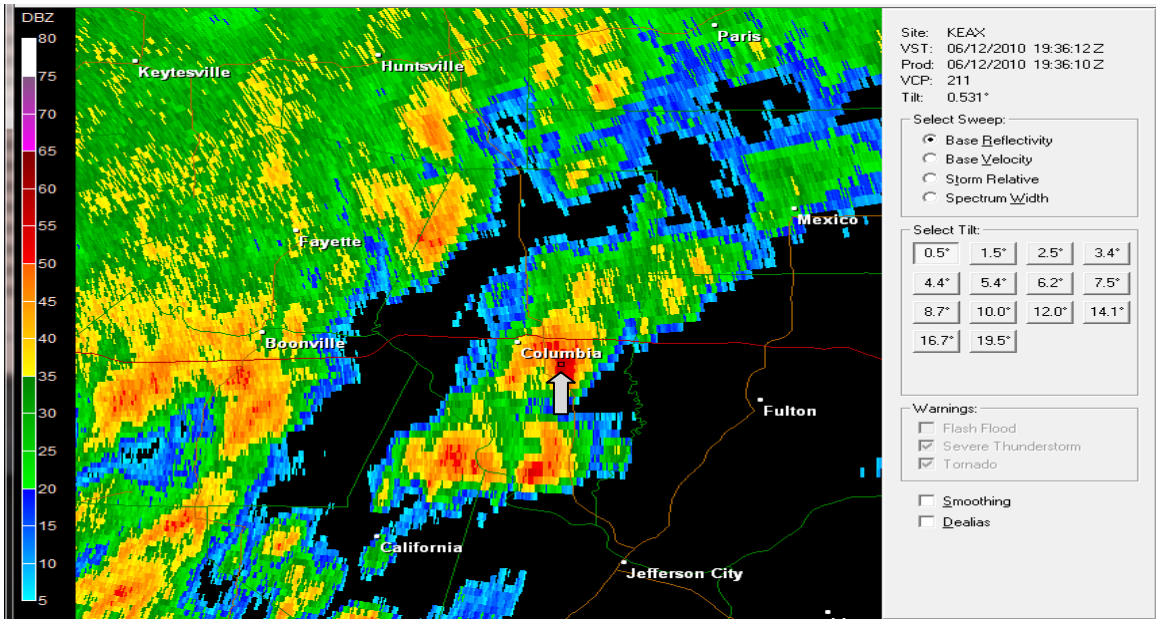

Figure 6.16: Radar reflectivity 0.5^0 tilt from the Pleasant Hill, MO Weather Forecast Office for the June 12, 2010 event. The red dot at the end of the gray arrow indicates the ACES South Farm location.

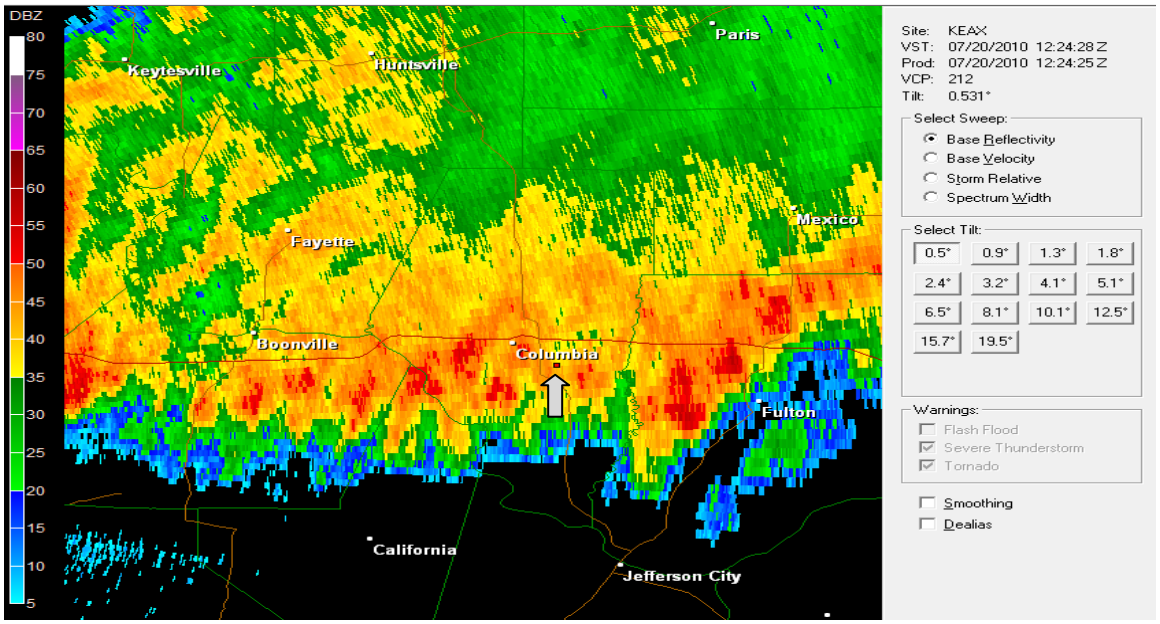

Figure 6.17: Radar reflectivity 0.5^0 tilt from the Pleasant Hill, MO Weather Forecast Office for the July 20, 2010 event. The red dot at the end of the gray arrow indicates the ACES South Farm location.

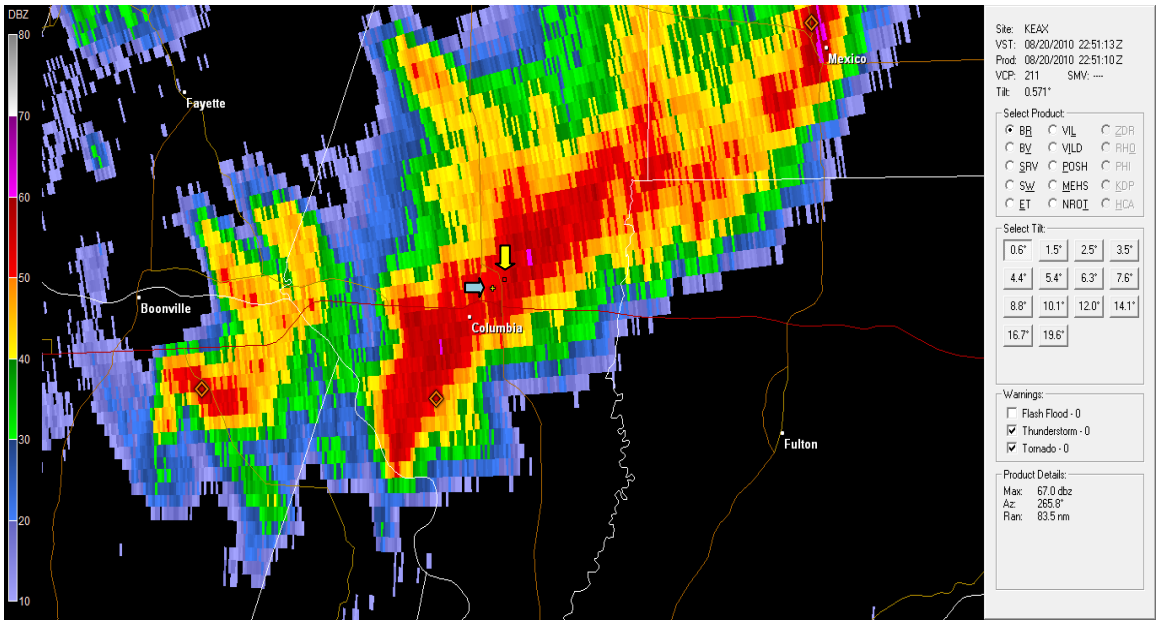

Figure 6.18: Radar reflectivity 0.5^0 tilt from the Pleasant Hill, MO Weather Forecast Office for the August 25, 2010 event. The red dot at the end of the gray arrow indicates the ACES South Farm location.

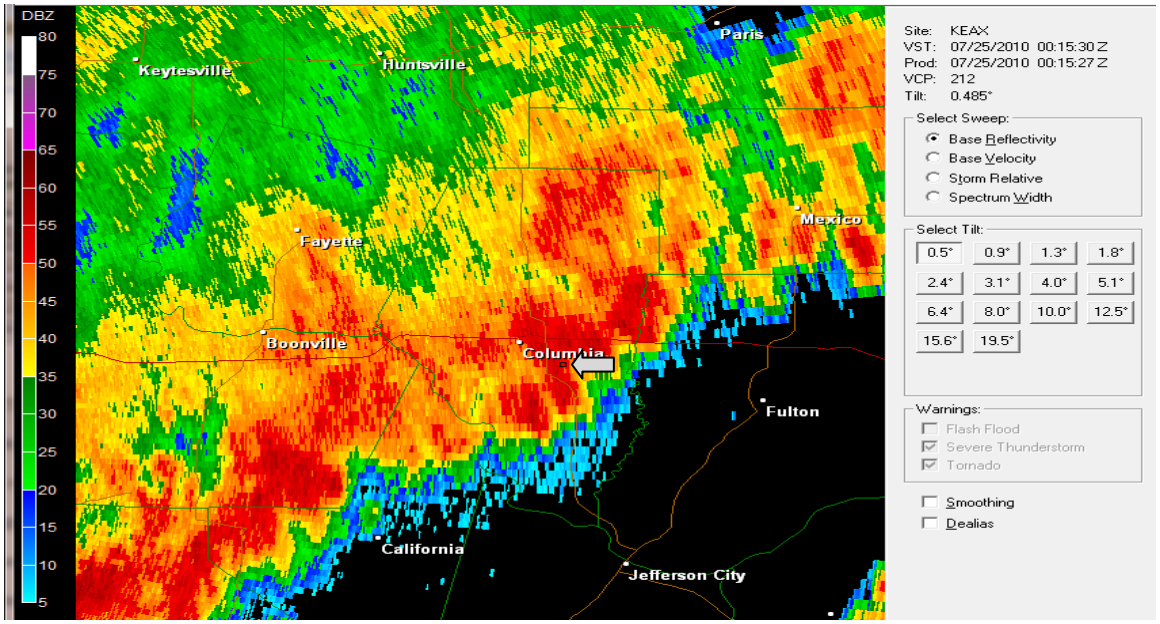

Figure 6.19: Radar reflectivity 0.5^0 tilt from the Pleasant Hill, MO Weather Forecast Office for the July 25, 2010 event. The red dot at the end of the gray arrow indicates the ACES South Farm location.

The radar images shown in Figures 6.14 through 6.19 indicated that many of the Category III events were sampled in the more intense portion of the storm with a majority of them actually sampled in the highest reflectivity. These events, overall, tended to be associated with more organized linear events with much heavier precipitation. It is very interesting to note that the more organized event with higher reflectivity in Figure 6.18 had a smaller maximum drop size than the less organized event in Figure 6.16; however, this appeared to be a fairly common occurrence throughout each event category. Figure 6.14 also appeared to be less organized than the linear event, yet the maximum drops size was 4.5 mm. One positive thing about the less organized events is that many times the storms will not last long enough to cause runoff to occur as many of them passed over the observation sight within the 10-minute interval. It is suspected that many of the pulse thunderstorm events that occur during the hot summer afternoons may also

have larger raindrops, but none of those events were captured during this study. If a similar trend holds true with those specific events, then raindrop detachment and surface runoff could be a greater issue in localized areas. This is due to the fact that many of these storms are very slow moving or even stationary at times and maintain very high rainfall rates.

6.1.5 KE Flux RUSLE vs. Summation

During the analysis it was necessary to evaluate how well the kinetic energy flux is represented by using Equation 2.1. To do this it was necessary to plot the kinetic energy flux summation for each bin with the aforementioned equation using first the rain rate measured by the rain gauge (RRG) and then the rain rate detected by the OTT Parsivel disdrometer. This graph can be seen below in Figure 6.20.

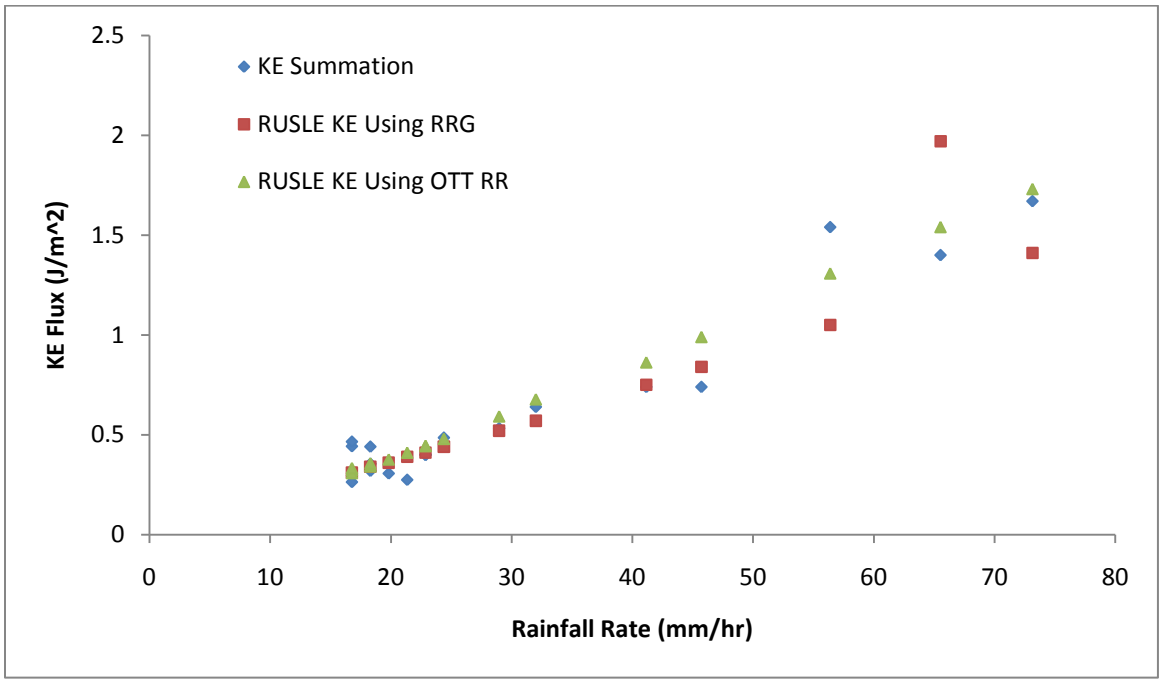

Figure 6.7: Comparison of KE flux, from Category II and III events, summed over each bin as well as KE flux shown using Equation 2.1 using rain rate from the rain gauge (RRG) and rain rate from the OTT disdrometer (OTT RR).

When evaluating Figure 6.20, it was noticeable that Equation 2.1 represents the summed kinetic energy flux with reasonable accuracy when the rainfall intensity was taken from the OTT measurements; however, in some cases there tends to be significant variance when comparing between or among events with similar rainfall rates. The rainfall intensity used from the rain gauge tended to underestimate the kinetic energy flux, especially during the more intense rainfall events. It is also notable that the data does not approach zero at any point and this is due to the fact that the very low intensity rainfall rates were not included in the KE flux evaluation as those events tend to have very little impact on soil erosion.

6.1.6 Summary

When analyzing the Category I, II and III events it was noticed that some of the events maintained very large errors, which were caused due to splash impacting the disdrometer lens. This type of issue impacted each drop size across the spectrum making it impossible to correct. It was also noticed that some of the events had splash that did not impact the lens, which made it possible to correct this issue by using the Gunn and Kinzer (1949) terminal velocity equation.

Overall, the larger drops were found in the less organized pulse-type thunderstorms while many of the more organized linear events had a much smaller maximum drop size. It is theorized that the reduced maximum drop size may be due to stronger horizontal winds associated with the linear events potentially shearing the drops apart. In each event classification it was noticed that not every event that had similar rainfall rates and similar drop counts had the same kinetic energy flux. It was also noticed that some events had higher rainfall rates with

lower kinetic energy fluxes. This was attributed to a greater amount of larger drop sizes in the distribution.

In some cases it was also shown that an increase in rainfall rate and kinetic energy flux can be attributed to a large increase in the total drops which increases the amount of mass falling through the sample area. This was also indicated in the Category III events as many of these events did not have any drops in the largest drop size bin, yet the kinetic energy flux increased significantly. Finally, when evaluating the value of Equation 2.1 for use in the RUSLE equation, it was noticed that both the rain gauge rainfall intensity and the OTT disdrometer rainfall intensity are useful in determining if the equation represents the summed kinetic energy flux. It appears that using the rainfall rate from the OTT disdrometer allows for a much better fit to the summation of kinetic energy over the bins and that Equation 2.1 may be useful in parameterizing the kinetic energy flux based on rain rate.

6.2 Theoretical Terminal Velocity

One of the objectives set in the beginning of this study was to determine if the Gunn and Kinzer (1949) equation was an accurate parameterization of the terminal velocity. In order to test this hypothesis it was necessary to calculate the kinetic energy flux in each event using the actual velocity of the raindrops as measured by the disdrometer, and also by using the aforementioned equation. Other methods such as comparing the actual velocity with that of the theoretical-terminal velocity proved to be very difficult as the actual velocity shown in each bin would need to be averaged each minute for comparison, so the previously mentioned calculation was sufficient since a significant change in velocity would cause large changes in the kinetic energy flux, due to the velocity term being squared. It was necessary to construct a table which shows these comparisons as well as the error between actual

velocity and terminal velocity, which can be seen in Table 6.5 with and without splash corrections.

When this table was examined, it was noticed that a majority of the events maintained kinetic energy flux differences that were very close; however, most of the events show that the Gunn and Kinzer (1949) equation overestimates the kinetic energy flux, especially when looking at the events that did not have the splash correction. This is due to the splashed drops being counted as moving at a set speed, where in reality, this is not the case. The splashed drops tended to move at greatly reduced velocities. The actual velocities that the disdrometer detects accounts for these slower moving drops, which caused the kinetic energy flux to be lower than that calculated by using the Gunn and Kinzer (1949) parameterization. An example of this can be seen below in Figure 6.21.

The difference between the kinetic energy fluxes using theoretical-terminal velocity and actual velocity is very similar after correcting for splash. This would be reasonable as the drops that were outliers, moving at greatly reduced velocities, were adjusted from the dataset effectively making the drops remain close to the Gunn and Kinzer curve. The large difference in total drop counts with splash (DC_S) and with the splash correction (DC_{NS}), would suggest that many of the drop corrections were performed on drops of very small diameters as the kinetic energy flux did not change a great deal. Overall it can be said that the Gunn and Kinzer (1949) equation represents the raindrop velocities reasonably well.

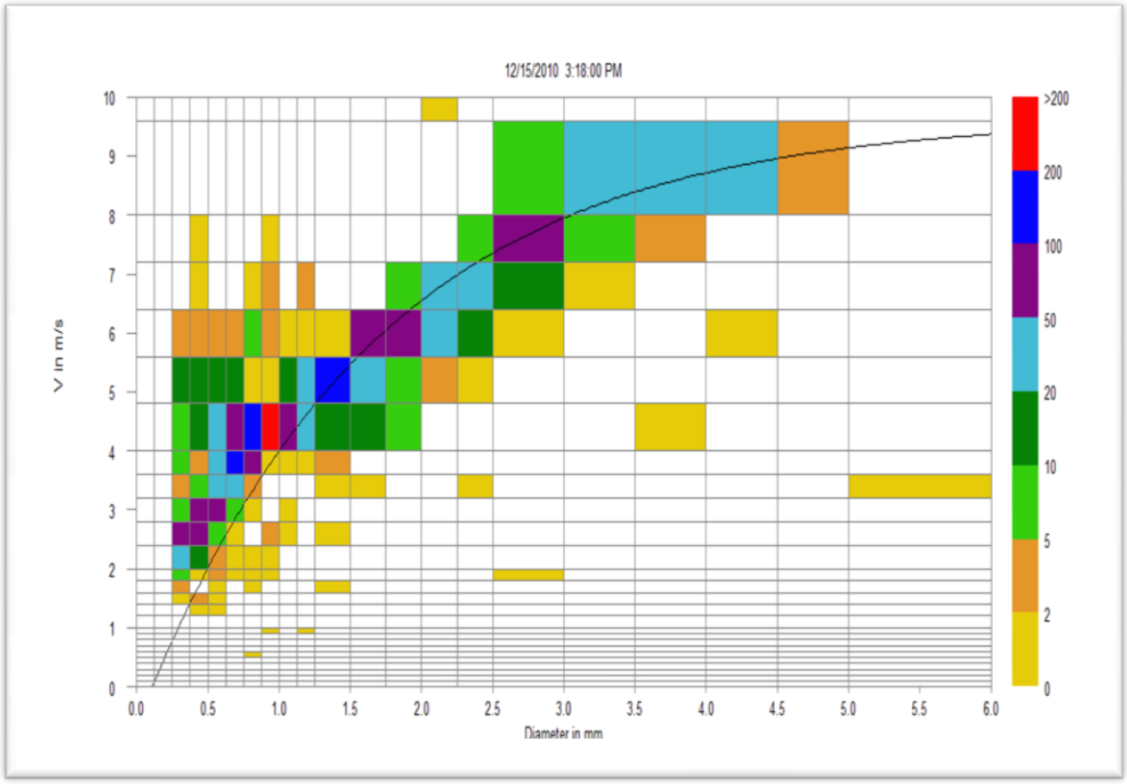

Figure 6.21: Example of the raindrop distribution in the gravity rainfall simulator. Drop diameter (mm) is across the x-axis and velocity (m s^{-1}) across the y-axis.

Table 6.5: Comparison of theoretic-terminal velocity and actual-terminal velocity. In the chart is kinetic energy flux with splash correction (KE_{NS}), with splash correction using terminal velocity (KE_T), without splash correction (KE_s) and without splash correction using terminal velocity (KE_{TS}).

Date	Time (UTC)	RR_G (mm hr^{-1})	KE_{NS} (J m^{-2})	KE_T (J m^{-2})	Diff $KE_T - KE_{NS}$	KE_S (J m^{-2})	KE_{TS} (J m^{-2})	Diff $KE_{TS} - KE_S$	DC_S	DC_{NS}
21-May	0244-0254	4.57	0.052	0.053	0.001	0.052	0.054	0.002	3578	3557
11-Jul	1948-1958	4.57	0.063	0.065	0.002	0.063	0.065	0.002	2257	2232
10-May	1948-1958	6.10	0.203	0.158	-0.045	0.203	0.158	-0.045	4686	4686
25-Jul	0040-0050	6.10	0.091	0.082	-0.009	0.092	0.083	-0.009	4689	4578
2-Jun	0830-0840	7.62	0.106	0.116	0.010	0.106	0.116	0.010	2665	2641
11-Jun	1724-1734	9.14	0.165	0.175	0.010	0.167	0.176	0.009	6280	5951
16-May	1830-1840	9.14	0.120	0.122	0.002	0.122	0.128	0.006	8900	8848
2-Jun	0716-0726	9.14	0.155	0.154	-0.001	0.155	0.155	0.000	5865	5799
26-Jul	2038-2048	12.19	0.335	0.315	-0.020	0.335	0.315	-0.020	4248	4248
2-Jun	0736-0746	13.72	0.246	0.247	0.001	0.254	0.263	0.009	3966	3823
12-Jun	1948-1958	13.72	0.180	0.164	-0.016	0.183	0.164	-0.019	8343	7940
15-Jun	1750-1800	13.72	0.264	0.259	-0.005	0.277	0.280	0.003	11511	9530
26-Jul	2022-2032	16.76	0.443	0.443	0.000	0.525	0.602	0.077	13739	10748
14-Aug	0424-0434	16.76	0.264	0.254	-0.010	0.27	0.267	-0.003	8853	8444
20-Aug	2330-2340	16.76	0.466	0.440	-0.026	0.475	0.453	-0.022	9713	9156
2-Jun	0700-0710	18.29	0.320	0.324	0.004	0.326	0.342	0.016	5450	5105
12-Jun	2008-2018	18.29	0.355	0.357	0.002	0.358	0.359	0.001	3913	3781
30-Jul	2220-2230	18.29	0.441	0.369	-0.072	0.451	0.379	-0.072	10437	9900
26-Jul	2012-2022	19.81	0.293	0.308	0.015	0.336	0.492	0.156	16217	12099
30-Jul	1714-1724	22.86	0.275	0.283	0.008	0.277	0.288	0.011	11608	11393
12-May	0632-0642	22.86	0.399	0.408	0.009	0.408	0.447	0.039	12720	11692
30-Jul	2210-2220	22.86	0.402	0.384	-0.018	0.416	0.409	-0.007	14279	12624
13-May	0934-0944	24.38	0.486	0.493	0.007	0.513	0.552	0.039	10318	9118
8-Jun	1634-1644	28.96	0.533	0.527	-0.006	0.562	0.584	0.022	15496	13227
30-Jul	2200-2210	32.00	0.640	0.555	-0.085	0.683	0.614	-0.069	26442	24023
24-Jun	0112-0122	41.15	0.740	0.650	-0.090	0.83	0.743	-0.087	16575	14131
12-Jun	1932-1942	45.72	0.740	0.707	-0.033	0.759	0.737	-0.022	26153	24666
20-Jul	1214-1224	56.39	1.540	1.660	0.120	1.54	1.660	0.120	52945	52945
20-Aug	2246-2256	65.53	1.400	1.350	-0.050	1.53	1.540	0.010	39688	34706
25-Jul	0010-0020	73.15	1.670	1.530	-0.140	1.67	1.530	-0.140	36168	36168

6.3 Simulated and Natural DSD Comparison

6.3.1 Rainfall Rate Comparison

The final objective in this study was to examine the natural DSD and compare it to the DSD from the rainfall simulator. In order to do this analysis, data were collected from the rainfall simulator using drop-redistribution screens at differing heights. The changes in the drop-redistribution height were to allow for larger drops to form at heights closer to the drippers and smaller drops to form at heights much farther away from the drippers. To determine if the disdrometer was accurately sampling the distribution it was necessary to collect the droplets in small buckets beneath the simulator within close proximity to the disdrometer with floor splash protection as previously mentioned. The buckets were weighed after each test to determine the amount of mass (kg) that fell through the sample area. This, coupled with the density of water, allowed for the calculation of the volume of water that fell through the sample area. That effectively gave the depth of water in millimeters that accumulated beneath the simulator. After this value was determined, it was then possible to compare the rainfall rate calculated by the disdrometer to that which was manually determined. In most cases the rainfall rates were very similar leading to a greater confidence in the disdrometer data. These values and comparisons can be seen below in Table 6.6.

Table 6.6: Shown in the table are the time (UTC), screen height, average rain rate measured (Avg RR_M) , rain rate measured by the disdrometer (RR_D) and percent difference.

Time (UTC)	Screen Height (cm)	RR_M (mm hr^{-1})	RR_D (mm hr^{-1})	% Difference
1518-1528	26	36.44	33.97	6.78
1538-1548	51	35.62	33.01	7.33
1602-1612	80	37.39	36.55	2.25
1618-1628	104	32.62	33.93	4.02
1636-1646	126	32.84	31.87	2.95
1702-1712	152	30.83	31.32	1.59
1720-1730	178	29.91	31.09	3.95
1736-1746	206	22.09	30.83	39.57

The only rainfall rate that had a large enough error to be questioned was the rate shown during the time interval of 1736-1746 UTC, where the disdrometer shows an amount that is roughly 9 mm hr^{-1} higher than the bucket measurements. There are several reasons that this might happen, one of which is the possibility that the buckets were too far away from the center of the simulator. This type of setup might allow for a greater concentration of drops near the disdrometer as it was actually placed in the center. The anomaly will be shown in a compilation of DSDs shown in Figure 6.22; however, the comparison will not be made with the natural events. This figure indicates that the closer the drop-redistribution screen is to the drippers the larger the drops tend to be. Also notable in Figure 6.22 is that the greater the distance is from the drippers to the drop-redistribution screen the greater the amount of smaller drops and total drops that occur. This is again due to the adhering of drops to the screen at lesser distances and the break-up of drops at greater distances from the drippers. Generally, the drops formed by the drippers will have a slower velocity before impacting the redistribution screen while the screen is closer to the drippers, allowing the drops to collect on the screen before dripping. This allows the drop sizes to grow to greater diameters before releasing from the redistribution screen. The greater the distance is between the redistribution screen

and the drippers, a greater velocity can be achieved before the drops impact the screen. This allows the drops to break apart upon impact, effectively reducing the drops size and increasing the total drop count. This graph supports the idea that the sampling buckets are too far away from the greater concentration of drops as the last two DSDs are very similar, but with very different rainfall rates.

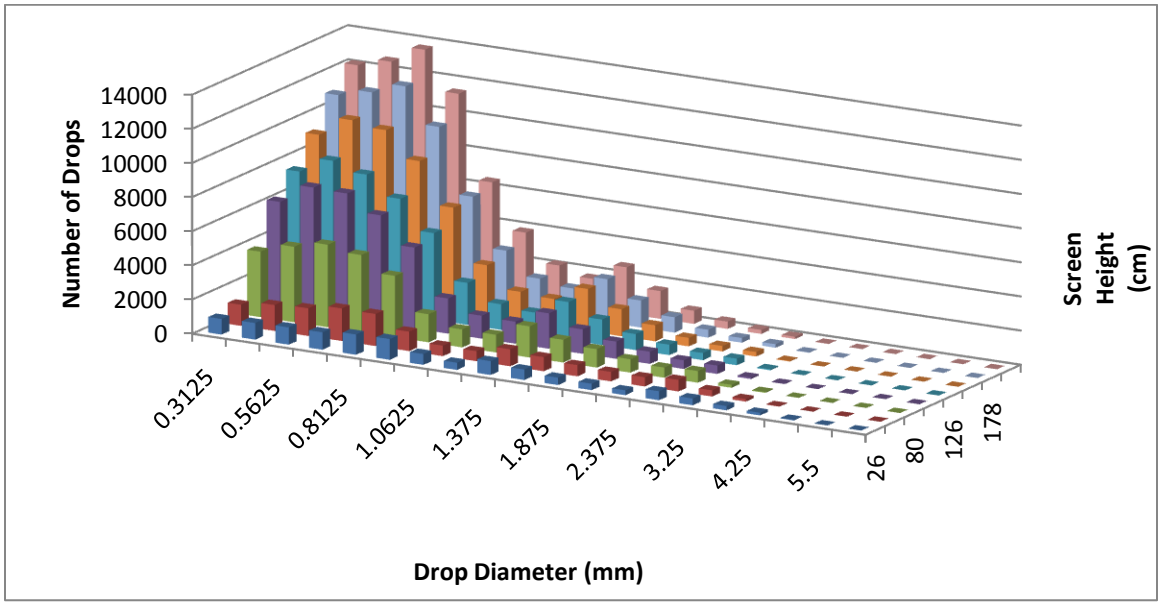

Figure 6.22: Comparison of DSDs based on the screen height adjustments.

The data discussed above could prove to be very useful if the distributions in the rainfall simulator are very similar to specific natural events. In this case most of the simulated events range between 31 and 36 mm hr^{-1}, so this analysis must be limited to this range of data. In order to do this, the natural rainfall events, with rainfall rates similar to the aforementioned rainfall rates, will be compared as these would be most likely to maintain similar DSDs. A graphical analysis will be completed first to determine if the distributions and largest drop size are similar and then a quantitative analysis will be completed to determine if the kinetic energy flux is similar using both theoretical and actual velocities. The natural events that are similar in rainfall rate are shown below in Table 6.7.

Table 6.7: Natural rainfall events used for simulator comparisons.

Date	Time (UTC)	R_T (mm)	RR_G (mm hr^{-1})	RR_{NS} (mm hr^{-1})	KE_{NS} (J m^{-2})	DC_{NS}
8-Jun	1634-1644	4.83	28.96	27.99	0.533	13227
30-Jul	2200-2210	5.33	32.00	35.56	0.64	24023
24-Jun	0112-0122	6.86	41.15	33.03	0.74	14131

6.3.2 Graphical Analysis

To determine if the rainfall simulator can be used to represent natural rainfall events it was necessary to overlay the DSDs from each. It is worth noting that not every simulated event was placed in each comparison as many of them did not maintain the larger drops necessary for an accurate comparison. The first event analyzed was the June 8, 2010 event which can be seen by looking at Table 6.7. The rainfall rate was 28.96 mm hr^{-1} which is very close to the range that the simulator produced. This event was compared with simulated events that maintained drop-redistribution screen heights of 51, 80 and 104 cm as these events contained a similar count of larger drop sizes. In Figure 6.23, it is noticeable that

the maximum drop size decreases as the screen distance is increased as was previously shown. In this case the June 8 event, shown in Figure 6.23-a, maintains a DSD very similar to that of the screen height of 51 cm, where the main difference is due to the maximum drop size. The June 8 event maintained 3 drops with a maximum drop size of 5.5 mm and the simulated event maintained 2 drops with a maximum drop size of 6.5 mm. The second event, shown in Figure 6.23-b, with a rainfall rate of 32 mm hr^{-1}, is the June 30, 2010 event, which maintained smaller drops as the maximum drop size is 4.75 mm and only one of these drops were detected. It can be seen that each of the simulated events were very similar to the natural event; however, the simulated events with the screen heights placed at 104 and 125 cm seems to fit much closer than the other simulated events and in many cases overlaps with the natural event. In this case either of the screen positions would be a good fit to the natural data. The last event analyzed is the June 24, 2010 event shown in 6.23-c, where the rainfall rate is shown to be 41.15 mm hr^{-1}. This event maintains a slightly larger maximum drop size than the July 30 event as the maximum drop size is 5.5 mm, where 15 of these drops were observed. In this case it appears as if the screen height of 26 cm fits best, which would suggest that the natural rainfall event maintains a greater deal of large raindrops as this height tends to allow drops to adhere to the screen and then release forming larger drop diameters as previously mentioned.

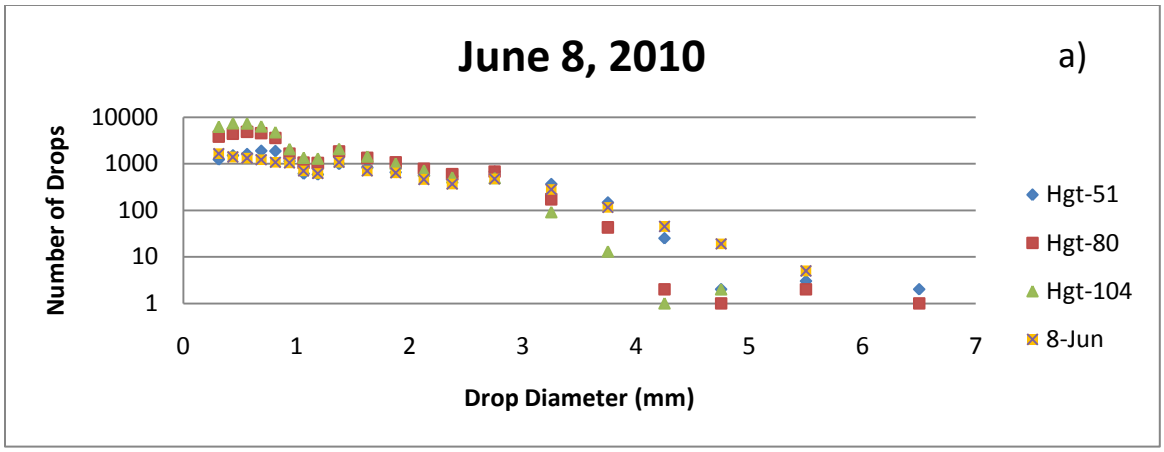

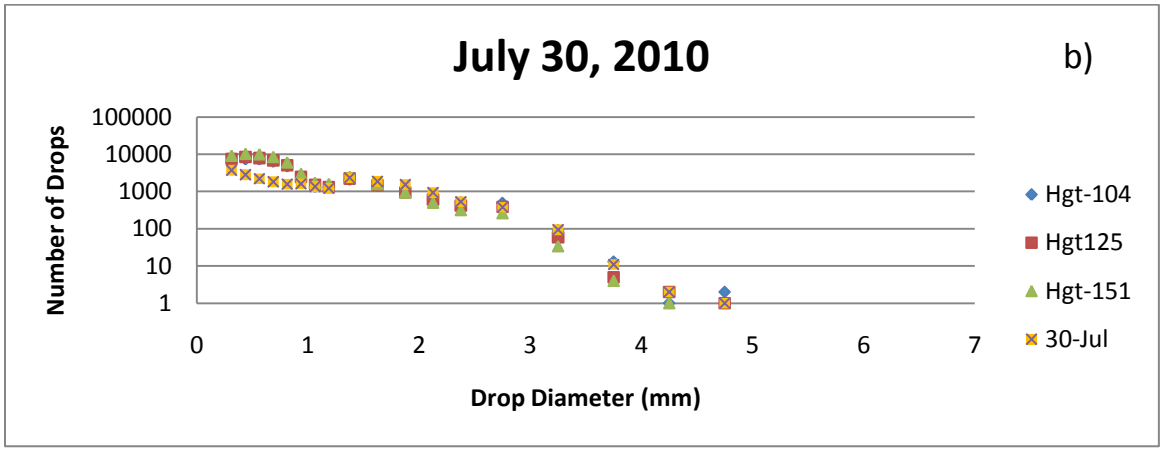

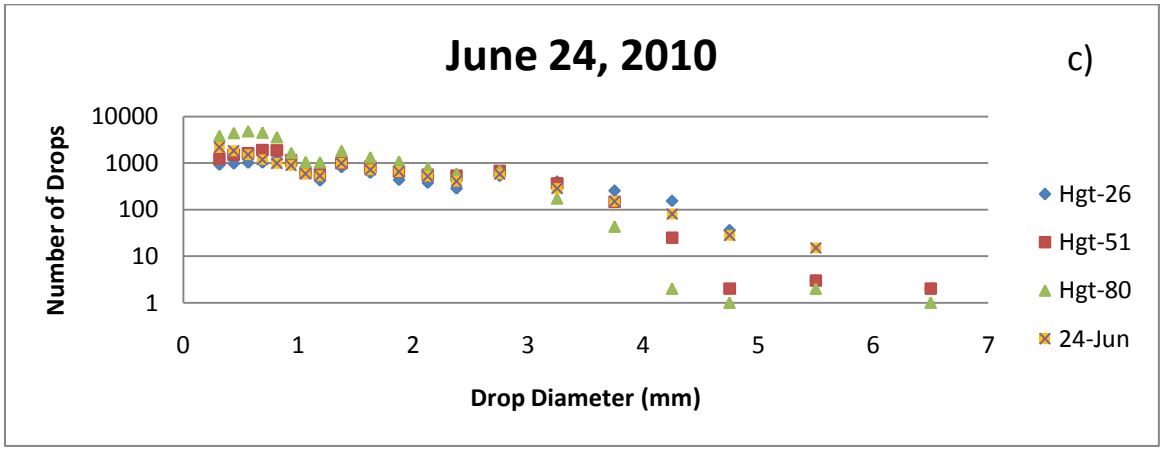

Figure 6.23: Log-scale DSD for each natural event listed previously as well as three simulated DSDs with maximum drop sizes that were similar to the Natural events.

Once the distributions were analyzed, it was necessary to see if rainfall events associated with these simulated data were due to certain storm types. To do this it was necessary to reference radar data as was completed in previous analyses. The first event, shown in Figure 6.24, indicates that the sampling occurred on an individual cell associated with a larger area of convection as was also the case in Figure 6.14. The difference in the two images is that one occurred on the leading edge of the line while the other occurred on the back side of the line. This could be an indication that the higher winds at the leading edge of a linear system could act to shear the drops apart causing the maximum drop size to be reduced. It is also a possibility that the area of highest reflectivity may not have been sampled in Figure 6.14; however, it appears as if the reflectivity was very similar in those areas. Figure 6.15 shows a different storm setup with the storm appearing as if it is more of a pulse thunderstorm, which may or may not maintain winds similar to that of a linear system. It is in this case that the overall drop sizes tended to be larger than the other events which compared more closely with screen positioned at 26 cm. A solid conclusion cannot be made as this study is only based on three events; however, it does appear as if the smallest two screen distances are more representative of pulse-type events and the linear events might be better represented by greater distances with the screen positioned at 104 and 125 cm.

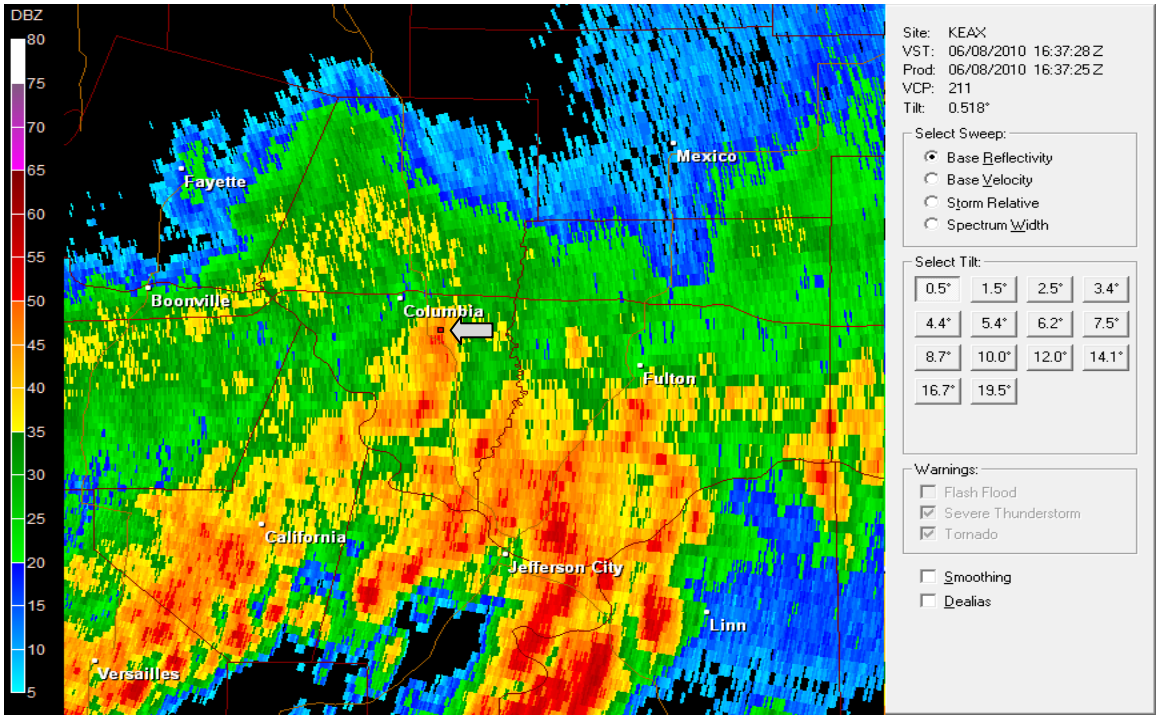

Figure 6.24: Radar reflectivity 0.5^0 tilt from the Pleasant Hill, MO Weather Forecast Office for the June 08, 2010 event. The red dot at the end of the gray arrow indicates the ACES South Farm location.

6.3.3 Quantitative Analysis

The final portion of the analysis was focused on the total kinetic energy flux as well as the total raindrop count associated with both the natural and simulated events. Ideally, one would wish to have these parameters very close to those of the natural events as this means that the distribution is more representative of that event. The most significant of these parameters is the kinetic energy flux as this is what researchers would likely need to reproduce to simulate soil loss due to rainfall. This comparison can be seen below in Table 6.8.

Table 6.8: A comparison of kinetic energy flux at different screen heights with natural rainfall events of similar rainfall rates.

Date	RR_{SIM} (mm hr^{-1})	RR_{GNE} (mm hr^{-1})	Screen Hgt (cm)	KE_{NE} (J m^{-2})	KE_{Sim} (J m^{-2})	KE_{SimT} (J m^{-2})	DC_{NE}	DC_{SIM}
8-Jun	33.01	28.96	51	.533	.565	.622	13227	15301
30-Jul	31.87	32.00	125	.640	.406	.442	24023	47147
30-Jul	31.87	32.00	104	.640	.450	.500	24023	43046
24-Jun	33.97	41.15	26	.740	.686	.703	14131	11277

This table shows the rainfall rates measured beneath the simulator (RR_{SIM}), rainfall rates measured by the tipping bucket rain gauge in natural events (RR_{GNE}), the screen heights used for comparison, kinetic energy flux from the natural events (KE_{NE}), simulated events (KE_{SIM}), simulated events with terminal velocity parameterization (KE_{SIMT}) and drop count both natural (DC_{NE}) and simulated (DC_{SIM}). The simulated data appears to be a reasonable representation of the natural rainfall events, especially the events with higher kinetic energy. The June 8 event shows that the kinetic energy flux is very similar when using the actual velocity measured by the disdrometer, but tends to be overestimated slightly when using the theoretical terminal velocity. This is logical as both the rainfall rate and total drop count are both higher for the simulated event. It should also be kept in mind that the reason for the difference in the actual and terminal velocity is due partially to the screen as well as the height of the simulator. In this situation, the best way to fix the reduced velocities would be to increase the height of the simulator so that the greatest screen distance tested would be at a height high enough that all drop sizes may reach terminal velocity.

The event that occurred July 30 shows that the screen at the distance of 125 cm may not be a good enough representation as the kinetic energy flux tends to be off significantly with both actual and terminal velocities. In this case it appears as if the secondary screen height of 104 cm represents the numerical data much better and

would be more representative of the data, which is likely due to the natural event maintaining larger drops which are better represented above 2 mm as shown in Figure 6.23. The simulated data also has nearly twice the drops of the natural event, which is partially the result of splash as well as drop break-up due to the drop-redistribution screen. The final event which occurred on June 24 shows that the simulated kinetic energy flux is representative of the natural event kinetic energy flux. It was expected that the simulated kinetic energy flux would be lower as the rainfall and total drop count were also lower, but the results are very similar.

One thing to note about the simulator is that the larger raindrops are forming on the screen as they pass through. This effectively decreases the distance that the drops have to fall, which keeps them from reaching terminal velocity. This may be the cause of the discrepancies in the kinetic energy flux comparisons. In order to evaluate this it was necessary to plot a curve of kinetic energy difference against screen height, which can be seen in Figure 6.25. The values in Figure 6.25 are not absolute values so the data represents the actual difference, where the theoretical terminal velocity gives values that are higher than the actual velocity measured by the instrument. In this figure it is curious that there is very little difference in the kinetic energy flux at the extremes of the screen distances and much larger differences as the screen is positioned near the middle height of 104 cm. It is likely that the difference is reduced near the 26 cm height since the drop height is only adjusted slightly lower. The difference is also reduced at the larger distances as the drops tend to pass through and remain at terminal velocity, since the terminal velocity of smaller drops is lower, as opposed to adhering to the screen and forming larger drops. The middle range would tend to have larger discrepancies, since there are more medium sized drops that adhere to the screen, thus reducing the fall height in which to reach terminal velocity.

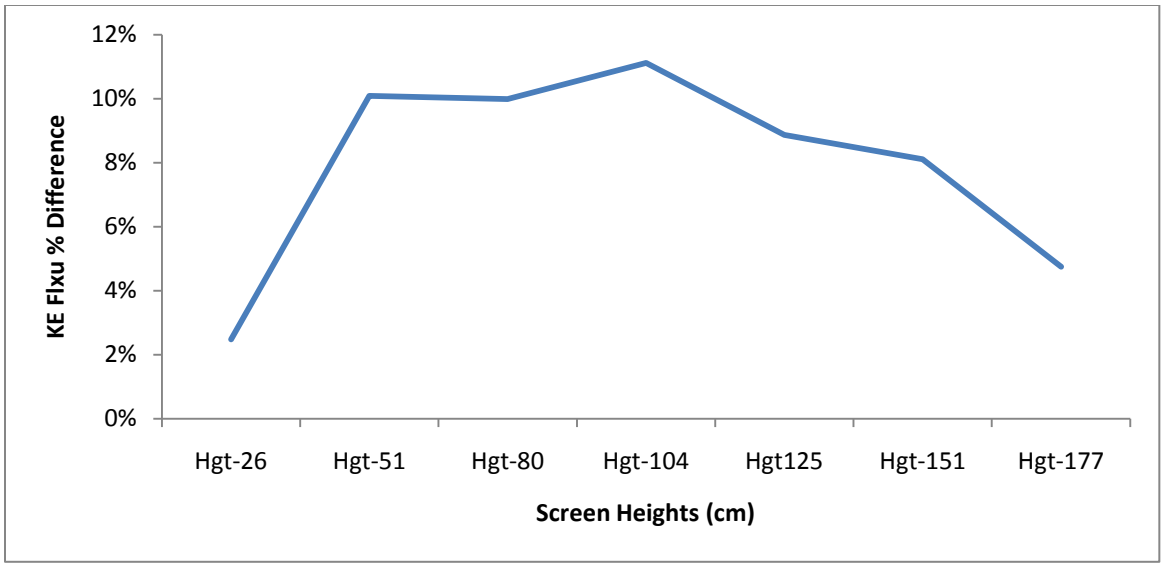

Figure 6.25: Percent difference between kinetic energy flux using actual and terminal velocity at each of the screen distances below the drippers. The percentages are not absolute, meaning that the theoretical terminal velocity is higher than the measured velocities.

6.3.4 Summary

In this section an analysis was completed to determine how the drop-redistribution screen height affects the DSD. When the screen height is closer to the drippers it was shown that the maximum drop size increases while the total number of drops decreases. The opposite occurs when the screen height is farther away from the drippers, causing a reduced maximum drop size and an increase in the total number of drops. To determine if the disdrometer was detecting the drops properly it was necessary to compare the rainfall rate detected by the disdrometer as well as the rainfall rate measured in the buckets. This evaluation showed that the disdrometer was indeed detecting the rainfall rate correctly, except in one sample, where it was likely that the buckets were not capturing as many drops as the disdrometer. This may have been a result of the buckets being farther away from the center causing fewer drops to fall into the sample area.

After it was determined that the disdrometer was sampling correctly, it was necessary to evaluate the distribution at each predetermined drop-redistribution screen height for comparison with natural rainfall events. The results from the analysis showed that greater distances from the drippers, such as the 104 and 125 cm heights, is more representative of linear events, while lesser distances of 26 and 51 cm heights are more representative of pulse-type thunderstorms. It must be noted that the analysis was based on three rainfall events as the range of rainfall rates tested in the simulator was limited; however, it appears as if the DSDs were very similar in most cases and the quantitative analysis suggested that many of the parameters were very close as well.

Some of the discrepancies were likely due to the drops forming on the screen and then falling from significantly reduced heights causing many of the drops to fall below terminal velocity as shown in Figure 6.25. It can be seen that the drops falling from the drop-redistribution screen, closer to the dripper, allows for the drop to obtain a greater percentage of terminal velocity, resulting in kinetic energy flux calculated using measured velocity being very similar to kinetic energy flux calculated using parameterized-terminal velocity. As the screen is positioned at 125 cm it is noticed that many of the drops are falling at greatly reduced velocities causing the kinetic energy flux to be reduced. It was theorized that this may be due to a larger percentage of the drops adhering to the screen and then falling from lower heights. The test at the greatest distance from the drippers, 178 cm, suggests that the velocities are very close to the parameterized velocities as the percent error is greatly reduced. It was theorized that this may be a result of the drops being sheared apart and splashing through the screen which allowed the smaller drops to fall at or slightly above terminal velocity. Further studies should be pursued with a greater range of rainfall rates to draw more solid conclusions.

Chapter 7
Conclusions
7.1 Summary

There is great interest in being able to model kinetic energy flux at the surface due to rainfall events, as higher kinetic energy fluxes have been associated with greater amounts of soil loss. This study was mostly focused on kinetic energy flux associated with both natural and simulated rainfall events of differing intensities, ranging from lighter stratiform events to very heavy convective events; however, there were other areas of focus as well. One focus area was placed on the instrumentation used in evaluating the kinetic energy flux based on the DSD. Simulated data were used in testing the RIS and the OTT Parsivel disdrometer and in doing a comparison between the instruments. The data collected from the simulated rainfall events, with drop-redistribution screens in place, were also compared to the natural rainfall events to determine if simulated data could be representative of natural data.

After completing the analysis it was shown that kinetic energy flux does increase overall as the rainfall rates increase; however, there are many times when this does not occur. It was discovered that, in some cases, the rainfall rate may remain similar to other events in the same class, but one of the events may have two to three times the amount of kinetic energy flux. In determining the cause of these differences, it was necessary to analyze the DSD to determine what may have contributed to these anomalies. It was shown that many of the anomalies tended to have a larger maximum drop size and similar rainfall rates, which would indicate that kinetic energy flux cannot always be accurately represented by rainfall rates. This would suggest that it would likely be better to parameterize the kinetic energy flux with the DSD as opposed to solely using the rainfall rate as is done for the RUSLE

equation. By further analyzing the events it was shown that the area of the storm sampled played a role in the DSD as it appeared that the pulse thunderstorm events generally had a larger maximum drop size than many of the linear events. Another of the objectives of this thesis was to determine if the Gunn and Kinzer (1949) equation for terminal velocity was representative of actual terminal velocity, as this would be needed if kinetic energy flux was parameterized by using the DSD. The analysis shows that only slight variances existed between the kinetic energy flux using the measured terminal velocity and the kinetic energy flux determined by using the Gunn and Kinzer (1949) equation.

Another objective was to determine if the rainfall simulator could be used to represent natural rainfall events. To do this comparison, the drop-redistribution screen was positioned at differing heights below the drippers. The DSDs collected during the simulated events were then compared to natural events that maintained similar rainfall rates and maximum drop sizes. It appears as if the rainfall simulator can give a reasonable representation of the natural rainfall events; however, this study was limited to only three rainfall events as time did not permit for the testing of rainfall rates outside of the 30 to 36 mm hr^{-1} range.

It is impossible to form solid conclusions with such a small number of events; however, looking at these events it appears as if the simulator represents pulse thunderstorms better when the screen is positioned at heights closer to the drippers, in this case 26 cm as this produced as larger maximum drop size and a similar amount of total drops. The linear events appeared to be better represented at distances farther away from the drippers, which were approximately 104 cm and 125 cm as the maximum drop size is similar in most cases and the total number of drops were similar, except for a larger amount of the very small drops below 1 mm. The quantitative analysis indicates that the kinetic energy flux determined by using the

simulated data is very similar to the natural rainfall events; however, there tended to be larger variances in the total number of drops detected. It must be kept in mind that there are many issues that arise when using simulated data. The largest issues are due to the inability to simulate turbulence, the steady rainfall rates of the simulator and the other is due to the simulator not being of significant enough height to allow the drops to reach terminal velocity. In this study it is shown that the rainfall simulator produces drops near terminal velocity when the screen is near the drippers as this allows the drops to adhere to the screen and fall from slightly reduced heights and also when the screen is positioned at distances greater than or equal to 178 cm from the drippers as this likely allows the drops to be sheared apart and splash through at or possibly above terminal velocity. In the central positions, the drops likely adhere to the screen causing the new drip height to be significantly lower resulting in the drops not being able to reach terminal velocity.

Another significant objective was to evaluate the instrumentation used in collection the DSDs. To be able to draw any type of conclusions from the rainfall data it is necessary to understand where the errors lie in both the hardware and the software that an individual uses. In this case the OTT Parsivel disdrometer and RIS were tested to determine these errors. The disdrometer appeared to have several issues when testing with a single dripper. The software was supposed to eliminate the drops that were out-of-focus, but it was determined that this was not happening, which resulted in an overestimation of the drop size. After further testing was completed with a range of drop sizes, it was then realized that it is likely that the RIS has an apparent sample volume that is highly dependent upon the drop size. The smaller the drop sizes in the sample volume, the smaller the apparent sample volume becomes. Other hardware and software problems resulted in a very limited amount of data collection with the RIS.

The OTT Parsivel disdrometer was also tested in the rainfall simulator where it was discovered that error existed due to the collocation of the sample area and the instrument, which resulted in a great deal of splash. It was possible to correct for some of the splash in the rainfall simulator by placing a wire mesh on the upward facing portion of the power supply box. This adjustment reduced splash significantly in the simulator, but as previously mentioned, the turbulence in the simulator is not representative of the turbulence experienced in natural rainfall events. After analyzing the natural rainfall events it was determined that wind was causing a great deal of splash to occur in the sample area. It was shown that an adjustment can be made to reduce the amount of splash by analyzing the velocity data. If a drop is moving at a velocity that is significantly lower than the others in the same class it is likely that it is due to splash. Once the drop is identified, then corrective action can be taken to adjust out the drop. Results were shown both with the splash and with the splash adjusted out. In this study it appears as if the disdrometer is a better instrument to use to detect the DSD.

7.2 Future Work

This study shows many of the interesting aspects of both natural and simulated rainfall events along with sources of error in detecting the DSD. The conclusions drawn from this study can be further expanded by comparing a larger range of rainfall rates using the rainfall simulator. The DSD found with the increased rainfall rates can then be compared to a wider range of natural rainfall events. If the range is expanded, it would also be possible to analyze a larger amount of radar data to determine if the simulator represents a particular classification of storm with the screen height positioned at the previously mentioned heights. Another possibility would be to use the instrumentation to compare with some of the other types of

simulators that were mentioned in previous sections to see if the simulated DSDs are a better fit to the natural DSDs. The gamma distribution could be fitted to the DSD data collected in this study, which would continue some of the work completed by Gilmore (2007) where a similar comparison was made. If the gamma distribution is fit to the DSDs shown in this study, then it might be possible to model the kinetic energy flux more accurately. The final suggestion is to consider changing the software for the RIS so that raindrop rejection occurs as it is meant to. The RIS has a lot of potential since the instrument has a very limited amount of splash in the sample volume.

References

Atlas, D., and C. W. Ulbrich, 1977: Path-and area-integrated rainfall measurement by microwave attenuation in the 1-3cm band. *J. Appl. Meteorology.*, **16**, 1322-1331.

Blanquies, J., M. Scharff and B. Hallock, 2003: The design and construction of a rainfall simulator. International Erosion Control Association (IECA), 34th Annual Conference and Expo

Fornis, R., H. R. Vermeulen and J. D. Nieuwenhuis, 2005: Kinetic energy–rainfall intensity relationship for Central Cebu, Philippines for soil erosion studies. *J. Hydrology*, **300**, 20-32.

Gilmore, W., 2007: Comparison of rainfall energy and soil erosion parameters from a rainfall simulator and natural rain. Available online at: https://mospace.umsystem.edu/xmlui/handle/10355/5101

Gunn, R., and G. Kizner, 1949: The terminal velocity for water droplets in stagnant air. *J. Meteorology*., **6**, 243–248.

Jones, B., J. Saylor and L. Bliven, 2003: Single-camera method to determine the optical axis position of ellipsoidal drops.

Kincaid, D., K. Solomon and J. Oiliphant, 1996: Drop size distributions for irrigation sprinklers. USDA

Marshall, J. S. and W. McK. Palmer, 1948: The distribution of raindrops with size. *J. Meteorology*., **5**, 165-166.

McDonald, J. E., 1954: The shape and aerodynamics of large raindrops. *J. Meteorology.*, **11**, 478–494.

OTT 2006: Manufacturers instruction manual. Available online at: http://www.esrl.noaa.gov/psd/data/obs/instruments/OpticalDisdrometer.pdf

Regmi, T. P. and A. L. Thompson, 2000: Rainfall simulator for laboratory studies, *Amer. Soc. Ag. Eng.*, **16(6)**, 641-647.

Renard, K, 1975: Rainfall simulators and USDA erosion research: History, perspective and future. Rainfall Simulator Workshop

Salmi, A., and J. Ikonen, 2005: New piezoelectric Vaisala RAINCAP® precipitation sensor. 19th Conf. of Hydrology, San Diego, Amer. Meteor. Soc., P2.6.

Schwab, G. O., D. D. Fangmeier, W. J. Elliot, and R. K. Frevert, 1993: *Soil and Water Conservation Engineering*. John Wiley and Sons, Inc., 93 pp.

Testud, J., S. Oury, R. A. Black, P. Amayenc, and D. Xiankang, 2001: The concept of "normalized" distribution to describe raindrop spectra: a tool for cloud physics and cloud remote sensing. *J. Appl. Meteorology*., **40**, 1118-1140

Tokay A., and D. A. Short, 1996: Evidence from tropical raindrop spectra of the origin of rain from stratiform versus convective clouds. *J. Appl. Meteorology*., 35, 355–371.

Sempere-Torres, D , C. Salles, J.D. Creutin, G. Delrieu, 1992: Quantification of soil detachment by raindrop impact:
performance of classical formulae of kinetic energy in Mediterranean storms. IAHS Publ. no. 210, 1992.

Ulbrich, C. W., 1983: Natural variations in the analytical form of the raindrop size distribution. *J. Clim. Appl. Meteorology*., **22**, 1764-1775.

Van Dijk, A. I. J. M., L. A. Bruijnzeel, and C. J. Rosewell, 2002: Rainfall intensity – kinetic energy relationships: a critical literature appraisal. *J. Hydrology.,* **261,** 1-23.

Yuter, S., D. Kingsmill, L. Nance and M. Mang, 2006: Observations of precipitation size and fall speed characteristics within coexisting rain and wet snow. *J. Clim. Appl. Meteorology.*